UNPUBLISHED PRELIMINARY DATA

FUNDAMENTAL RESEARCH IN SOLID STATE ENERGY CONVERSION PROCESSES

CENTER FOR SPACE RESEARCH

and

Energy Conversion and Semiconductor Laboratory
Department of Electrical Engineering

MASSACHUSETTS INSTITUTE OF TECHNOLOGY
Cambridge 39, Massachusetts

Semiannual Technical Summary Report No. 3
June 1, 1964 to November 30, 1964

on

Contract: NASA Grant NsG 496 (part)
M. I. T. Task: 9827

November 30, 1964

FUNDAMENTAL RESEARCH IN SOLID STATE ENERGY CONVERSION PROCESSES

CENTER FOR SPACE RESEARCH

and

Energy Conversion and Semiconductor Laboratory
Department of Electrical Engineering

MASSACHUSETTS INSTITUTE OF TECHNOLOGY
Cambridge 39, Massachusetts

Semiannual Technical Summary Report No. 3

June 1, 1964 to November 30, 1964

on

Contract: NASA Grant NsG 496 (part)
M.I.T. Task: 9827

November 30, 1964

TABLE OF CONTENTS

PROJECT PERSONNEL

John Blair, Associate Professor of Electrical Engineering

G.S. Almasi, Research Assistant, Electrical Engineering

A.W. Carlson, Research Assistant, Electrical Engineering

J.W. Conley, Research Assistant, Electrical Engineering

P.J. Shaver, Instructor, Electrical Engineering

W. Brennan, Technician

Barbara A. Smith, Secretary

FELLOWSHIP AND THESIS STUDENTS

Nguyen Duc Cuong

17531

INTRODUCTION

During the past reporting period the work continued in the areas of photovoltaic and thermoelectric processes.

Additional progress was made in the theoretical characterization of the properties of graded heterogeneous transitions between dissimilar semiconductors. The theoretical properties of such regions was examined with and without an applied magnetic field. The work on the characterization of the processes at the absorption edge of CdTe is complete. The complete theoretical and experimental results of this work will be published in a doctoral thesis in January 1965. The investigation of the feasibility of a multiple transitional process via impurity levels in CdS continues with a view towards the feasibility of a multi-transitional solar cell.

The work on the experimental characterization of the thermal and electrical transport properties of ZnSb is essentially complete. The pertinent coefficients of the galvanomagnetic tensor have been evaluated experimentally. The thermal conductivity measurements are essentially complete. With the completion of the work on ZnSb, the work will continue on the investigation of mixed crystals of $(CdSb)_x(ZnSb)_{1-x}$.

Two doctoral theses, one on the optical properties of CdTe and one on the transport properties of ZnSb are essentially complete. Two Ph.D degrees will be granted, one in January 1965 and the other in June 1965 on the basis of work supported in these areas.

arthur

CHAPTER 1

GEORGE ALMASI

GRADED ENERGY GAP HETEROSTRUCTURES

1.0 Introduction

Work since the last report has centered on the theoretical analysis of a graded-gap photocell. Earlier results of the present author[6] have been revised and combined with work done during the last reporting period, resulting in a comprehensive theoretical treatment of graded-gap photodevices which is presented on the following pages.

1.1 Theoretical Background

The idea for a graded-energy-gap photocell arose from a desire for a high-efficiency, wide-spectral-response solar cell. In a normal solar cell, in which the bandgap is the same throughout the device, photons with energy below the bandgap contribute nothing to the output power, whereas photons with energy greater than the bandgap contribute no more than photons with energy equal to the bandgap. It would seem that this source of inefficiency would be avoided by a device with a range of bandgaps built in, so that the low-energy photons are absorbed where the bandgap is small, whereas the high-energy photons are absorbed where the bandgap is large.

To set up a photovoltage it is necessary to separate the excess carriers produced by the photons. In a normal photocell this involves carrier motion by diffusion. In a graded-gap photocell, as will be shown later, "quasi-electric" fields enter into the charge separation. These "quasi-electric" fields are proportional to the gradients of the respective band edges.[1]

The first problem which comes up is the characterization of such a device. This was discussed briefly by Aigrain[2] in a seminar at M.I.T. The configuration he suggested is shown in Fig. 1. This lecture has not been published, and the author is grateful to Professor Bruce Wedlock for making his private notes available to him.

Tauc[4] has considered the problem of setting up a potential between the faces of a graded-gap photocell in the absence of a magnetic field. He considers an illuminated semiconductor region in which the bandgap changes from E_{G1} to E_{G2}, but which is otherwise homogeneous. The excess carrier concentration is assumed to be uniform inside the illuminated region and zero outside. Tauc uses irreversible thermodynamics and the "Quasi-Fermi levels" of Shockley[15] to derive an expression for the open circuit voltage.

For a strongly p-type sample with a uniform equilibrium hole concentration p_o, his expression yields

$$V_{oc} = \frac{\mu_n \Delta_n}{p_o \mu_p + \Delta n(\mu_n + \mu_p)} \quad \frac{E_{G2} - E_{G1}}{e}$$

where Δn is the excess carrier density, E_G the energy gap, and μ the mobility. A similar expression holds for a strongly n-type sample.

Tauc considered only the open-circuit case and did not calculate any I-V characteristics or efficiencies.

Segall and Pell[3] used the open circuit voltage expression of Tauc as a starting point in a brief "exploratory" investigation of the potentialities of a graded-gap photocell. Mobilities and other quantities besides the energy gap were assumed to be constant. Uniform doping was assumed. They calculate short-circuit current, assume ohmic behavior, and derive an expression for efficiency; using the properties of a material like GaAs and a doping level of 10^{17} cm^{-3}, they obtain an efficiency of about 2% in sunlight. For a Ge-Si alloy cell, they obtain an efficiency of 3% in sunlight.

Segall and Pell display a very good physical understanding of the processes in and problems of a graded-gap device. However, it is hard to criticize or comment on their paper because many of their results are stated without proof or derived from physical reasoning. It so happens that their results agree with the more detailed analyses to be discussed below, and in retrospect it is interesting to see that they can be "derived" by such simple techniques but by their own admission, it is not meant to be a rigorous discussion.

Before leaving this paper, it may be appropriate to point out that the doping level of 10^{17} cm^{-3} used by Segall and Pell is determined by present-day GaAs material technology; the intrinsic concentration of GaAs at room temperature is about 10^{7} cm^{-3}. Now, the open-circuit voltage and thus the efficiency are inversely proportional to the dark carrier concentration, at least until the open-circuit voltage saturates. Thus a decrease in doping level to 10^{16} cm^{-3} would increase the efficiency in sunlight to 20%.

A more extensive treatment of a graded-gap photocell without a magnetic field is presented by Emtage.[5] He starts by setting his partial currents equal to the gradients of suitably defined pseudo-electrochemical potentials,

the "quasi-Fermi levels" introduced by Shockley.[15] Emtage states without proof that " it is easily verified either from the Boltzmann equation or from thermodynamic arguments that these forms hold even when the band gap and effective masses vary". One supposes that he is relying here partially on the results of Tauc, who did use "thermodynamic arguments".

These current equations are combined with Poisson's equation and with the continuity equation; the pseudo-electrochemical potentials are then combined into two new dimensionless quantities which allow Emtage to reduce the entire problem to a pair of simultaneous nonlinear second order differential equations which, by his own admission, "cannot be solved in their entirety." Emtage then makes a number of assumptions (to be discussed shortly) and goes on to calculate the I-V characteristics of a cell combining a p-n junction and an energy-gap gradient normal to the junction. Using numbers for a GaAs-InAs alloy system and illumination having a uniform spectrum extending between the greatest and least bandgaps only, he calculates an efficiency of 3% for sunlight intensity and a maximum of 43% for an intensity 2000 times greater than sunlight.

Several months after the publication of the papers by Segall and Pell and by Emtage, Almasi* presented an independent analysis of a graded-gap cell operating with a magnetic field in the original PEM configuration suggested by Aigrain. This work will be discussed in detail later. In this work, the present author chose to start with the Boltzmann equation as a more physically motivated treatment than the quasi-Fermi level approach. As was noted at the time, the Boltzmann equation approach does indeed bear out the validity of Emtage's partial current equations for the inhomogeneous semiconductor case.

Having derived the partial-current equations by different means, the two analyses differ chiefly in their assumptions and in the stages at which the assumptions are made, although of course Emtage does not include a magnetic field in his treatment. Both papers combine the partial current equations with Poisson's equation and with the continuity equation and eventually come out with expressions for quantities of interest such as open-circuit voltages and short-circuit currents.

*Reference 6, the author's M.S. thesis, henceforth abbreviated M.S.

It is true that Emtage's approach has a good deal of generality, but it is the present author's personal opinion that the mathematical complexity tends to obscure the physical processes involved. For example, the importance of excess carriers and the excess carrier distribution in understanding semiconductor device action has become increasingly apparent in recent years, and yet the action of the excess carriers in the various cases considered by Emtage is all but lost in the dimensionless quantities with which he is dealing. Excess carriers are barely even mentioned.

As a more important example, Emtage is eventually forced to assume that the change in bandgap in an extrinsic Debye length is small compared to kT in order to solve his system of equations. As pointed out by Almasi[6] M.S., this is equivalent to assuming quasi-neutrality and can be done much earlier in the analysis with the "safety check" of self-consistency. The physical significance of this assumption is not at all apparent from Emtage's analysis.

As a third example, Almasi showed in M.S. that the diffusion current due to the excess carriers in the graded region can be safely neglected in most cases when compared to the drift current. Realizing this would have simplified Emtage's analysis considerably.

Emtage's treatment of the high illumination case is more detailed than that of Tauc or the present author. However, Emtage's expression for the open-circuit voltage is substantially* the same as that derived by Tauc, and if it can be assumed that the fields in the x- and y directions are simply related by the Hall angle, that is, that $\mathcal{E}_y = (B\mu_n)_{eff}\mathcal{E}_x$, then the open-circuit voltage which would be derived on the basis of M.S. also agrees substantially** with Emtage's result.

At present, Emtage's paper is the only published work which considers the I-V characteristics of a graded-gap device with current flowing along the direction of the gap gradient. (Later on in this paper, the developments in the present author's M.S. thesis will be applied to this situation.) Tauc has not done this at all, and the present author's M.S. thesis considered only net current flowing perpendicular to the gap gradient. Emtage allowed

*Expect for some "end corrections", which Emtage admits are small.
**Some uncertainty is caused by the fact that Emtage has assumed constant mobilities whereas the present author uses a certain average of a linearly varying mobility.

for departures from ohmic behavior and found these departures to be small.

On other counts, Emtage's assumptions are more restrictive than either those of Tauc or the present author. Emtage assumes constant mobilities; Tauc discusses varying mobilities very briefly; the present author incorporated a linearly varying mobility into his model. Emtage assumes constant effective masses, although he admits that both this and the constant mobilities are very poor assumptions. Tauc states (without proof) that such effects are "usually very small." The present author assumed effective masses proportional to the energy gap* and showed under what conditions the effects were "very small."

This last point was also considered by Verie[25] in a paper published more than two years after M.S. Verie also made the assumption, based on k·p theory, that the effective masses were proportional to the bandgap, and came to the same conclusions as the present author, namely, that band-gap variations and effective mass variation give rise to quasi-electric fields of opposite signs, but that the band-gap variation will be the dominant effect as long as $E_G >> kT$.

In 1963, an analysis of photoelectric effects in a graded-gap region in the presence of a magnetic field appeared in a paper by Fortini and Saint-Martin.[27] Constant mobilities were assumed, and the band-edge gradients were simply inserted into the current equations without any derivation. The analysis is valid for small Hall angles and low illumination. Quasi-neutrality was assumed, but the conditions necessary for this assumption to hold were not discussed. No reference level was defined for the energy levels under discussion.

These omissions aside, however, the work which is done in this paper is done well. The normal PEM effect is considered alongside the PEM effect arising from the gap gradient, and the authors point out the importance of the new mobility coefficient

$$\mu' = \frac{n + p}{n/\mu_p + p/\mu_n}$$

*An assumption suggested by k·p perturbation theory and borne out experimentally for the HgTe-CdTe system.[16] See Appendix A, P. 39.

which is associated with the gap gradient and which is to be compared with the normal ambipolar mobility coefficient

$$\mu = \frac{n - p}{n/\mu_p + p/\mu_n} .$$

This coefficient μ' is the same as the quantity μ^* defined in M.S.

The short-circuit PEM due to the gap gradient is calculated for arbitrary surface recombination velocities* at the front and back faces and for two different excess carrier generation functions: a uniform and constant generation rate and a generation rate localized near the illuminated front face.

This is as far as the analysis is carried; there is no discussion of the power output of such a device, and no calculation of efficiency. The experimental work (to be discussed later in the section on experimental background) consisted of setting up a small energy gap gradient by straining a germanium crystal, and then measuring the PEM voltage as a function of strain. There is no discussion of what material parameter values are desirable for efficient device operation. The main purpose of the paper seems to be to establish the fact that a gap gradient will contribute to the PEM effect.

This completes the summary and comparison of existing analyses of graded-gap devices; the next few sections are devoted to a more detailed consideration of a simplified version of the analysis in M.S.

1.2 Analysis of a Graded-Gap Device: General

The theoretical part of the author's thesis[6] derived an analysis applicable to the problem of the graded-gap device. The graded region was treated using three basic assumptions:

(1) That the effective mass approach could be used and that the effect of a band-edge gradient was equivalent to that of an electric field acting on the carriers in the band under consideration.

(2) That Boltzmann transport theory could be used to derive the equations of motion of carriers in inhomogeneous regions moving under the influence of forces such as discussed above.

*In M.S., the equations for arbitrary surface recombination velocities were set up and the solutions were sketched out, but not carried to completion.

(3) That the electrostatic potential distribution could be found by assuming quasi-neutrality throughout the graded region.

The limitations on the validity of these assumptions are examined in Appendix A of this paper (p. 39)

As shown in Appendix A, the main result of the effective mass treatment is that the current carriers can be treated as free particles with an effective mass m^* appropriate to the energy band under consideration, and that the force acting on them [in the absence of a magnetic field] is given by

$$F_e = -e\left[-\frac{d\phi}{dx} + \frac{1}{e}\frac{dE_c}{dx} - \frac{\hbar^2 k^2}{2m_e}\frac{1}{m_e}\frac{dm_e}{dx}\right]$$

[for electrons] where ϕ is the electrostatic potential and $\frac{dE_c}{dx}$ is the conduction band-edge gradient.* For holes in the valence band, the result is

$$F_h = e\left[-\frac{d\phi}{dx} + \frac{1}{e}\frac{dE_v}{dx} + \left[\frac{\hbar^2 k^2}{2m_h}\right]\frac{1}{m_h}\frac{dm_h}{dx}\right].$$

These are then the force terms to be inserted into the Boltzmann equation for the distribution function f,

$$f = f_o - \tau\hbar^{-1} F\cdot\nabla_k f - \tau v\cdot\nabla_r f \qquad (1.2)$$

The heart of the analysis which follows is contained in the author's M.S. thesis,[6] and the reader is referred to that paper for details. However, the organization of the analysis presented here is different and (hopefully) clearer, and the analysis itself is expanded to include further work by the author, both on the PEM graded gap device analyzed in M.S. and on graded-gap devices operating without a magnetic field. Comparisons with the work of other authors will be made where possible.

The author's M.S. thesis treated the transport of carriers in a section of inhomogeneous semiconductor by the standard Boltzmann equation approach

*The conduction band lower edge (Fig. 1) is also called the "electron affinity;" it is important to note that it is a property of the material only, and does not depend on such things as the doping or excess carrier density. Thus $E_c(x)$ is fixed once the variation in composition with distance x is fixed.

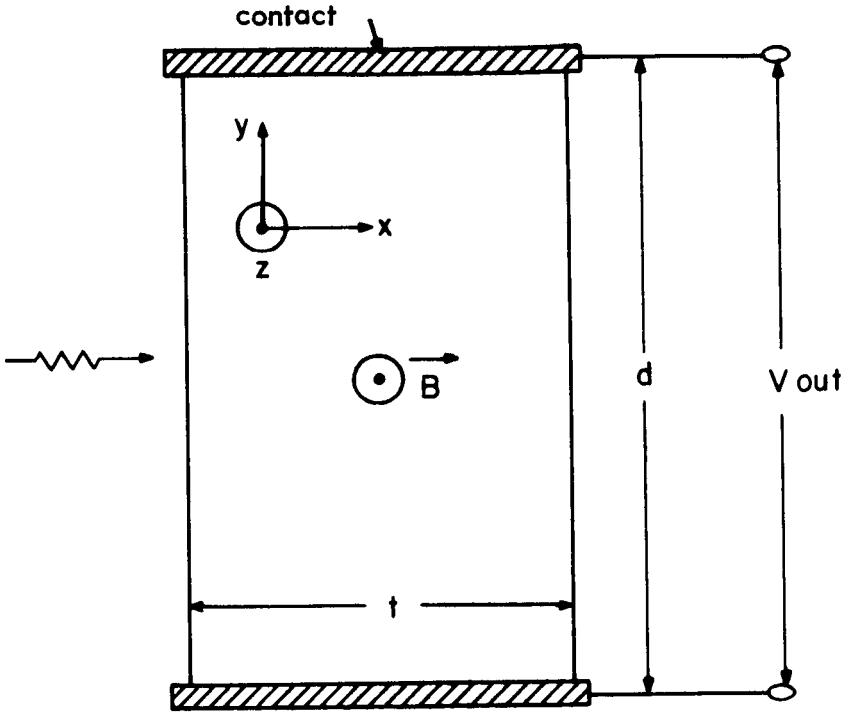

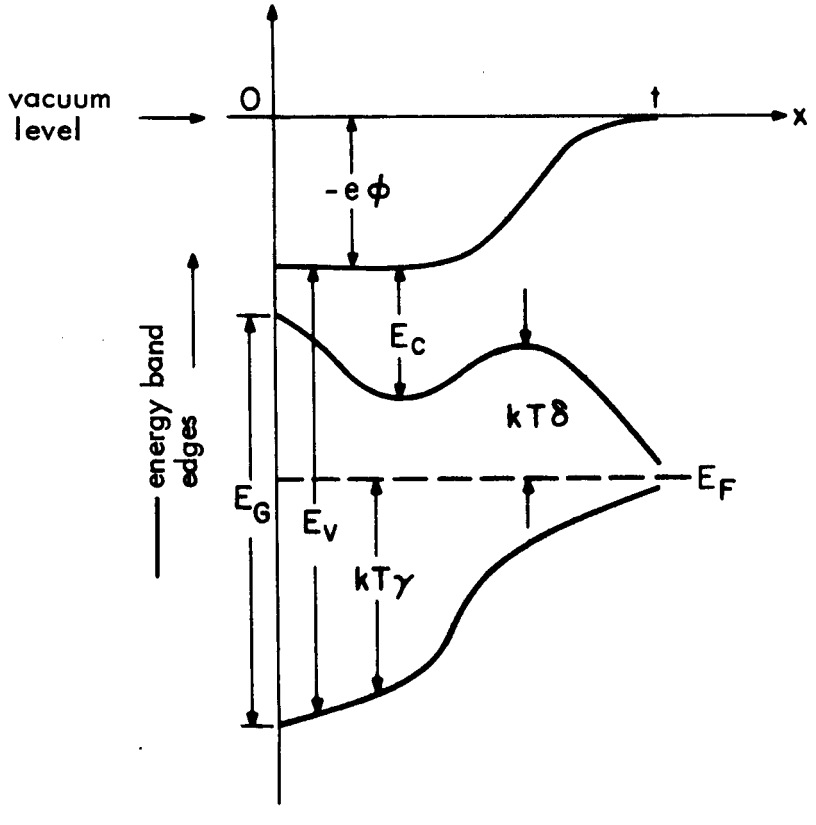

Fig. 1.1 Configuration and energy levels in PEM Graded-gap device. (Behavior of ϕ selected arbitrarily for illustration purposes)

described by Smith.[17] Only the handling of the force term was slightly different from that described in the last section. Instead of taking the force expression resulting from the effective mass treatment and inserting it directly into the Boltzmann equation, the author took the following attitude: Kromer has shown that such things as quasi-electric fields do exist; insert them into the equations of motion as unknowns and see what form they must have from equilibrium considerations alone, without going through any quantum mechanics. This approach is not quite as straightforward or clear as the one used in this paper, but it is satisfying in that it yields the same values for the "quasi-electric fields" as does the quantum-mechanical approach.

Using the force terms derived in Appendix A, the Boltzmann equation in the presence of a magnetic field B becomes

$$f = f_o + \tau/\hbar\ e\left(-\frac{d\phi}{dx} + \frac{1}{e}\frac{dE_c}{dx} - \left[\frac{\hbar^2 k^2}{2m_e}\right]\frac{1}{m_e}\frac{dm_e}{dx} + vxB\right)\cdot\nabla_k f - \tau v\cdot\nabla_r f \qquad (1.2a)$$

for conduction band electrons and

$$f = f_o - \tau/h\ e\ \left(-\frac{d\phi}{dx} + \frac{1}{e}\frac{dE_v}{dx} + \left[\frac{\hbar^2 k^2}{2m_h}\right]\frac{1}{m_h}\frac{dm_h}{dx} + vxB\right)\cdot\nabla_k f - \tau v\cdot\nabla_r f \qquad (1.2b)$$

for valence band holes. Figure 1 should be consulted for the references on the various energy levels. The steps involved in solving the Boltzmann equation are identical to those outlined in the author's thesis, and the resulting equations of motion, to first order in magnetic field, are

$$J_{xn} = n\mu_n\left(\frac{dE_c}{dx} - e\frac{\partial\phi}{\partial x} - kT\frac{\partial\delta}{\partial x} - \frac{5}{2}\frac{kT}{m_e}\frac{dm_e}{dx}\right) + B\mu_n J_{yn} \qquad (1.3a)$$

$$J_{yn} = -en\mu_n\frac{\partial\phi}{\partial y} + B\mu_n J_{xn}$$

for electrons, and

$$J_{xp} = p\mu_p \left(\frac{dE_v}{dx} - e\frac{\partial\phi}{\partial x} + kT\frac{\partial\gamma}{\partial x} + \frac{5}{2}\frac{kT}{m_h}\frac{dm_h}{dx} \right) + B\mu_p J_{yp}$$

$$J_{yp} = -e\, p\mu_p \frac{\partial\phi}{\partial y} - B\mu_p J_{xp} \qquad (1.3b)$$

for holes.* The quantities δ and γ are defined in Figure 1. The assumptions made up to this point are

1) No temperature gradients
2) Non-degenerate material
3) Uniform B-field in the z-direction
4) Parabolic, spherical bands, e.g., $E_c = \frac{\hbar^2}{2m^*}(k_x^2 + k_y^2 + k_z^2)$
5) Variation in the x-direction only
6) $\tau_n^2 = \tau_n^2$, i.e., Hall mobility equals conductivity mobility
7) $(B\mu)^2 << 1$

Now since $n = N_c\, e^{-\delta}$

$$-n\frac{d\delta}{dx} = \frac{dn}{dx} - \frac{n}{N_c}\frac{dN_c}{dx}$$

and equations (3) may be re-written

$$\left.\begin{aligned} J_{xn} &= n\mu_n \left(\frac{dE_c}{dx} - e\frac{\partial\phi}{\partial x} - \frac{kT}{N_c}\frac{dN_c}{dx} - \frac{5}{2}\frac{kT}{m_e}\frac{dm_e}{dx}\right) + kT\,\mu_n\frac{dn}{dx} - B\mu_n J_{yn} \\ J_{xp} &= p\mu_p \left(\frac{dE_v}{dx} - e\frac{\partial\phi}{\partial x} + \frac{kT}{N_v}\frac{dN_v}{dx} + \frac{5}{2}\frac{kT}{m_h}\frac{dm_h}{dx}\right) - kT\,\mu_p\frac{dp}{dx} + B\mu_p J_{yp} \end{aligned}\right\} \qquad (1.4)$$

However,

$$N_c = \text{const} \times m_e^{3/2}$$

$$N_v = \text{const} \times m_h^{3/2}$$

and if we assume, as discussed in Apendix A, that the effective masses are

*The quantity $(dE_c/dx - e\,\partial\phi/\partial x - kT\,\partial\delta/\partial x)$ is exactly equal to the pseudo-electrochemical potential gradient defined by Emtage. Thus it is seen that for B = 0, the Boltzmann equation does indeed bear out the validity of the Quasi Fermi level approach used by Emtage, since then the present equations (3) become identical with his equations (4). [Emtage assumed uniform effective masses.]

proportional to the energy gap, then $\frac{1}{N_c}\frac{dN_c}{dx} = \frac{1}{N_v}\frac{dN_v}{dx} = \frac{3}{2}\frac{1}{E_G}\frac{dE_G}{dx}$. Thus equations (4) may be re-written

$$\left.\begin{aligned} J_{xn} &= n\mu_n \left(\frac{dE_c}{dx} - e\frac{\partial\phi}{\partial x} - 4\frac{kT}{E_G}\frac{dE_G}{dx} \right) + kT\,\mu_n \frac{dn}{dx} - B\mu_n J_{yn} \\ J_{xp} &= p\mu_p \left(\frac{dE_v}{dx} - e\frac{\partial\phi}{\partial x} + 4\frac{kT}{E_G}\frac{dE_G}{dx} \right) - kT\,\mu_p \frac{dp}{dx} + B\mu_p J_{yp} \end{aligned}\right\} \qquad (1.4a)$$

In equilibrium, $n = n_o$, $J_{yn} = J_{yp} = J_{xn} = J_{xp} = 0$; thus

$$n_o\,\mu_n \left(\frac{dE_c}{dx} - 4\frac{kT}{E_G}\frac{dE_G}{dx} - e\frac{d\phi_o}{dx} \right) + kT\,\mu_n \frac{dn_o}{dx} = 0 \qquad (1.5)$$

In the presence of excess carriers $\Delta n = \Delta p$,

$$\begin{aligned} J_{xn} &= \Delta n\,\mu_n \left(\frac{dE_c}{dx} - e\frac{\partial\phi_o}{\partial x} - 4\frac{kT}{E_G}\frac{dE_G}{dx} \right) + kT\,\mu_n \frac{d\Delta n}{dx} \\ &\quad - e(n_o + \Delta n)\mu_n\, \partial/\partial x\,(\phi-\phi_o) + B\mu_n J_{yn} \\ &\quad + n_o\,\mu_n \left(\frac{dE_c}{dx} - e\frac{\partial\phi_o}{\partial x} - 4\frac{kT}{E_G}\frac{dE_G}{dx} \right) + kT\,\mu_n \frac{dn_o}{dx} \end{aligned} \qquad (1.6)$$

But from equation (5), the last four terms of equation (6) add up to zero, so that the currents may be re-written*

$$\left.\begin{aligned} J_{xn} &= e\,\Delta n\mu_n \mathcal{E}^n_{xo} - e\,n\mu_n\, \partial/\partial x\,(\phi-\phi_o) + e\,D_n \frac{d\Delta n}{dx} - B\mu_n J_{yn} \\ J_{xp} &= e\,\Delta n\mu_p \mathcal{E}^p_{xo} - e\,p\mu_p\, \partial/\partial x\,(\phi-\phi_o) - e\,D_p \frac{d\Delta n}{dx} + B\mu_p J_{yp} \end{aligned}\right\} \qquad (1.7)$$

where we have defined

*Note that the second terms in equation 7 is the standard drift term, the third is the standard diffusion-of-excess-carriers term, and the fourth the standard Hall effect term. The first term corresponds to the band-edge gradients.

$$\left.\begin{aligned}
\mathcal{E}^{n}_{xo} &= \frac{1}{e}\left(\frac{dE_c}{dx} - e\frac{d\phi_o}{dx} - \frac{kT}{N_c}\frac{dN_c}{dx} - \frac{5}{2}\frac{kT}{m_e}\frac{dm_e}{dx}\right) \\
&= \frac{kT}{e}\frac{d\phi_o}{dx} - \frac{4kT}{eE_G}\frac{dE_G}{dx} \\
\mathcal{E}^{p}_{xo} &= \frac{1}{e}\left(\frac{dE_v}{dx} - e\frac{d\phi_o}{dx} + \frac{kT}{N_v}\frac{dN_v}{dx} + \frac{5}{2}\frac{kT}{m_h}\frac{dm_h}{dx}\right) \\
&= -\frac{kT}{e}\frac{d\phi_o}{dx} + 4\frac{kT}{eE_G}\frac{dE_G}{dx}
\end{aligned}\right\} \qquad (1.8)$$

Note that $\mathcal{E}^{n}_{xo}$ and $\mathcal{E}^{p}_{xo}$ are independent of the level of injection. In order to find their individual values we must know ϕ_o, which involves solving Poisson's equation. However, this is not necessary at this stage of analysis, and will be done later.

The two other quantities involved in this analysis are the photo potential $(\phi-\phi_o)$ and the excess carrier distribution Δn. It will be shown that $(\phi-\phi_o)$ is found from $\nabla\cdot J = 0$, and that Δn is determined by the continuity equation

$$\nabla\cdot J_n = e\frac{\Delta n}{\tau_1} - eg \qquad (1.9)$$

where $g = g(x)$ is the external rate of hole-electron pair generation due to photons and τ_1 is the lifetime of excess carriers. (One should not lose sight of the fact, however, that in general we have five equations for the five unknowns Δn, Δp, J_{xn}, J_{xp}, and ϕ, namely, the two equations 7, two continuity equations like equation 9, and Poisson's equation, and that in general these five equations must be solved simultaneously.)

The condition that $\nabla\cdot J = 0$ reduces to

$$J_x = \text{const}$$

therefore, since $J_{xn} + J_{xp} = J_x$,

$$\frac{\partial}{\partial x}(\phi-\phi_o) = \frac{-J_x}{\sigma(x)} + \left[\frac{\Theta_n\mu_n n + \Theta_p\mu_p p}{\mu_n n + \mu_p p}\right] \frac{\partial}{\partial y}(\phi-\phi_o)$$
$$+ \left[\frac{\mu_n \mathcal{E}^n_{ox} + \mu_p \mathcal{E}^p_{ox}}{\mu_n n + \mu_p p}\right] \Delta n + \left[\frac{D_n - D_p}{\mu_n n + \mu_p p}\right] \frac{d\Delta n}{dx} \qquad (1.10)$$

where we have defined

$$\sigma(x) = e(n\mu_n + p\mu_p)$$
$$\Theta_n = B\mu_n$$
$$\Theta_p = B\mu_p$$
$$D = \frac{kT}{e}\mu$$

Now J_{nx} becomes

$$J_{nx} = \frac{n\mu_n}{n\mu_n + p\mu_p} J_x + e\frac{\mu_n\mu_p}{\mu_n\frac{n}{p} + \mu_p}\left[(\Theta_n-\Theta_p)n\frac{\partial}{\partial y}(\phi-\phi_o) + \Delta n(\mathcal{E}^n_{ox} - \frac{n}{p}\mathcal{E}^p_{ox}) + \frac{kT}{e}(1+\frac{n}{p})\frac{d\Delta n}{dx}\right] \qquad (1.11)$$

The inclusion of the term J_x makes these expressions a little more general than those in M.S.

M.S. treated only the PEM case, for which $J_x = 0$; therefore we proceed to find the terminal characteristics in the y direction, leaving the discussion of a device utilizing the x-directed voltage until later.

1.3 Analysis of a Graded-Gap PEM Device

We define

$$I_y = \int_o^t J_y\, dx,$$

and since $\nabla\cdot\vec{\mathcal{E}} = \rho/\epsilon = 0$, and the material properties are not assumed to vary in the y-direction, we can also define

$$\frac{\partial}{\partial y}(\phi-\phi_o) = \frac{V_y}{d}.$$

Recognizing that

$$J_y = J_{ny} + J_{py} = e(n\mu_n + p\mu_p)\frac{\partial}{\partial y}(\phi-\phi_o) + \Theta_n J_{xn} - \Theta_p J_{xp}$$

and realizing that in this case $J_{xn} = -J_{xp}$, it is easy to show that*

$$I_y = -\int_o^t \sigma \frac{V_y}{d}\,dx + \int_o^t (\Theta_p + \Theta_n)J_{xn}\Big|_{V_y=0}\,dx$$

(Equation 11) shows that the expression for J_{nx} also contains V_y, but this term enters into the expression for J_y multiplied by a second-order term in B, and is therefore neglected.) Then

$$I_y = -\frac{V_y}{R_{int}} + I_{ySC} \tag{1.12}$$

where

$$\frac{1}{R_{int}} = \frac{1}{d}\int_o^t \sigma(x)\,dx \tag{1.13}$$

and the short circuit current I_{ySC}

$$I_{ySC} = \int_o^t (\Theta_p + \Theta_n)J_{nx}\Big|_{V_y=0}\,dx \tag{1.14}$$

Thus it is seen that the terminal characteristics of the device are those of a Norton equivalent circuit, that is, an internal resistance in parallel with an ideal current source. The current source depends on magnetic field and on J_{nx}. All necessary information may thus be obtained by treating the short circuit case only. The remaining problem is thus the evaluation of J_{nx} under short circuit conditions ($\partial/\partial y\,(\phi-\phi_o) = 0$.)

---

*M.S. thesis[6] p. 35

In the short circuit condition, J_{nx} can be written

$$J_{nx} = e\mu^* \mathcal{E}^* \Delta n + e D^* \frac{d\Delta n}{dx} \tag{1.15}$$

where we have defined

$$\mu^* = \frac{\mu_n \mu_p}{\mu_n \frac{n}{p} + \mu_p}$$

$$\mathcal{E}^* = \mathcal{E}^n_{ox} - \frac{n}{p} \mathcal{E}^p_{ox}$$

$$D^* = \frac{kT}{e} (1 + \frac{n}{p}) * = \frac{D_n D_p}{D_n \frac{n}{p} + D_p} (1 + \frac{n}{p})$$

Thus the problem becomes that of finding $\mathcal{E}^*$ and Δn for the cases of interest.

1.3.1 Finding the effective electric field $\mathcal{E}^*$:

Using the values in equation 8, $\mathcal{E}^*$ becomes

$$\mathcal{E}^* = \frac{kT}{e} \left(\frac{d\delta_o}{dx} + \frac{n}{p} \frac{d\gamma_o}{dx} \right) - 4 \frac{kT}{eE_G} \frac{dE_G}{dx} (1 + \frac{n}{p}) \tag{1.16}$$

It is tempting at this point to go ahead, make the approximations of intrinsic or strongly doped material ($\frac{n}{p} = 1$ or $\frac{n}{p} << 1$ or $\frac{n}{p} >> 1$), and come out with some compact results. However, a little reflection will show that we are assuming that the carrier concentrations and thus the values of δ_o and γ_o are determined simply by the doping. This is true only if Quasi-Neutrality can be shown to hold. The conditions under which quasi-neutrality holds for the type of non-uniform semiconductors under consideration here are discussed in some detail in Appendix B.

The results of Appendix B show that as long as N_c, N_v, E_G/kT vary slowly in a Debye length, then for intrinsic or uniformly strongly doped graded-gap regions, the electrostatic potential can be found from

$$\sin h \, (\Phi - \Phi_i) = \frac{\tilde{N}}{2} \tag{1.17}$$

where $\Phi = \frac{e\phi}{kT}$, $\Phi_i = \frac{1}{kT}(E_c - E_G/2 - E_F - \frac{1}{2} kT \ln N_c/N_v)$ and $\bar{N} = \frac{N_d - N_a}{n_i}$ where N_d = # of donors and N_a = # of acceptors and complete ionization of impurities is assumed.

Once Φ is determined, δ and γ are also determined, since

$$\delta = \frac{E_c - E_f}{kT} - \Phi \tag{1.18}$$

and

$$\delta + \gamma = \frac{E_G}{kT} .$$

Now let us evaluate $\mathcal{E}^*$ for the cases of interest. For strong p-type material such that $|\bar{N}| >> 1$ everywhere, equation 17 yields

$$\Phi_o = \frac{E_v - E_f}{kT} - \ln \frac{|N_d - N_a|}{N_v} \tag{1.19}$$

and

$$\left.\begin{aligned} \delta_o &= \frac{E_G}{kT} + \ln \frac{|N_d - N_a|}{N_v} \\ \gamma_o &= - \ln \frac{|N_d - N_a|}{N_v} \end{aligned}\right\} \tag{1.20}$$

therefore

$$\mathcal{E}^n_{ox} = \frac{1}{e}\frac{dE_G}{dx} - \frac{kT}{e}\left(\frac{1}{N_c}\frac{dN_c}{dx} + \frac{1}{N_v}\frac{dN_v}{dx}\right) - \frac{5}{2}\frac{kT}{em_e}\frac{dm_e}{dx}$$

$$\mathcal{E}^p_{ox} = + \frac{5}{2}\frac{kT}{em_h}\frac{dm_h}{dx}$$

and

$$\mathcal{E}^* = \frac{1}{e}\frac{dE_G}{dx}\left(1 - \frac{11kT}{2E_G}\right) \tag{1.21}$$

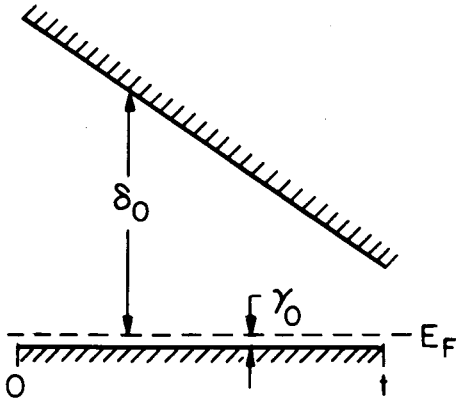

Fig. 1.2 P-type device

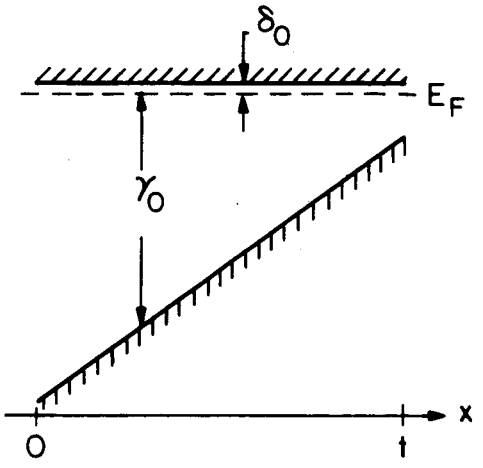

Fig. 1.3 N-type device

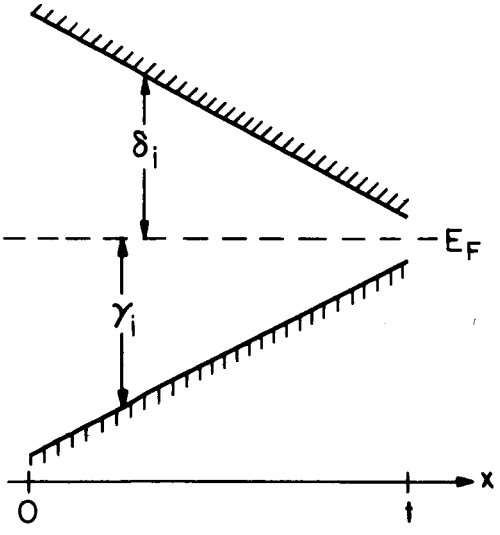

Fig. 1.4 Intrinsic device

where the effective masses have again been assumed proportional to the energy gap.* Since regions where $E_G < 6$ kT are already being neglected through the assumption of non-degeneracy, $\mathcal{E}^*$ may be taken as constant and equal to the gap gradient. If the variations in N_v are ignored, then equation 17 can be interpreted as saying that if the hole affinity does not vary with position in this case, then no electrostatic field will be set up in equilibrium.

For a strong n-type material such that $\bar{N} >> 1$ everywhere, equation 15 yields

$$\phi_o = \frac{E_c - E_f}{kT} + \ln \frac{N_d - N_a}{N_c}$$

$$\delta_o = -\ln \frac{N_d - N_a}{N_c}$$

$$\gamma_o = \frac{E_G}{kT} + \ln \frac{N_d - N_a}{N_c}$$

therefore

$$\mathcal{E}^n_{ox} = -\frac{5}{2} \frac{kT}{em_e} \frac{dm_e}{dx}$$

$$\mathcal{E}^p_{ox} = -\frac{1}{e} \frac{dE_G}{dx} + \frac{kT}{e} \left(\frac{1}{N_c} \frac{dN_c}{dx} + \frac{1}{N_v} \frac{dN_v}{dx}\right) + \frac{5}{2} \frac{kT}{em_h} \frac{dm_h}{dx}$$

and

$$\mathcal{E}^* = \frac{n}{p} \frac{1}{e} \frac{dE_G}{dx} \left(1 - \frac{11kT}{2E_G}\right) ; \qquad (1.22)$$

this result seems less strange where it is realized that for this strong n-type case, $\mu^* = p/n\ \mu_p$ thus we may take

$$\mu^* \mathcal{E}^* = \mu_p \frac{1}{e} \frac{dE_G}{dx}$$

---

*See Appendix A.

whereas for the p-type case,

$$\mu^* \mathcal{E}^* = \mu_n \frac{1}{e} \frac{dE_G}{dx}$$

For intrinsic material ($\bar{N} = 0$),

$$\Phi_i = \frac{1}{kT} (E_c - E_f - E_G/2) - \frac{1}{2} \ln N_c/N_v \qquad (1.24)$$

$$\delta_i = \frac{1}{2} \frac{E_G}{kT} + \frac{1}{2} \ln \frac{N_c}{N_v}$$

$$\gamma_i = \frac{1}{2} \frac{E_G}{kT} - \frac{1}{2} \ln \frac{N_c}{N_v}$$

$$\mathcal{E}^n_{ox} = \frac{1}{2e} \frac{dE_G}{dx} - \frac{kT}{2} \left[\frac{1}{N_c} \frac{dN_c}{dx} + \frac{1}{N_v} \frac{dN_v}{dx} \right] - \frac{5}{2} \frac{kT}{em_e} \frac{dm_e}{dx}$$

$$\mathcal{E}^p_{ox} = -\frac{1}{2e} \frac{dE_G}{dx} + \frac{kT}{2} \left[\frac{1}{N_c} \frac{dN_c}{dx} + \frac{1}{N_v} \frac{dN_v}{dx} \right] + \frac{5}{2} \frac{kT}{em_h} \frac{dm_h}{dx}$$

$$\mathcal{E}^* = \frac{1}{e} \frac{dE_G}{dx} \left(1 - \frac{3kT}{E_G}\right)$$

and

$$\mu^* = \frac{\mu_n \mu_p}{\mu_n + \mu_p}$$

$$\mu^* \approx \mu_p$$

if $\mu_n >> \mu_p$, as is common. Thus the product $\mu^* \mathcal{E}^*$ is $\mu_p \frac{1}{e} \frac{dE_G}{dx}$ for the intrinsic and n-type cases and $\mu_n \frac{1}{e} dE_G/dx$ for the p-type case.

(Equation (24) may be interpreted as saying that no equilibrium electrostatic field is set up if the electron affinity and hole affinity have the same magnitude.)

1.3.2 Finding the excess carrier distribution: constant mobilities

The next problem is that of finding $\Delta n(x)$. This is somewhat more involved. When equation (15) for J_{nx} is inserted into the continuity equation (9), and it is assumed that $J_x = 0$, the equation for Δn becomes

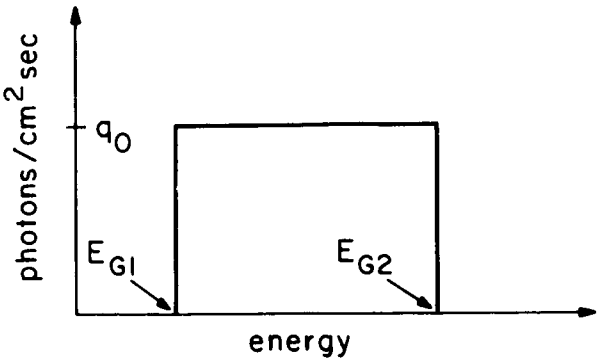

Fig. 1.5 Illumination spectrum

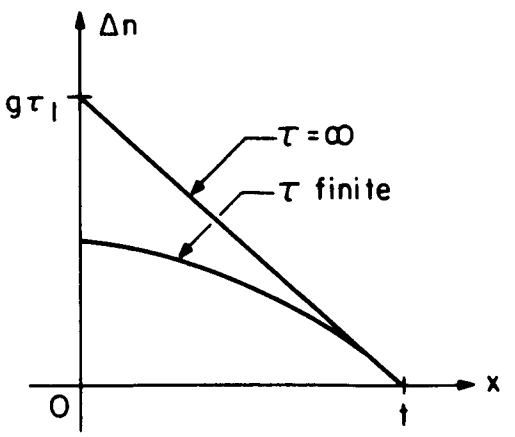

Fig. 1.6 Excess carrier distribution

$$\frac{d^2\Delta n}{dx^2} + \frac{\mu^* \mathcal{E}^*}{D^*} \frac{d\Delta n}{dx} - \frac{\Delta n}{L^2} = - g/D^* \qquad (1.25)$$

where $L = \sqrt{D^* \tau_1}$ is the diffusion length. It can be seen that if $\mathcal{E}^*$ were zero and the volume generation term were absent, this would be the equation for the excess carrier distribution in a normal, homogeneous PEM cell.

Since μ^* (and thus D^* and L) are in general functions of position, this is in general a non-constant coefficient differential equation. Simplifying assumptions must be made in order to obtain closed-form solutions.

Our first assumption will be that the mobility is constant. This is a very poor assumption for most material systems; in CdTe-HgTe, for instance, the electron mobility can vary from 600 cm^2/v-sec in CdTe to 20,000 cm^2/v-sec in a HgTe-rich alloy. However, it results in a workable model which shows the effects of the gap gradient. Another model will be derived later which does include mobility variations.

The illumination spectrum assumed is shown in Figure 5. It is assumed that the absorption is so strong that all the photons of a given energy are absorbed at the point which has the appropriate energy gap within a distance which is small compared to the width of the graded region.* This assumption is taken to mean that the generation rate can be taken as constant throughout the entire graded region and equal to q_o/t cm^{-3} sec^{-1}.

$\mathcal{E}^*$ is also taken to be constant, since we are considering $E_G >> kT$ everywhere.

The solution using these assumptions is outlined in the author's M.S. thesis starting on page 40. The solution takes the form

$$\Delta n = g\tau_1 + e^{\frac{\mu^* \mathcal{E}^*}{D^*}} [C_1 e^{rx} + C_2 e^{-rx}] \qquad (1.26)$$

where**

$$r = \frac{1}{2} \sqrt{\left(\frac{\mu^* \mathcal{E}^*}{D^*}\right)^2 + 4/L^2}$$

*In CdTe, this condition should be easily achieved.

**Again, it can be seen that if $\mathcal{E}^* = 0$, $r = 1/L$

and C_1 and C_2 depend in a rather complicated way on the boundary conditions at $x = 0$ and $x = t$.

An additional assumption makes the solution easier and also throws more light on the processes involved. Although never explicitly stated, one of the reasons for interest in this device is the possibility that the excess carriers move primarily by drift rather than diffusion. This intuitive feeling will be checked by neglecting the diffusion current compared to the drift current, and then checking the assumption for self-consistency.

If the diffusion term in equation 15 for J_{xn} is neglected, the equation for Δn becomes

$$\frac{d\Delta n}{dx} - \frac{\Delta n}{\mathcal{E}^*\mu^*\tau_1} = - g/\mu^*\mathcal{E}^* . \qquad (1.27)$$

It will be assumed that the illuminated surface is very carefully prepared, so that the surface recombination velocity s_1 there is zero. At the back surface, the opposite approximation will be made, namely $s_2 = \infty$. This means that all excess carriers which reach this surface recombine immediately, and that the excess carrier density at the back surface is zero.*

In the two special cases of intrinsic material and uniformly doped material, μ^* will be constant if the individual mobilities μ_n and μ_p are constant.

Under these conditions the solution for Δn is

$$\Delta n = g\tau_1 \left(1 - e^{\frac{x - t}{\tau_1 \mu^* \mathcal{E}^*}} \right) \qquad (1.28)$$

We now wish to check our assumption neglecting the diffusion current. The diffusion current due to this excess density is $e D^* \frac{d\Delta n}{dx}$. Thus the ratio of drift current to diffusion current is found to be

$$\frac{J_{drift}}{J_{diff}} = \frac{\Delta E_G}{kT} \left(\frac{\mathcal{E}^*\mu^*\tau_1}{t}\right) \left(e^{\frac{t - x}{\mathcal{E}^*\mu^*\tau_1}} - 1\right) \qquad (1.29)$$

*It is shown in the section on efficiency that a much more desirable condition would be $s_1 = 0$ and s_2 also $= 0$. However, these values were chosen in M.S. in the spirit of a "worst-case" analysis.

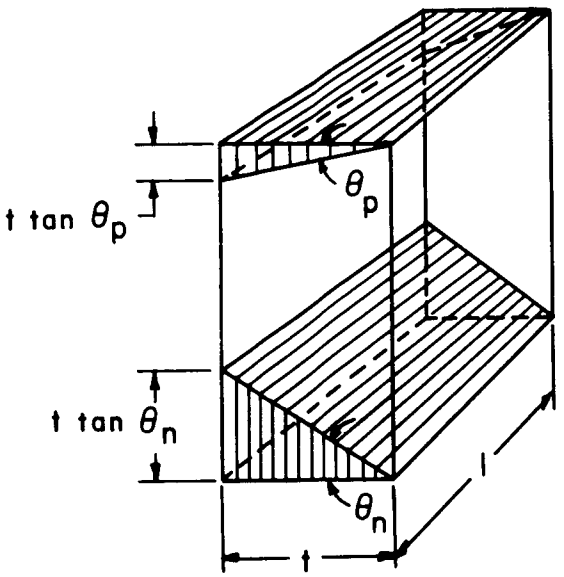

Fig. 1.7 Maximum current

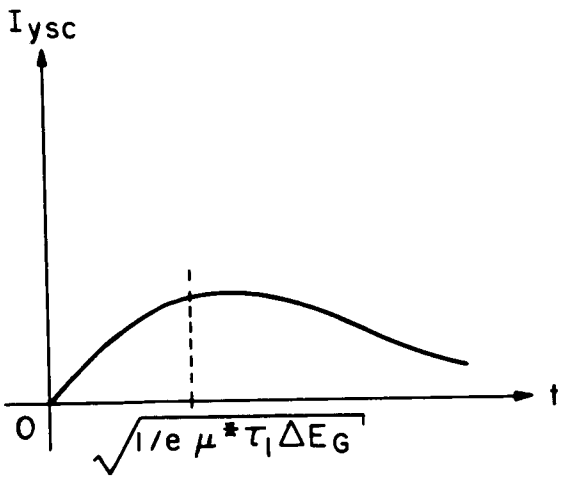

Fig. 1.8 Shortcircuit current as a function of sample width

A "worst-case" analysis for CdTe using values of $\mu^* = 100\ cm^2/v\text{-}sec$, $\tau_1 = 10^{-8}$ sec, and $t = 10^{-3}$ cm shows that at $x = 0$, the ratio in equation 29 has a value of 57, and that the ratio does not reach unity until $x = .98\ t$. Thus for this material system at least, it is valid to neglect the diffusion current. In general, the approximation gets better as the quantity

$$\frac{\mathcal{E}^*\mu^*\tau_1}{t} = \frac{\Delta E_G \mu^* \tau_1}{et^2}$$

increases.

Now that neglect of the diffusion current has been justified, the short-circuit current per unit width can be computed. Since

$$I_{y\ SC} = \int_o^t J_{y\ SC}\, dx = (\Theta_p + \Theta_n) \int_o^t J_{nx}\, dx$$

there results for the PEM case

$$I_{y\ SC} = eg(\Theta_p + \Theta_n)t^2 \left[\frac{z - 1 + e^{-z}}{z^2} \right] \qquad (1.30)$$

where $z = \dfrac{e\,t^2}{\mu^*\tau_1 \Delta E_G}$.

In the limit, as $z \to 0$ while t remains constant,

$$I_{y\ SC} = \frac{1}{2}\, eg\, t^2(\Theta_p + \Theta_n).$$

This represents the maximum current output for a given thickness t. The interpretation is simple when one refers to Figure 7. It will be recalled that $\tan \Theta_n = \Theta_n$, $\tan \Theta_p = \Theta_p$ by assumption. Thus the maximum current occurs when all the carriers generated in the shaded triangular volumes of Figure 7 reach the contacts.*

*It is interesting to calculate how near to the condition z=0 an actual case might be. Using the same "worst-case" analysis for CdTe as that used after equation 29, i.e., $\tau_1 = 10^{-8}$sec, $\mu^* = 100\ cm^2/v\text{-}sec$, $t = 10^{-3}$cm, $\Delta E_g = 1.5$ ev, z will be 1.5, and therefore

$$I_{y\ SC} = .34\ eg(\Theta_p + \Theta_n)t^2 = .68\ I_{y\ SC}\Big|_{z=0}$$

Thus for a 10-micron wide intrinsic graded-gap region, the material properties assumed above result in a short-circuit current whose magnitude is about 2/3 of the maximum available.

Since the quantity z seems to be some sort of figure of merit, it may be informative to see what happens to Δn as $z \to 0$. Using equation 28 it can easily be shown that if z goes to zero because τ_1 goes to infinity the result is

$$\Delta n = \frac{g(t-x)}{\mu^* \mathcal{E}^*}$$

whereas if z goes to zero because $\mu^* \to \infty$ or $\mathcal{E}^* \to \infty$, then Δn vanishes. This corresponds to the carriers being "whisked away" as fast as they are generated.

Another quantity of interest is the value of z for maximum power transfer. This time the values of τ_1, μ^*, and ΔE_G will be considered as given and the optimum value of t will be found.

The maximum transferable power will be proportional to $(I_{y\ SC})^2 R_{int}$. Now,

$$I_{y\ SC} = \text{const } q_o \frac{t^2 - K(1-e^{-t^2/K}}{t^3} \tag{1.31}$$

where $K = 1/e\ \mu^* \tau_1\ \Delta E_G$. It can be shown that $R_{int} = \text{const.}\ 1/t$. Therefore the maximum power will vary as

$$p_m = \text{const.} \frac{[t^2 - K(1 - e^{-t^2/K})]^2}{t^7} \tag{1.32}$$

Setting $\frac{dp_m}{dt} = 0$ results in a transcendental equation

$$e^{-z} = \frac{7 - 3z}{7 + 4z}$$

which can be solved graphically or numerically to yield the value of z corresponding to maximum power transfer. This value is about 0.9. The thickness corresponding to this value is $t = \sqrt{.9\ K}$. For the CdTe HgTe system this turns out to be about 12 microns, which is quite encouraging in view of the fact that we are thinking of 10-micron wide transition regions.

The main result of this section is the appearance of the quantity $z = \frac{e\ t^2}{\mu^* \tau_1\ \Delta E_G}$, which is a critical parameter of the device. It will be shown later that it is indeed a figure of merit which is uniquely related to the efficiency of the device.

The preceeding section has been considering μ^* to be constant. However, as pointed out earlier, this is a very poor assumption for most material systems. Therefore the next section treats the problem of a variable mobility in the graded-gap region. It will be shown that this situation may be reduced to a case with a constant "effective" mobility.

1.3.3 Excess carrier distribution, variable mobility

It is assumed that the diffusion current is still negligible compared to the drift current, which means that $J_{nx} = e\mu^*\mathcal{E}^*\Delta n$. Thus the continuity equation becomes

$$\frac{d\Delta n}{dx} + \Delta n \frac{1}{\mu^*}\left[\frac{d\mu^*}{dx} - \frac{1}{\tau_1 \mu^* \mathcal{E}^*}\right] = -g/\mu^*\mathcal{E}^*$$

and its solution is

$$\Delta n(x) = e^{-\int \left[\frac{1}{\mu^*}\frac{d\mu^*}{dx} - \frac{1}{\tau_1\mu^*\mathcal{E}^*}\right]dx} \int -\frac{g}{\mu^*\mathcal{E}^*} e^{\int\left[\frac{1}{\mu^*}\frac{d\mu^*}{dx} - \frac{1}{\tau_1\mu^*\mathcal{E}^*}\right]dx} dx + C\, e^{-\int\left[\frac{1}{\mu^*}\frac{d\mu^*}{dx} - \frac{1}{\tau_1\mu^*\mathcal{E}^*}\right]dx} \qquad (1.34)$$

τ_1, g, and $\mathcal{E}^*$ are again assumed constant.

If a linear behavior of the "ambipolar" mobility μ^* is assumed, i.e.,

$$\mu^* = \mu_o (1 + \alpha\, x/t)$$

then the solution for Δn is

$$\Delta n(x) = (1 + \alpha \frac{x}{t})^{\left[\frac{t}{\tau_1 \mathcal{E}^* \mu_o^* \alpha} - 1\right]} \left\{ C - \frac{gt}{\mu_o^* \mathcal{E}^*} \int (1 + \frac{x}{t})^{-\left[\frac{t}{\tau_1 \mathcal{E}^* \mu_o^* \alpha}\right]} d(\frac{x}{t}) \right\} \qquad (1.35)$$

The integral can be evaluated analytically for integer or half-integer values* of $\frac{t}{\tau_1 \mathcal{E}^* \mu_o^* \alpha}$, i.e., 0, 1/2, 1, 3/2, 2, -----.

---

*For an intrinsic HgTe-CdTe graded-gap region, the quantity $\tau_1 \mathcal{E}^* \mu_o^* \alpha$ will be about 3×10^{-3} cm = 30 microns. For a p-type sample it will be about 3×10^{-1} cm = 3 mm.

The integral will first be evaluated using a "thin sample" approximation namely, $\frac{t}{\tau_1 \mathcal{E}^* \mu_o^* \alpha} \ll 1$. Then

$$\Delta n(x) = \frac{gt}{\mu_o^* \mathcal{E}^*} \quad \frac{t-x}{t+\alpha x} = \frac{g\,(t-x)}{\mu^*(x)\mathcal{E}^*} \tag{1.36}$$

where the condition that $\Delta n = 0$ at $x = t$ has again been applied. This solution is seen to have exactly the same functional form as the solution for the case of constant mobility and infinite lifetime, except that the constant mobility has been replaced by a variable mobility. This is a plausible result, since both the thin sample approximation and the infinite lifetime approximation are equivalent to neglecting the recombination process.

The short-circuit current in the thin sample is

$$I_{y\ SC} = e \int_o^t (\Theta_p + \Theta_n) \mu^* \mathcal{E}^* \Delta n dx.$$

If a p-type sample is assumed, then $\mu^* \approx \mu_n$. Furthermore, Θ_n is generally much larger than Θ_p.* Thus if it is assumed that $\mu_n = \mu_{no}(1 + \alpha_n x/t)$ then

$$I_{y\ SC} = \frac{1}{2} eg\, B\mu_{no} t^2 \int_o^t 2(1 - x/t)(1 + \alpha_n x/t)\frac{dx}{t} . \tag{1.37}$$

The term outside the integral in the above expression is the maximum current available from a graded-gap region with a constant mobility μ_{no} and a width t, while the integral itself may be interpreted as an average value of α_n. For this case

$$\int_o^t 2(1 - x/t)(1 + \alpha_n x/t)\, \frac{dx}{t} = 1 + \frac{\alpha_n}{3} ;$$

thus

$$I_{y\ SC} = \frac{1}{2} eg\, t^2\, B\mu_{no} \left(1 + \frac{\alpha_n}{3} \right) \tag{1.38}$$

or

$$I_{y\ SC} = \frac{1}{2} eg\, t^2\, B\mu_{n\ eff}$$

*This is certainly true in the HgTe-CdTe system, where $\Theta_p/\Theta_n \approx 0.1$ for CdTe and ≈ 0.01 for HgTe.

where $\mu_{n\ eff}$ is approximately one-third of the maximum value of $\mu_n(x)$.

The case where $\frac{t}{\tau_1 \mathcal{E}^* \mu_o^* \alpha} = 1$ may be treated by the same process. Here the result will be

$$\Delta n(x) = \frac{gt}{\mathcal{E}^* \mu_o^* \alpha} \log \left[\frac{1 + \alpha}{1 + \alpha\, x/t} \right] \tag{1.39}$$

and

$$I_{y\ SC} = \frac{1}{2} eg\, t^2\, B\mu_{no} \int_o^t \frac{2}{\alpha_n}\left(1 + \alpha_n \frac{x}{nt}\right)^2 \log\left[\frac{1 + \alpha_n}{1 + \alpha_n\, x/t} \right] \frac{dx}{t} \tag{1.40}$$

and while in this case the integral may require numerical evaluation, it is still clear that it represents a certain average of α_n.

If we assume a graded region width of 10 microns, then for HgTe-CdTe, $\mathcal{E}^* = \frac{1}{e}\ \Delta E_G/t = 1.5 \times 10^3$ v/cm; τ_1 is assumed to be 10^{-8} sec; then for a p-type sample with $\mu_o^* \alpha = 20{,}000$ cm^2/v-sec, $\tau_1\, \mathcal{E}^* \mu_o^* \alpha = 3{,}000$ microns, whereas for an intrinsic structure with $\mu_o^* \alpha = 200$ cm^2/v-sec, $\tau_1 \mathcal{E}^* \mu_o^* \alpha = 30$ microns. Thus the thin-sample approximation $\frac{t}{\tau_1 \mathcal{E}^* \mu_o^* \alpha} \approx 0$ is a very good one for the p-type sample, whereas $\frac{t}{\tau_1 \mathcal{E}^* \mu_o^* \alpha} = 1/2$ might be more appropriate for an intrinsic sample.

Different situations will lead to different average values of α_n, but the main point is that the output current is the same as that of a constant-mobility graded-gap device with $\mu^* = \mu_{o\ eff}$.

A similar argument applies to the intrinsic case where $\mu^*(x) \approx \mu_p(x)$. Thus a graded-gap device with a linearly varying mobility is equivalent, at least as far as output current is concerned, to a graded-gap device with a constant mobility which is some fraction of the maximum value of the actual mobility. It will therefore be assumed that the calculations of the previous section can be applied to a variable-mobility graded-gap device by treating it as a device with a constant effective mobility.

The rest of the theoretical chapter of the author's M.S. thesis was devoted to a comparison of the graded-gap device with a standard PEM cell made out of either one of the individual semiconductors or some intermediate alloy. The conclusion reached was that under any realistic conditions of illumination, the graded-gap device would be more efficient, due primarily

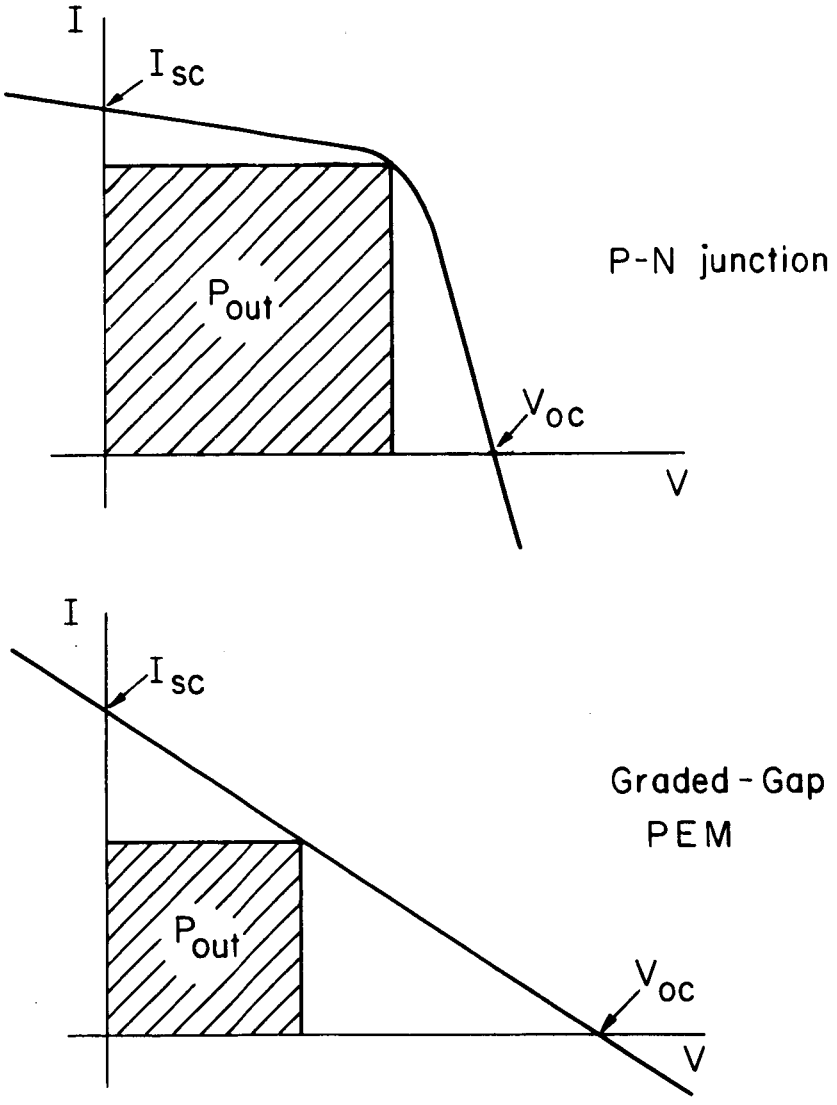

Fig. 1.9 Comparison of I-V characteristics

to the fact that the "drift length" for excess carriers in the graded region is much longer than the diffusion length, the ratio being given by

$$\sqrt{\frac{\Delta E_G}{kT} \quad \frac{\mu_{eff \ \ graded \ gap}}{\mu_{eff \ \ standard \ cell}}} \ .$$

Instead of going into this, it might be more interesting to make some comments of a preliminary nature on the absolute efficiency of a graded-gap PEM device. These will be somewhat speculative and approximate in nature, since the exact analysis for the case of high illumination and high magnetic field has not yet been carried out. However, it should be possible to show at least some of the basic limitations on the efficiency of such a device.

1.4 Efficiency of the Graded-Gap PEM Device

For a given illumination, the output power will be maximum when the product I V is maximum. This in turn depends on the I-V characteristics.

The maximum output power for a photocell is thus usually written

$$P_{max} = f \, V_{oc} \, I_{sc}$$

where f is a "fillfactor which depends on the I-V characteristics. As the sketches in Figure 9 show, the fill factor for a pn junction cell can be greater than 0.8; for the graded-gap PEM cell under consideration, the linear I-V characteristic results in a fill factor of 0.25.

1.4.1 The case s(0) = 0, s(t) = ∞

Recombination will be neglected at first, for simplicity; this is equivalent to making the "thin sample" approximation. This results in

$$I_{y \ SC} = \frac{1}{2} eg \, t^2 \, B\mu_{n \ eff}$$

where g is the uniform generation rate equal to q_o/t, where q_o is the number of photons per cm^2 per sec incident on the sample.

The open-circuit voltage is given by

$$V_{OC} = I_{SC} \, R = \frac{I_{SC} \, d}{\int_o^t \sigma(x) dx} \qquad (1.41)$$

but for a p-type sample with equilibrium concentration p_o and low injection conditions ($\Delta n = \Delta p << p_o$),

$$\int_o^t \sigma(x)dx = e\, p_o \int_o^t \mu_p(x)dx = ept\, \frac{(\mu_{p1} + \mu_{p2})}{2}$$

$$= e\, p_o t\, \mu_{p\ AV}$$

thus

$$V_{OC} = \frac{1}{2}\left[\frac{q_o\, Bd}{p_o}\ \frac{(\mu_n)_{eff}}{(\mu_p)_{AV}}\right] \tag{1.42}$$

Now, the input power is $q_o\, E_{AV}$, where E_{AV} is the average photon energy. For the illumination spectrum shown in Figure 5, $E_{AV} = \frac{E_{G2} + E_{G1}}{2}$. Thus the expression for efficiency is

$$\eta = \frac{\frac{1}{4} V_{OC}\, I_{SC}}{q_o \left(\frac{E_{G1}+E_{G2}}{2}\right)d} = \frac{1}{8} (B\mu_n)^2_{eff}\ \frac{e\, q_o t}{p\, \mu_{pAV}(E_{G1} + E_{G2})}$$

Now, by noting that $\Delta n(x=0) = \frac{gt}{\mu^* \mathcal{E}^*}$ and that thus $q_o = \Delta n(x=0)\mu^* \frac{1}{e} \frac{\Delta E_G}{t}$ the efficiency expression can be rewritten

$$\eta = \frac{1}{8} (B\mu_n)^2_{eff}\ \frac{\Delta n(x=0)}{p}\ \frac{\mu^*(x=0)}{\mu_{p\ AV}}\ \frac{\Delta E_G}{E_{G1} + E_{G2}} \tag{1.43}$$

It is obvious from the form of equation 43 that, up to a point, at least, the efficiency will increase as the magnetic field and the illumination are increased.

An inquiry into the ultimate efficiency of the device thus requires a knowledge of its behavior both at high magnetic fields and at high illumination. This analysis has not been carried out in detail, but what follows should at least give an idea of the limiting factors involved, even though the exact numerical values of the efficiency may be somewhat open to question.

1.4.2 High magnetic fields

In his treatment of conduction in a magnetic field, Smith[17] takes the solution to the Boltzmann equation through one further order of approximation to include B^2 terms. The net result is that in the expressions for the currents which he derived earlier, the term $B\mu$ is replaced by a term $\frac{B\mu}{1 + B^2\mu^2}$. The author feels that, based on the developments in his M.S. thesis, it is entirely reasonable to expect the same thing to happen in this case. This would enter directly into the expression for efficiency (43).

Exactly how it will enter in is another question; since the mobility in general will vary quite strongly in the graded region, $B\mu(x_1)=1$ may imply $B\mu(x_2) >> 1$ elsewhere. However, even if the mobility is constant throughout the graded region, the maximum value of $\frac{B\mu}{1+B^2\mu^2}$ is $\frac{1}{2}$. So for a "best case" analysis, it will be assumed that the magnetic field factor $(B\mu_n)^2_{eff}$ in the efficiency is $\frac{1}{4}$.

1.4.3 High illumination

High illumination will be treated by considering the resulting conductivity modulation, and its effect on the open-circuit voltage. Since $V_{OC} = I_{SC} R$ and

$$\frac{d}{R} = \int_o^t \sigma(x)dx = \int_o^t e\,[p\mu_p(x) + n\mu_n(x)]dx$$

$$= \int_o^t e\,[p_o + \Delta n)\mu_p(x) + (n_o + \Delta n)\mu_n]dx$$

Now, if recombination is neglected and a strongly p-type sample is assumed,

$$\Delta n = \frac{q_o}{t}\,\frac{(t - x)}{\mu^*\mathcal{E}^*}$$

and thus $\frac{d}{R} = e\,p_o t\mu_{pAV} + e\,\frac{q_o}{t}\int_o^t \frac{(t-x)[\mu_p(x) + \mu_n(x)]}{\mu^*(x)\mathcal{E}^*}\,dx$

Since the material is p-type, $\mu^* \approx \mu_n$, and if it is also assumed that $\mu_n >> \mu_p$, then

$$\frac{d}{R} = e\, p_o t \mu_{p\ AV} + e\, \frac{q_o t}{2\mathcal{E}^*} \tag{1.44}$$

Conductivity modulation thus begin to take place when

$$q_o \approx 2\mathcal{E}^*\, \mu_{p\ AV}\, p_o \tag{1.45}$$

The open-circuit voltage is given now by

$$V_{OC} = \frac{1}{2}\ \frac{q_o d\ B\mu_{n\ eff}}{p_o \mu_{p\ AV} + q_o/2\,\mathcal{E}^*} \tag{1.46}$$

Thus the behavior of the open circuit voltage should be, for low illumination

$$V_{OC} = \frac{1}{2}\ \frac{q_o\ Bd}{p_o}\ \frac{(\mu_n)_{eff}}{(\mu_p)_{AV}} \tag{1.47}$$

in other words, linear with illumination intensity q_o, and for high illumination

$$V_{OC} = \mathcal{E}^*\ (B\mu_n)_{eff}\ d$$

and since $\mathcal{E}^* = \frac{1}{e}\frac{\Delta E_G}{t}$

$$V_{OC} = \frac{\Delta E_G}{e}\ \frac{d}{t}\ (B\mu_n)_{eff} \tag{1.48}$$

In other words, for high illumination, the open circuit voltage should saturate and become independent of illumination. The "breakpoint" or dividing line between the two types of behavior occurs for a value of illumination such that $q_o = 2\ \mathcal{E}^*\ \mu_{p\ AV}\ p_o$.

The efficiency is directly dependent on the behavior of the open-circuit voltage. The expression is

$$\eta = \frac{1}{8}\ (B\mu_n)^2_{eff}\ \frac{eqt}{(E_{G1} + E_{G2})(p_o \mu_{p\ AV} + \frac{eqt}{2\Delta E_G})} \tag{1.49}$$

Making the previous assumption about the high-magnetic-field dependence and let $(B\mu_n)^2_{eff} = \frac{1}{4}$, then the expression for maximum efficiency, occuring at high illumination, becomes

$$\eta_{max} = \frac{1}{16} \frac{E_{G2} - E_{G1}}{E_{G2} + E_{G1}} \tag{1.50}$$

Thus it is easy to see that, based on the model under discussion thus far, it is not at all reasonable to expect efficiencies greater than 5% from <u>any</u> graded-gap device operated in the PEM mode, at least not with the type of illumination spectrum we have assumed. However, it must be borne in mind that our model makes very specific assumptions about bulk and surface recombination. The effect of these assumptions will now be considered briefly.

Bulk recombination and the effects of finite surface recombination velocity enter into the efficiency calculation as follows: It has been shown that if recombination is included, the short circuit current can be written as

$$I_{y\ SC} = eq_o t\ (B\mu_n)_{eff}\ F(z)$$

where $z = \frac{et^2}{\mu^* \tau_1 \Delta E_G}$. The exact form of F(z) depends on $\Delta n(x)$ and thus on the surface recombination velocities s_1 and s_2, as well as on the spatial variation of μ^*, etc. For the case discussed earlier ($s_1 = 0$, $s_2 = \infty$)

$$F(z) = \frac{z - 1 + e^{-z}}{z^2}$$

and has the property that $F(0) = 1/2$, $F(\infty) = 0$.
z thus brings in the effects of finite thickness t, mobility μ^*, lifetime τ_1, and gap gradient $\mathcal{E}^*$, whereas the surface effects come in through the <u>form</u> of F(z). The expression for efficiency is then simply multiplied by a factor $[F(z)]^2$. Thus, including the bulk recombination usually lowers the efficiency. However, it is important to remember that only a very special set of surface recombination velocities has been considered. A simple example will illustrate.

<u>1.4.4 The case s(0) = 0, s(t) = 0</u>

In the constant mobility case and for $s_1 = 0$, $s_2 = \infty$, we obtained

$$\frac{d}{R} = e\, p_o t \mu_{p\ AV} + e\, \frac{q_o t}{2\mathcal{E}^*} \tag{1.44}$$

Conductivity modulation thus begin to take place when

$$q_o \approx 2\mathcal{E}^*\, \mu_{p\ AV}\, p_o \tag{1.45}$$

The open-circuit voltage is given now by

$$V_{OC} = \frac{1}{2}\, \frac{q_o d\, B\mu_{n\ eff}}{p_o \mu_{p\ AV} + q_o/2\,\mathcal{E}^*} \tag{1.46}$$

Thus the behavior of the open circuit voltage should be, for low illumination

$$V_{OC} = \frac{1}{2}\, \frac{q_o\, Bd}{p_o}\, \frac{(\mu_n)_{eff}}{(\mu_p)_{AV}} \tag{1.47}$$

in other words, linear with illumination intensity q_o, and for high illumination

$$V_{OC} = \mathcal{E}^*\, (B\mu_n)_{eff}\ d$$

and since $\mathcal{E}^* = \frac{1}{e}\, \frac{\Delta E_G}{t}$

$$V_{OC} = \frac{\Delta E_G}{e}\, \frac{d}{t}\, (B\mu_n)_{eff} \tag{1.48}$$

In other words, for high illumination, the open circuit voltage should saturate and become independent of illumination. The "breakpoint" or dividing line between the two types of behavior occurs for a value of illumination such that $q_o = 2\ \mathcal{E}^*\, \mu_{p\ AV}\, p_o$.

The efficiency is directly dependent on the behavior of the open-circuit voltage. The expression is

$$\eta = \frac{1}{8}\, (B\mu_n)^2_{eff}\, \frac{eqt}{(E_{G1} + E_{G2})(p_o \mu_{p\ AV} + \frac{eqt}{2\Delta E_G})} \tag{1.49}$$

Making the previous assumption about the high-magnetic-field dependence and let $(B\mu_n)^2_{eff} = \frac{1}{4}$, then the expression for maximum efficiency, occuring at high illumination, becomes

$$\eta_{max} = \frac{1}{16} \frac{E_{G2} - E_{G1}}{E_{G2} + E_{G1}} \tag{1.50}$$

Thus it is easy to see that, based on the model under discussion thus far, it is not at all reasonable to expect efficiencies greater than 5% from <u>any</u> graded-gap device operated in the PEM mode, at least not with the type of illumination spectrum we have assumed. However, it must be borne in mind that our model makes very specific assumptions about bulk and surface recombination. The effect of these assumptions will now be considered briefly.

Bulk recombination and the effects of finite surface recombination velocity enter into the efficiency calculation as follows: It has been shown that if recombination is included, the short circuit current can be written as

$$I_{y\ SC} = eq_o t\ (B\mu_n)_{eff}\ F(z)$$

where $z = \frac{et^2}{\mu^* \tau_1 \Delta E_G}$. The exact form of F(z) depends on $\Delta n(x)$ and thus on the surface recombination velocities s_1 and s_2, as well as on the spatial variation of μ^*, etc. For the case discussed earlier ($s_1 = 0$, $s_2 = \infty$)

$$F(z) = \frac{z - 1 + e^{-z}}{z^2}$$

and has the property that $F(0) = 1/2$, $F(\infty) = 0$.
z thus brings in the effects of finite thickness t, mobility μ^*, lifetime τ_1, and gap gradient $\mathcal{E}^*$, whereas the surface effects come in through the <u>form</u> of F(z). The expression for efficiency is then simply multiplied by a factor $[F(z)]^2$. Thus, including the bulk recombination usually lowers the efficiency. However, it is important to remember that only a very special set of surface recombination velocities has been considered. A simple example will illustrate.

<u>1.4.4 The case s(0) = 0, s(t) = 0</u>

In the constant mobility case and for $s_1 = 0$, $s_2 = \infty$, we obtained

$\Delta n(x) = g\tau_1\left[1 - e^{\frac{x - t}{\tau_1 \mu^* *}}\right]$. However, for $s_1 = 0$, $s_2 = 0$, we would obtain $\Delta n(x) = g\tau_1$ with

$$I_{y\ SC} = eq_o t(B\mu_{n\ eff})\ \frac{1}{z}$$

thus $F(z) = \frac{1}{z}$ now. This means that for $z = 1$ (not unreasonable for the HgTe-CdTe system), $F(z)$ for $s_2 = \infty$ is $e^{-1} = .37$, whereas for $s_2 = 0$, $F(z) = 1$; this corresponds to a seven-fold increase in efficiency. In HgTe-CdTe this would correspond to $7/16 \times \frac{\Delta E}{E_{G2} - E_{G1}} \approx 30\text{-}40\%$.

Obviously our assumptions start to break down for small values of z, since otherwise we would have a infinitely efficient device. However, this example does show that the efficiency of the device is quite sensitive to the surface recombination velocities and would probably be improved by reducing the surface recombination velocity s_2 at the back face. A more detailed discussion of the effects of finite surface recombination velocities will be possible when the equations for $\Delta n(x)$ for the general case [which were set up in the author's M.S. thesis] are solved.

Let us summarize this section. We derived an expression for the efficiency of a graded-gap PEM device valid for small magnetic fields and low illumination. We then extrapolated results obtained by Smith[17] for homogeneous materials and assumed that the magnetic-field-dependent factor in the efficiency had a maximum value of 1/4. We also assumed that the main effect of high illumination was conductivity modulation. We then showed that with an input spectrum matched to give a uniform generation rate and with the assumptions on surface recombination velocity ($s_1 = 0$, $s_2 = \infty$) which our analytical model includes, that the maximum efficiency* is only slightly greater than 5%. However, we then changed the assumption about surface recombination velocity and showed that for a case in which $s_1 = 0$, $s_2 = 0$, the efficiency for $z = 1$ was seven times greater than for $s_1 = 0$, $s_2 = \infty$.

Both the assumptions on high magnetic field and high illumination ignore some quantum effects and statistical effects. However, these should result only in second-order corrections to the model.

---

*This maximum occurs for $z = 0$.

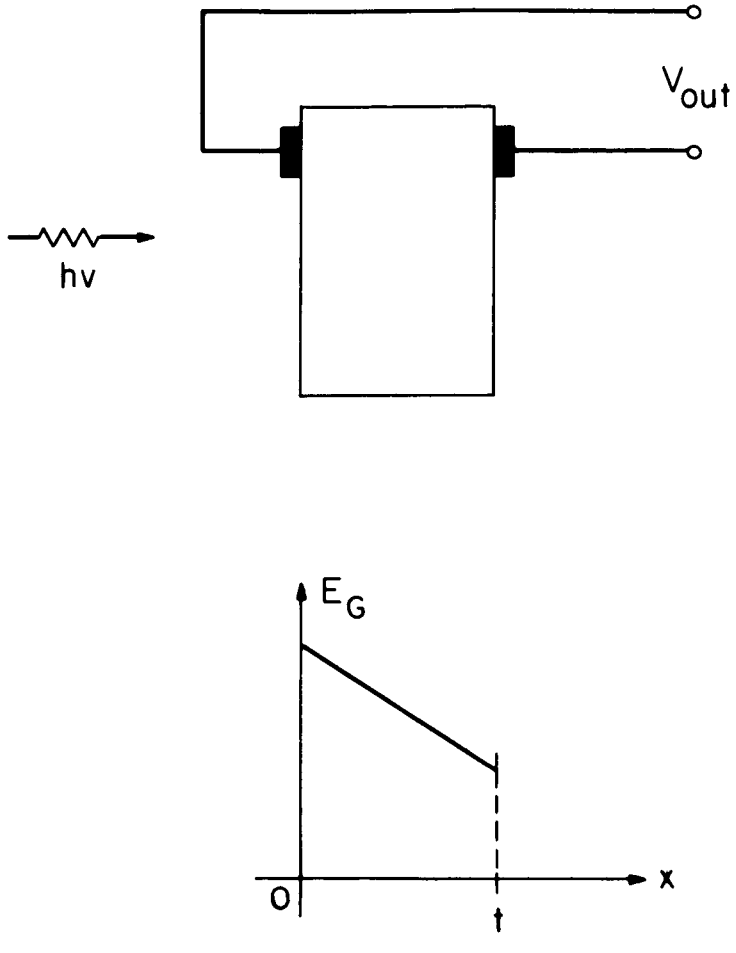

Fig. 1.10 Graded-gap photocell without magnetic field

1.5 Operation Without a Magnetic Field

This section considers the possible operation of a graded gap device without a magnetic field. Our purpose will not be to derive detailed I-V characteristics, but just to show that a potential can be set up between the two faces of a graded-gap photocell even in the absence of a magnetic field.

The devices considered by Tauc, Emtage, and Segall and Pell all operated without a magnetic field, and the conclusion reached by these authors have already been discussed in the section on "Theoretical Background." We will be interested in deriving the open-circuit voltage in the x-direction by using the procedures and results of the author's M.S. thesis.

Our starting point is equation 10 (of this paper) for the photopotential $\phi-\phi_o$. B = 0, of course, and we also assume $\Delta n \approx$ const. to ignore diffusion effects. Then equation 10 becomes

$$\frac{d}{dx}(\phi-\phi_o) = -\frac{J}{\sigma} + \frac{\Delta n}{n_o\mu_n+p_o\mu_p+\Delta n(\mu_n+\mu_p)}\left[\frac{\mu_n}{e}\frac{dE_c}{dx} + \frac{\mu_p}{e}\frac{dE_v}{dx} - (\mu_n+\mu_p)\frac{d\phi_o}{dx}\right] \quad (1.51)$$

If the material is strongly p-type so that $p_o\mu_p >> n, \mu_n$ then

$$\frac{d}{dx}(\phi-\phi_o) = -\frac{J}{\sigma} + \frac{\Delta n\mu_p}{p_o\mu_p+\Delta n(\mu_n+\mu_p)}\left[\frac{\mu_n}{\mu_p}\mathcal{E}_o^n + \mathcal{E}_o^p\right] \quad (1.52)$$

Inserting the values for $\mathcal{E}_o^n$ and $\mathcal{E}_o^p$ derived in connection with equation 21 and integrating yields for the p-type case

$$V_{OC} = \frac{\mu_n}{\mu_p}\frac{\Delta n}{p_o}\frac{\Delta E_G}{e} \quad (1.53)$$

for low illumination, and

$$V_{OC} = \frac{\mu_n}{\mu_n+\mu_p}\frac{\Delta E_G}{e} \quad (1.54)$$

for high illumination. This agrees with the results of Tauc and Emtage.

For n-type material, the corresponding results are

$$\left.\begin{aligned} V_{OC} &= -\frac{\mu_p}{\mu_n}\,\frac{\Delta n}{n_o}\,\frac{\Delta E_G}{e} \quad \text{for low illumination, and} \\ V_{OC} &= -\frac{\mu_n}{\mu_p+\mu_n}\,\frac{\Delta E_G}{e} \quad \text{for high illumination} \end{aligned}\right\} \tag{1.55}$$

For intrinsic material, equation 51 becomes

$$\frac{d}{dx}(\phi-\phi_o) = -\frac{J}{\sigma} + \frac{\Delta n}{n_i+\Delta n}\,\frac{1}{2e}\,\frac{dE_G}{dx}\left[\frac{\mu_n-\mu_p}{\mu_n+\mu_p}\right] \tag{1.56}$$

and thus

$$\left.\begin{aligned} V_{OC} &= +\frac{\Delta n}{n_{i2}}\,\frac{kT}{e}\,\frac{\mu_n-\mu_p}{\mu_n+\mu_p} \quad \text{for low illumination, and} \\ V_{OC} &= \frac{\mu_n-\mu_p}{\mu_n+\mu_p}\,\frac{\Delta E_G}{2e} \quad \text{for high illumination} \end{aligned}\right\} \tag{1.57}$$

where n_{i2} is the intrinsic concentration at the small-gap side of the device.*

To go further than this with an exact treatment it is necessary to find Δn for this situation with a net current flowing along the direction of the gap gradient. This should present no new difficulties, but will not be carried out here for reasons of space. Our original purpose of using the approach developed by the author to show that a graded-gap device can operate without a magnetic field has certainly been accomplished, and the results agree with those of others where available. In particular, the expressions for open-circuit voltages tend to verify the statement by Emtage that if $\mu_n > \mu_p$, it will generally be desirable to use acceptor doping in the variable band-gap material.

*Equation 57 bears out the statement by Segall and Pell that for an intrinsic device with $\mu_n = \mu_p$, there is no output.

APPENDIX A

BASIC THEORETICAL ASSUMPTIONS

1. Effective-Mass Treatment of Band-Edge Gradients

Krömer[1] has given the most detailed discussion of the effect of band-edge gradient on carrier motion, but to find out the limitations of his treatment it is worthwhile to review briefly the work of Slater[18] in his paper on "Electrons in Perturbed Periodic Lattices", which forms the basis for Krömer's work.

The perfectly periodic semiconductor crystal is described by the Schrödinger equation

$$H_o \psi_o(k,r) = E_o(k)\psi_o(k,r) \tag{A1}$$

where H_o is the hamiltonian describing the perfectly periodic crystal and $\psi_o(k,r)$ is one of the eigenfunctions, corresponding to an eigenvalue $E_o(k)$. The effective mass, of course, enters in through the form of $E_o(k)$.

If we now consider a perturbation to the perfectly periodic hamiltonian H_o of the form

$$H = H_o + H_1$$

where H_1 is "slowly varying", and is to be specified in more detail later, then the new eigenvalues E_n are given by the equation

$$H \psi_n(r) = E_n \psi_n(r)$$

We choose to form the eigenfunctions $\psi_n(r)$ as a sum of Wannier functions[19]

$$\psi_n = \sum_i \Phi_n(r_i)\, a(r-r_i) \tag{A2}$$

where $a(r-r_i)$ is the Wannier function on the ith atomic site and $\Phi_n(r_i)$ is an appropriate amplitude function. The form of $\Phi_n(r_i)$ is found by inserting the expansion for ψ_n into the Schrödinger equation, pre-multiplying by the complex conjugate of ψ_n, and integrating. If H_1 varies so slowly with r that

it can be regarded as approximately constant over the atomic wave function of an atom, then it can be taken outside the integral, and the orthogonality properties of the Wannier functions are such that $\Phi_n(r_i)$ is given by

$$[E_o(\nabla) + H_1(r_i) - E_n]\ \Phi_n(r_i) = 0 \qquad \text{(A3)}$$

which corresponds to a particle with an effective mass determined by the form of E_o and with an eigenvalue E_n moving under the influence of an electrostatic potential H_1.

It is easily seen that whether the perturbation $H_1(r)$ is taken to be $e\ \phi(r)$ due to some external electric field or whether it is taken to be a position dependent band edge, for instance, $H = P^2/2m^* + E_c(x)$, the problem is the same in either case.

From here on we proceed by standard methods; that is, the center of mass of a wave packet moves according to the classical Hamilton's equations, so that

$$\frac{d}{dt}\ (\vec{p}) = -\vec{\nabla}_r(H)$$

and so forth, with the result being that the net force term to be inserted into the Boltzmann transport equation is given by

$$\left.\begin{aligned} F_e &= -e\left(-\frac{d\phi}{dx} + \frac{1}{e}\frac{dE_c}{dx} - \left[\frac{\hbar^2k^2}{2m_e}\right]\frac{1}{m_e}\frac{dm_e}{dx}\right) \\ &\text{for conduction band electrons, and} \\ F_h &= e\left(-\frac{d\phi}{dx} + \frac{1}{e}\frac{dE_v}{dx} + \left[\frac{\hbar^2k^2}{2m_h}\right]\frac{1}{m_h}\frac{dm_h}{dx}\right) \end{aligned}\right\} \qquad \text{(A4)}$$

for valence band holes. If the bandgap varies with position, $\frac{dE_c}{dx} \neq \frac{dE_v}{dx}$, and the forces on electrons and holes will not be the same. For this reason Krömer described the forces as arising from "quasi-electric fields."

With the references shown in Fig. 1, E_c and E_v are also called the "electron affinity" and "hole affinity". They are properties of the material

alone, and do not depend on such things as the doping or excess carrier density. They are fixed once the variation in composition is fixed as a function of distance.

The terms containing the effective-mass gradients in equation (A4) show the tendency of the carriers to move from regions of small effective mass to regions where the effective mass is larger. In order to eventually compare magnitudes of currents due to gap variations and currents due to effective mass variations, it will be assumed that the effective masses are proportional to the energy gap. This possibility is predicted by k·p band structure calculations[21] if the conduction and the valence bands are the only bands which are interacting. For the HgTe-CdTe system, at least, the experimental results of Harman et al[16] show that the effective masses are very nearly proportional to the energy gap.

If this assumption is made, then both $\frac{1}{m_e}\frac{dm_e}{dx}$ and $\frac{1}{m_h}\frac{dm_h}{dx}$ in equation (A4) are replaced by $\frac{1}{E_G}\frac{dE_G}{dx}$.

Let us see what limitations the assumption that H_1 is "slowly varying" puts on this approach. Let us assume that we have a more or less linear variation in E_c between two values, and let us specify that not more than 1% of this change shall occur over the extent of one atomic wave function. Let us take this extent to be 10 angstroms. Thus the transition region should not be narrower than 10^3 Å or 0.1 microns in order for this effective mass treatment to apply.

2. Boltzmann Transport Theory

Very few words will be said about Boltzmann transport theory and its limitations because a good discussion of this topic is given by Smith.[17] He shows that Boltzmann theory can be used to explain most "low-field" magnetic-field effects, but that quantum-mechanical and other effects arise at high magnetic fields which disagree with many of the predictions of Boltzmann theory.

In all cases the dividing line between low- and high-field behavior is the condition $B\mu = 1$. It is difficult to predict precisely how these high-field considerations will affect the operation of the graded-gap device without further analysis. However, Lawson[7] and Nielsen have reported mobilities in excess of 100,000 cm^2/v-sec in their investigation

of HgTe-CdTe alloys, and it may be interesting to point out that for such a large mobility, the condition $B\mu = 1$ is reached for B = 1 kilogauss.

3. Quasi-Neutrality

Jonscher[20] gives a good description of the use of the "quasi-neutral" approximation in finding the electrostatic potential distribution in a non-uniform semiconductor. This is a kind of "self-consistent" process in which it is first assumed that the semiconductor is strictly neutral. The potential is then calculated on this basis.

This treatment is exactly correct only in very special cases, because any spatial variation in the potential gradient must be accompanied by a net space charge. Thus the next step in the procedure is to calculate the net space charge necessary to support the potential calculated on the assumption of strict neutrality. If this net space charge is small compared to the net mobile carrier concentration, then the assumption of quasi-neutrality is justified.

In a constant band-gap semiconductor, the quasi-neutral approximation is usually good if the doping density change is less than some specified percentage in a certain characteristic length called the Debye length. In a graded gap region with uniform doping, it was shown in the author's M.S. thesis (and also in the next appendix) that the condition of self-consistency for the quasi-neutral treatment becomes that the change in energy gap in a Debye length be small compared to kT.

APPENDIX B

QUASI-NEUTRALITY IN THE GRADED-GAP DEVICE

The electrostatic potential* must satisfy Poisson's equation

$$-\nabla\cdot(\varepsilon\nabla\phi) = \rho$$

where ε = dielectric constant and ρ = charge distribution. It is assumed that the dielectric constant does not vary in the inhomogeneous region. (As Emtage points out, this is probably a good assumption.)

The electrostatic potential is also related to the carrier concentration by

$$n = N_c e^{-\delta} = N_c e^{-\frac{(E_c - E_f - e\phi)}{kT}}$$

Now, since the net charge density ρ is given by

$$\rho = e(p-n + N_d - N_a)$$

(N_d and N_a are donor and acceptor concentrations, respectively, and are assumed to be completely ionized), Poisson's equation can be rewritten

$$\frac{-\varepsilon}{e^2 n_i}\frac{\partial^2\phi}{\partial x^2} = -2\sinh\left[\frac{e(\phi-\phi_i)}{kT}\right] + \bar{N} \qquad \text{(B1)}$$

where $\bar{N} = \frac{N_d - N_a}{n_i}$ and ϕ_i is defined by

$$n_i = N_c e^{\frac{-(E_c - E_f - e\phi_i)}{kT}} = N_c e^{-\delta_i} \qquad \text{(B2)}$$

---

*This treatment follows that of Jonscher[20] (p. 17 and p. 154) quite closely.

or

$$\phi_i = \frac{1}{e}\left(E_c - \frac{E_G}{2} - E_f - \frac{1}{2}kT \ln N_c/N_v\right) \tag{B3}$$

Applying the quasi-neutral approximation to equation (B1) consists of assuming that ϕ is given with sufficient accuracy by the strictly neutral solution

$$\sinh(\Phi-\Phi_i) = -\frac{\bar{N}}{2} \tag{B4}$$

(Here we have defined $\Phi = \frac{e\phi}{kT}$). This would mean that $\Phi-\Phi_i$ would be determined by the spatial variation of the doping and the intrinsic concentration n_i.

In a homogeneous semiconductor, the quasi-neutral approximation is enough to specify the electrostatic potential distribution ϕ. However, equation (B3) shows that ϕ_i contains the band edge variation as well as the bandgap variation. Putting it another way, one would have to know the electron affinity as well as the bandgap as a function of alloy composition in order to calculate ϕ. It will be shown later that, fortunately, as long as the variations are sufficiently gradual, the electron affinity does <u>not</u> enter into the behavior of the device.

The quantity which <u>is</u> determined once $N_d(x)-N_a(x)$ and $E_G(x)$ are specified is $\delta(x)$, since equation (B4) can be converted to*

$$\sinh(\delta-\delta_i) = -\frac{\bar{N}}{2} \tag{B5}$$

where

$$\delta_i = \frac{1}{2}E_G/kT + \frac{1}{2}\ln N_c/N_v \tag{B6}$$

The quasi-neutral approximation is valid only when departures from neutrality are quite small, and $-\varepsilon/e^2 n_i \, \partial^2\phi/\partial x^2$ is much smaller than either term on the right-hand side of Poisson's equation (B1). Two cases will be checked for self-consistency: undoped material ($\bar{N} = 0$) and uniformly extrinsic material ($N_d - N_a$ = const).

*Tauc calls δ the chemical potential.

1. Undoped Material

For undoped material, equation B4 yields $\phi=\phi_i$. The condition of self-consistency may then be written as

$$\frac{\varepsilon}{en_i}\ \frac{d^2\phi_i}{dx^2} << 1.$$

Substituting the value of ϕ_i from equation (B3) we have

$$\frac{kT\varepsilon}{e^2n_i}\ \frac{d^2}{dx^2}\left(\frac{E_c - E_f - E_G/2}{kT}\right) - \frac{kT\varepsilon}{e^2n_i}\ \frac{d}{dx}\left[\frac{N_v}{N_c}\frac{d}{dx}\left(\frac{N_c}{N_v}\right)\right] << 1$$

To keep the situation from becoming overly complicated, a linear variation of band edges will be assumed; this eliminates the second derivative of E_c and E_G from equation B7. Also, since we are considering the equilibrium case, $dE_f/dx = 0$. Thus we are left with

$$L_i^2\ \frac{d}{dx}\ \frac{N_v}{N_c}\ \frac{d}{dx}\left(\frac{N_c}{N_v}\right) << 2$$

where $L_i = (kt\varepsilon/e^2n_i)^{1/2}$ is called the Debye length. If we assume a linear variation in N_c/N_v, i.e.

$$\frac{N_c}{N_v} = \left(\frac{N_c}{N_v}\right)_o + \left(\frac{N_c}{N_v}\right)_1 \frac{x}{L_{io}}$$

where L_{io} is constant and is equal to the Debye length somewhere in the graded region, then the self-consistency condition becomes

$$\left[\frac{\left(\frac{N_c}{N_v}\right)_1}{\left(\frac{N_c}{N_v}\right)_o + \left(\frac{N_c}{N_v}\right)_1 \frac{x}{L_{io}}}\right]^2 << 2 \qquad \text{(B8)}$$

In other words, if N_c/N_v changes only a little in a Debye length and if the departures of E_c and E_v from linearity are small in a Debye length, then the

undoped graded-gap region may be treated by the quasi-neutral assumption. As pointed out in the author's M.S. thesis, none of these are drastic assumptions.**

2. Uniformly Doped Material

The second case to be treated is that of $N_d - N_a$ = constant and large enough so that $|\bar{N}| >> 1$ everywhere. If an almost-linear bandgap and an almost-constant N_c/N_v are again assumed, the situation is exactly the same as that treated by Jonscher, p. 154, the condition for self-consistency is that the relative change in $\bar{N}$ within an extrinsic Debye length* L_N be small. This means

$$\left| \frac{1}{\bar{N}} \frac{d\bar{N}}{dx} L_N \right| << 1$$

but

$$\frac{d\bar{N}}{dx} = \frac{d}{dx} \left(\frac{N_d - N_a}{n_i}\right) = \bar{N} \left(\frac{1}{2kT} \frac{dE_G}{dx} - \frac{1}{N_c} \frac{dN_c}{dx}\right)$$

To estimate the relative sizes of these terms, it is again assume that m_n is proportional to E_G. The term $1/N_c \; dN_c/dx$ then becomes $3/2 \; 1/E_G \; dE_G/dx$ and

$$\frac{d\bar{N}}{dx} = \frac{\bar{N}}{2kT} \frac{dE_G}{dx} \left(1 - \frac{3kT}{E_G}\right)$$

The self-consistency condition then becomes

$$\left| \frac{L_N}{2kT} \frac{dE_G}{dx} \left(1 - \frac{3kT}{E_G}\right) \right| << 1$$

As long as $E_G > kT$, this will be satisfied if

---

*$L_N^2 = L_i^2/\bar{N} = \epsilon kT/e^2 n$ where $n \quad N_d - N_a$.

**Since N_c = const x $m_n^{3/2}$ and N_v = const x $m_p^{3/2}$, (N_c/N_v) = const $(m_n/m_p)^{3/2}$. Then if we make the assumption discussed in Appendix A that the effective masses are each proportional to the energy gap, the ratio (N_c/N_v) would indeed be constant.

$$\frac{d(E_G/kT)}{d(x/L_n)} \ll 1 \qquad \text{(B9)}$$

That is, the change in bandgap in the space of an extrinsic Debye length must be much less than kT.

As an example of what all this means, if at room temperature and a doping of 10^{17} cm^{-3}, L_N is approximately 10^{-6} cm for CdTe. If we assume that E_G changes by 1.5 ev in 10^{-3} (10 microns) then the change in E_G in one Debye length is a little less than 1/10 kT. Quasi-neutrality is just barely preserved. Smaller band-gap gradients and heavier doping improve the assumption.

It is interesting to note that although quasi-neutrality in the above example was valid only for transition widths greater than 10 microns, the effective-mass treatment and the resulting force expressions are valid for transition widths of 1/10 micron and probably less. Thus it is valid and perhaps worthwhile to consider in the future other ways of obtaining the potential distribution besides that of assuming quasi-neutrality.

1.6 List of Symbols

B = magnetic field strength

D_n = electron diffusion constant

D_p = hole diffusion constant

D^* = effective diffusion constant

E_c = conduction band edge

E_f = equilibrium Fermi level

E_g = energy gap

E_v = valence band edge

$\mathcal{E}$ = electric field strength

F_e = force on electrons

F_h = force on holes

g = rate of generation of excess carriers

$\hbar$ = $h/2\pi$ = Planck's constant

H = Hamiltonian

I_x, I_y = currents

J_{nx}, J_{ny} = electron current densities

J_{px}, J_{py} = hole current densities

k = Boltzmann constant

k_x, k_y, k_z = wave vectors

$|k| = k_x^2 + k_y^2 + k_z^2$

L = diffusion length

m^* = effective mass

m_e = effective mass of electrons

m_h = effective mass of holes

n = total electron concentration

n_o = equilibrium electron concentration

Δn = excess electron concentration

$N_c = 2\left(\frac{2\pi m_e kT}{h^2}\right)^{3/2}$ = effective conduction band edge density

$N_v = 2\left(\frac{2\pi m_h kT}{h^2}\right)^{3/2}$ = effective valence band edge density

N_a = acceptor concentration

N_d = donor concentration

p = total hole concentration

p_o = equilibrium hole concentration

Δp = excess hole concentration

$\vec{p}$ = momentum

q_o = incident photon flux

s = surface recombination velocity

t = length of graded region

V_x, V_y = terminal voltages

w = width of sample

x, y, z = Cartesian coordinates

$\gamma = -\ln p/N_v$

$\delta = -\ln n/N_c$

ε = dielectric constant

η = efficiency

θ = $B\mu$ = Hall angle

λ = wavelength

μ_n = electron mobility

μ_p = hole mobility

μ^* = effective mobility

ρ = charge density

σ = conductivity

τ = relaxation time

τ_l = excess carrier lifetime

ϕ = electrostatic potential

ψ = electron wave function

1.7 References

1. H. Kroemer, "Quasi-Electric and Quasi-Magnetic Fields in Non-Uniform Semiconductor", R.C.A. Review, V. 18, p. 332 (1957).

2. P. Aigrain, Seminar given for Semiconductor and Energy Conversion Laboratory at M.I.T. in 1960.

3. B. Segall and E. Pell, "An Evaluation of Graded Band Gap Photovoltaic Solar Cells", G.E. Research Laboratory Report # 62-RL-(3051G), June 1962.

4. J. Tauc, "Generation of an emf in Semiconductors with Non-Equilibrium Current Carrier Concentrations", Review of Modern Physics, V. 29, p. 308 (1957).

5. P. Emtage, "Electrical Conduction and the Photovoltaic Effect in Semiconductors with Position-Dependent Band Gaps", Journal of Applied Physics, V. 33, p. 1950 (1962).

6. G. Almasi, "Cadmium-Telluride-Mercury Telluride Graded-Gap Device", M.I.T. M.S. Thesis, 1962.

7. Lawson et al, "Preparation and Properties of HgTe and Mixed Crystals of HgTe-CdTe", J. Phys. Chem. Solids, V. 9, p. 325 (1959).

8. J. Blair, "Investigation into the Thermal and Electrical Properties of the Mercury-Telluride-Cadmium Telluride Semiconductor Solid Solution System", M.I.T. Electronic Systems Laboratory Energy Conversion Group Scientific Report No. 2, Contract No. AF 19(604)-4153 (1960).

9. Strauss et al, "Optical and Electrical Properties of $Cd_xHg_{1-x}Te$ Alloys", paper presented at the Exeter Conference, Summer, 1962.

10. J. Conley, "The Optical Absorption Edge in CdTe", Fundamental Research in Solid State Energy Conversion Processes, Semiannual Technical Summary Report No. 2 of the M.I.T. Center for Space Research and Energy Conversion and Semiconductor Laboratory, (June, 1964).

11. De Nobel, "Phase Equilibria and Semiconducting Properties of CdTe", Philips Research Reports, V. 14, pp 361-399 and 430-492 (1959).

12. Davis and Shilliday, "Some Optical Properties of CdTe", Physical Review, V. 118, p. 1020 (1960).

13. Marple and Segall, "Optical Absorption Edge in CdTe", Bull. Am. Phip. Soc., V. 9, p. 223 (1964).

14. M. Lorenz, "High-Purity CdTe by Sealed-Ingot Zone Refining", J. Electrochem. Soc., V. 110, p. 343 (1963).

15. W. Shockley, Electrons and Holes in Semiconductors, Van Nostrand, 1950.

16. T.C. Harman et al, "Band Structure of HgTe and HgTe-CdTe Alloys", to be published in Solid State Communications, 1964.

17. R.A. Smith, Wave Mechanics of Crystalline Solids, John Wiley, 1961.

18. J.C. Slater, "Electrons in Perturbed Periodic Lattices", Phys. Rev. 76, 1592 (1949).

19. G.H. Wannier, "The Structure of Electronic Excitation Levels in Insulating Crystals", Phys. Rev., 52, 191 (1937).

20. A.K. Jonscher, "Principles of Semiconductor Device Operation, John Wiley, 1960.

21. C. Kittel, Solid State Physics, John Wiley, 1964.

22. H. Rodot and J. Henoc, "Diffusion a 1 etat solide entre des materiaux semi-conducteurs", Comptes Rendus, 256, 1954 (1963).

23. F. Bailly et al, "Preparation et controle de structures a largeur de bande interdite variable", Comptes Rendus, 257, 103 (1963).

24. G. Cohen-Solal et al, "Effects Photoelectriques et Photomagneto-electriques dans les structures a largeur de bande interdite variable", Comptes Rendus, 257, 863 (1963).

25. C. Verie, "Effect des gradients de largeur de bande interdite et de masse effective dans les structures heterogenes", Comptes Rendus, 258, 533 (1964).

26. H. Rodot, "Etude des equilibres thermodynamiques dans le tellurure de mercure et ses solutions solides avec le tellurure de cadmium", Comptes Rendus, 258, 6386 (1964).

27. A. Fortini and J.P. Saint-Martin, "Photomagneto-Electric Effect in Graded-Gap Semiconductors", Phys. Stat. Solid, 3, 1039 (1963).

28. R. Hinrichs, "Impurity Control in CdTe", S.B. Thesis, M.I.T., 1963.

CHAPTER 2

THE OPTICAL ABSORPTION EDGE IN CADMIUM TELLURIDE

2.0 Introduction

Detailed measurements on the temperature and energy dependence of optical absorption near the fundamental edge in CdTe have been performed. The process which was hypothesised on the basis of preliminary measurements, i.e., absorption of photons by excitons with assistance from LO phonons, has been confirmed.[1] One significance of this identification is that the existence of a band structure model which has a "direct" forbidden energy gap is also confirmed. These considerations are consistent with the results of D.T.F. Marple and B. Segall in their independent investigation of the optical properties.[2,3]

2.1 Experimental Considerations

Precise measurements of both energy and temperature are required. The sensitivity with respect to temperature arises because the magnitude of the effect is proportional to the (Bose) occupation probability of the LO phonon modes, i.e.,

$$\bar{n} = \frac{1}{e^{\theta/T} - 1} \simeq e^{-\theta/T}$$

where

$$\theta = 247^{\circ}K$$

is the "temperature" of the modes. Further, the magnitude of the optical absorption coefficient varies over several orders of magnitude in an energy range comparable to the LO phonon quantum

$$h\omega_{LO} = k\theta = .0213 \text{ ev.}$$

This necessitates both precise measurement of the photon energy and establishes the requirement of high resolution.

To establish isothermal conditions at the low temperature required, an optical cryostat was constructured in which the sample was immersed in helium exchange gas.

2.1.1 The optical cryostat

A metal helium dewar of commercial manufacture[4] was modified to provide a low temperature environment around and access to the transmission sample. The details of this are represented in Figure 2.1. The sample on its supporting structure fits into the inner most tube. This tube is filled with helium gas. The gas is cooled by contact with the lower section of the tube which is made of copper. Provision is made to cool the tube through a thermal "leak" to the helium reservoir and to add heat electrically for the purpose of adjusting temperature. For economy, the "heat leak" was made of annealed copper wire which has a negative coefficient of thermal conductivity. The thermal time response of the system is long, on the order of 15 minutes. Automatic control means were not required. The system was capable of operating in a constant power mode for 20 minutes with $\pm$ .5° maximum thermal fluctuation. Equilibrium is established in 15 minutes. There is, however, an additional factor which contributes to this performance. The heater resistor[5] has a negative coefficient of electrical resistance and is supplied from a relatively high impedance source. This arrangement proved useful both in reaching and maintaining the required equilibrium.

The supporting structure was provided with nylon brushings to prevent excessive communication of heat from the ambient. A low temperature of 16°K could be attained in the exchange gas mode. Liquid helium transferred directly into the inner tube provided an optically quiet 4.2+°K environment.

Optical windows were of Pyrex which is a satisfactory transmission medium in the .8 micron wavelength range. The "cold window" was a reworked Kovar of Pyrex seal[6] of commercial origin. No difficulty with thermal mismatch was encountered with this type of window. Helium could be pumped to below the λ point without experiencing a superfluid leak.

A radiation shield which is made of heavy-walled copper tube and is cooled by contact with the liquid nitrogen reservoir surrounds the inner tube. Slits were milled in this shield to provide optical access.

The sample is exposed to ambient radiation over .7% of the total solid angle.

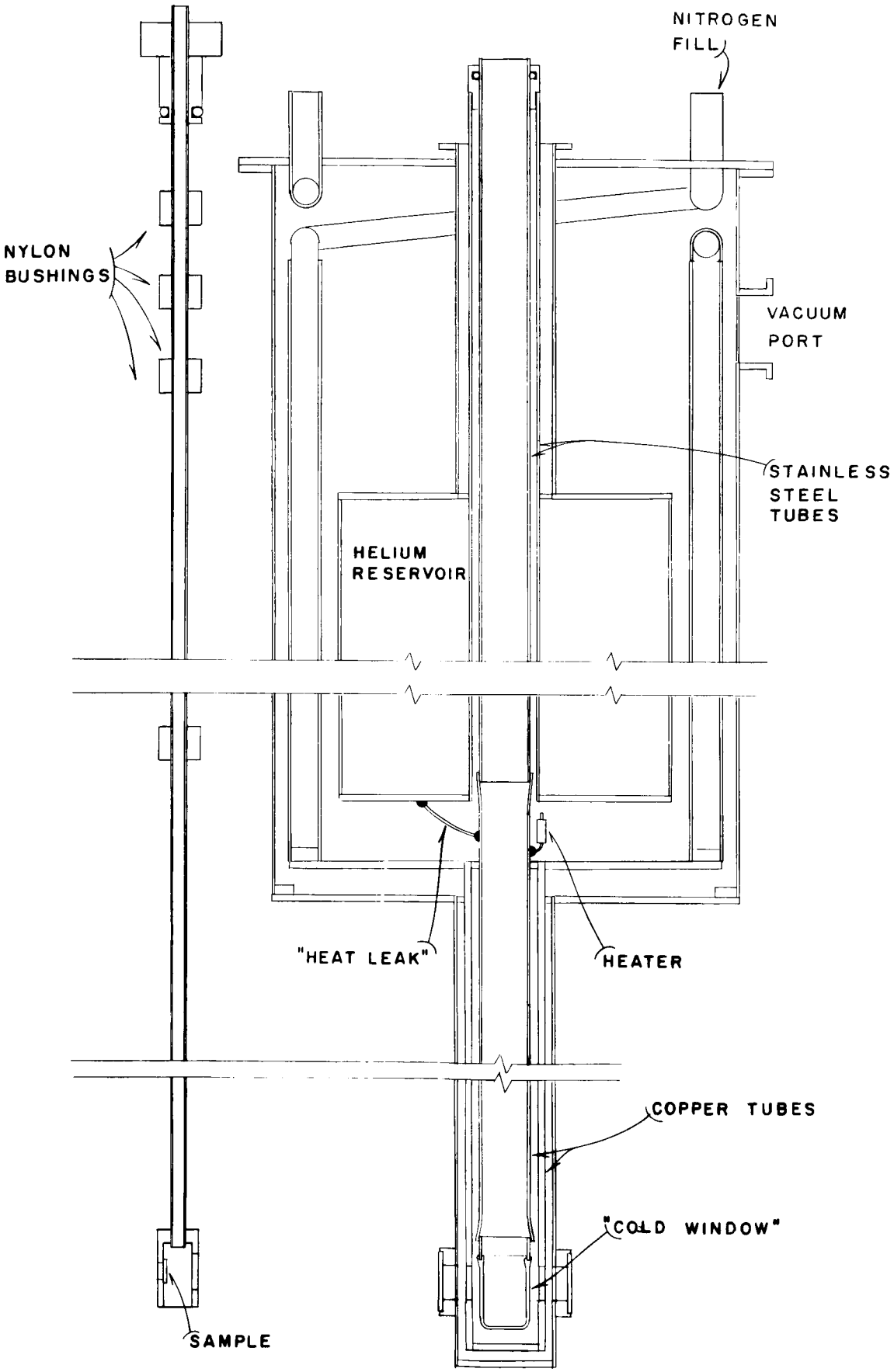

Fig. 2.1 Design of the Optical Cryostat

2.1.2 Thermocouple thermometry

A premium grade Copper-Constantan thermocouple[7] was calibrated with respect to normal points of melting ice, boiling helium and boiling nitrogen. The reference data of Powell et al.[8] corrected with a quadratic function based on this calibration was used for interpolation.

2.1.3 Spectral calibration

The monochrometer was calibrated against emission lines from a cesium lamp. Established wavelength values[9] were converted to their equivalent energy by the relation[10]

$$E(\text{ev.}) = \frac{1.23978}{\lambda(\mu)}$$

The grating employed[11] was nominally ruled at 1200 lines per mm. The theoretical dependence of energy on micrometer drum number, N, is

$$E(N) = \frac{A_1}{\sin A_2(N-A_3)}$$

(The grating angle is very nearly proportional to the drum number, N.)

A least square error fit[12] of 9 calibration points to this dependence yielded a standard error of $\pm$.00007 ev. The calibration data and parameters obtained are shown in Table 2.1. The parameters so obtained were used in subsequent interpolation.

2.1.4 The exciton position

The temperature dependent of the lowest exciton energy is required in normalization of the reduced data. This is known from emission and reflection measurements.[13] For the purpose of interpolation, the known positions were fit empirically with the function

$$E(\text{ev.}) = B_1 - [B_2 + B_3\, T^2(^\circ K)]^{1/2}$$

A least equare error of .0002 ev. was obtained for the data and parameters shown in Table 2.2.

Drum Number	Energy in ev. of Cs lines	
1.278	1.5894152	Rb impurity
2.531	1.5606279	
3.158	1.5466876	
3.710	1.5345764	
7.615	1.4549529	
9.766	1.4150510	
11.414	1.3862358	
13.505	1.3516654	
13.839	1.3463489	

Parameters Obtained

A_1 = .72389922

A_2 = .00754939

A_3 = 61.3600482

Table 2.1 Cs calibration data and parameters for spectral calibration of 1200/mm grating in a Perkin-Elmer model 99G monochrometer

Temperature (°K)	Exciton Energy (ev.)
2.1	1.5955
24.	1.5946
39.	1.5930
63.	1.5890
80.	1.5848
90.	1.5827
102.	1.5794
115.	1.5750
130.	1.5691

Parameters

$B_1 = 3.155764788$

$B_2 = 2.434919089$

$B_3 = .0000048787$

Table 2.2 Exciton energy in CdTe vs. temperature and parameters of an empirical function for purposes of interpolation.

2.1.5 Aquisition, reduction, and normalization of the experimental data

The physical process hypothesised dominates in determining the observed dependence of optical absorption on energy and temperature. A demonstration of this is effected by a systematic procedure of reducing an normalizing the experimental data.

Absolute transmission values were measured by a sample-in, sample-out method for several sample of various thickness. Factorial data was obtained as a continuous record of transmitted intensity vs. wavelength drum number for several temperatures (thermocouple voltages). Similarly, a continuous record of transmitted intensity for the sample-out condition was also taken to provide reference values. This was taken on a relative scale. Normalization was provided by a single sample-in, sample-out measurement at a fixed wavelength drum number for each sample and temperature involved. Because of the convenient appearance of wavelength markers at each 0.1 drum number, this was adopted as the mesh in sampling the continuous record. A data point results at about every 0.0023 ev. in energy.

The large amount of data generated and the requirement of retaining the precision inherent in the measurements necessitated the application of digital computer techniques. To illustrate the method, a sequence of four graphical figures has been prepared. The sample chosen for this example is one of five for which detailed results are reported. This particular sample was chosen in order to demonstrate both the range of agreement with an existing theory and the departure from agreement.

In reducing the experimental data, the quantity of physical interest required is the temperature dependent component of the bulk absorption as a function of photon energy, $h\nu$. The surfaces of the samples are chemically prepared. This results in an irregular surface. A discussion of the motivation for this preparation appears in section 2.1.6. One consequence of this is that the multiple reflection correction required in obtaining accurate values of the absorption coefficient for small losses is not readily applied. However, this information is not required as an intermediate quantity in obtaining the result of importance.

The first step in the reduction is to process the experimental data to produce values of the absolute transmission as a function of photon energy and temperature, i.e.,

$$t_{abs}\ (h\nu,T)$$

Next, values of the function

$$\alpha(h\nu,T) = -\frac{1}{D}\log\ (t_{abs})$$

are computed. The results of this are shown in Figure 2.2. Also shown are positions of the exciton for the temperatures of measurement.

The temperature dependence arising from the shift of the exciton (or alternately stated, the band gap) is removed by normalizing the observed absorption with respect to energy. This is most conveniently done by introducing the coordinate

$$\Delta = E_o(T) - h\nu$$

The results so obtained are shown in Figure 2.3.

The remaining temperature dependence of the absorption at 41.7, 57.1, and 72.°K, is proportional to the (Bose) occupation probability of the LO phonon modes, $\bar{n}$. This can be demonstrated in a sequence of two operations. The temperature dependence which appears in comparison of the 4.2 and 29.2°K data is finite but far too small to be proportional to $\bar{n}$. For this reason, the 29.2°K data is considered to be a "background" arising from unspecified processes. When these values are subtracted from those of the higher temperatures, the results shown in Figure 2.4 are obtained.

In performing this subtraction, it is apparent that the gradually increasing dependence of absorption on energy as shown in Figure 2.2 is removed. Another feature of this procedure is that a correction for reflection is effected. This is similar to that correction which is made when the absorption values from a thin sample are subtracted from corresponding values from a thicker sample.

That the component of absorption obtained in this manner is proportional in magnitude to the phonon occupation, $\bar{n}$, is demonstrated by dividing by $\bar{n}$ and plotting as shown in Figure 2.5. Also shown are theoretical results for the process in which excitons with the assistance of one LO phonon produce absorption. It is apparent that the higher absorption values converge to

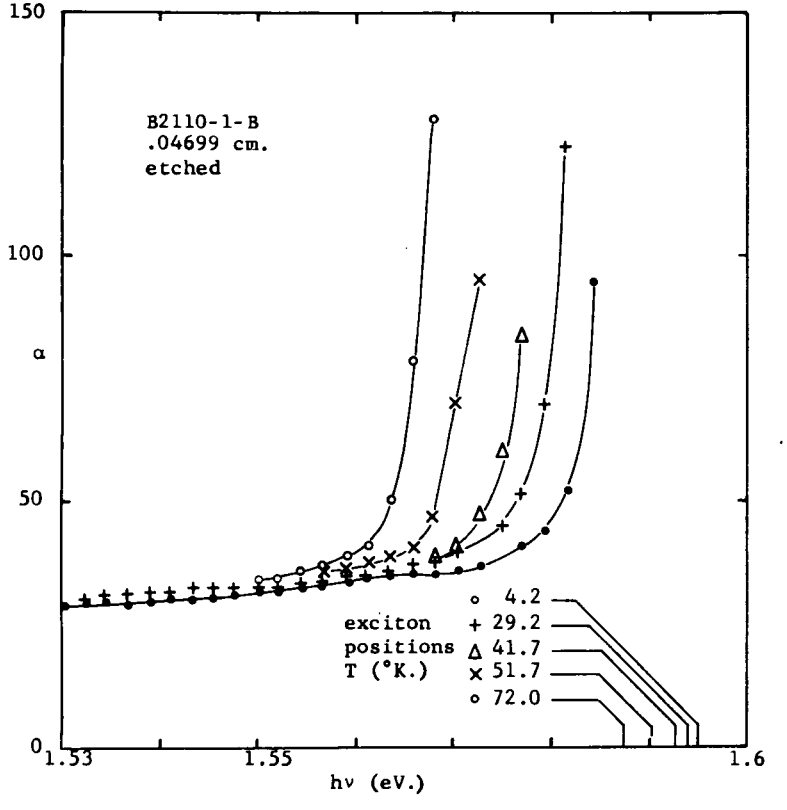

Fig. 2.2 TRANSMISSION DATA REDUCED ACCORDING TO $\alpha = \frac{1}{D} \log t_{abs}$

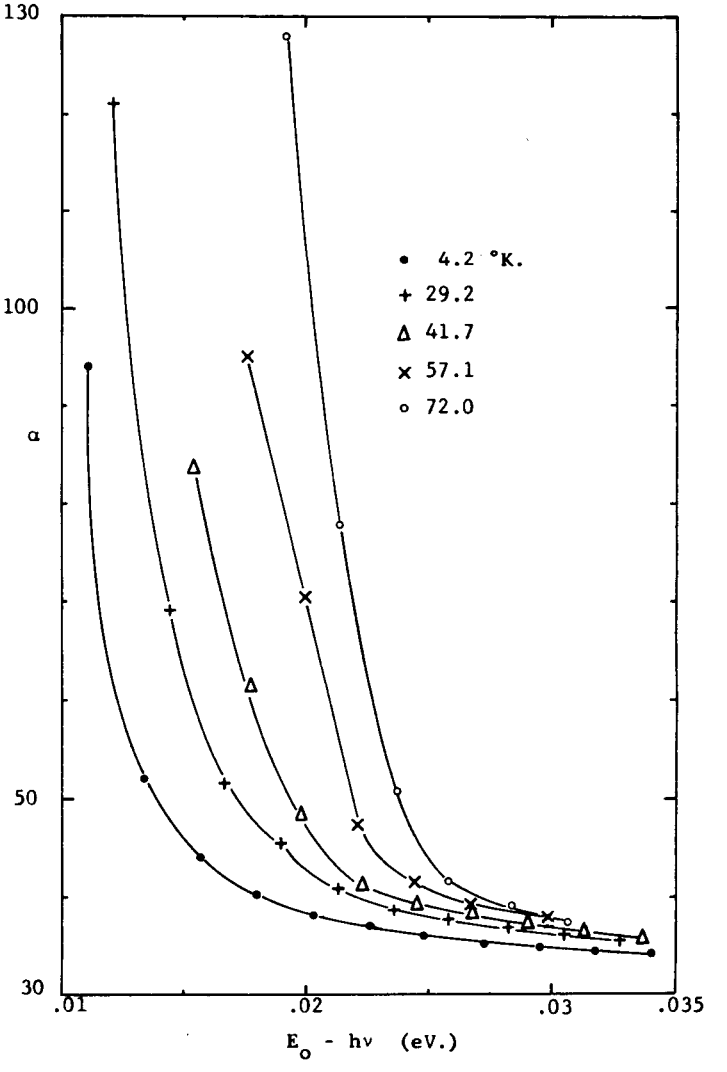

Fig. 2.3 REDUCED TRANSMISSION DATA NORMALIZED WITH RESPECT TO THE EXCITON POSITION

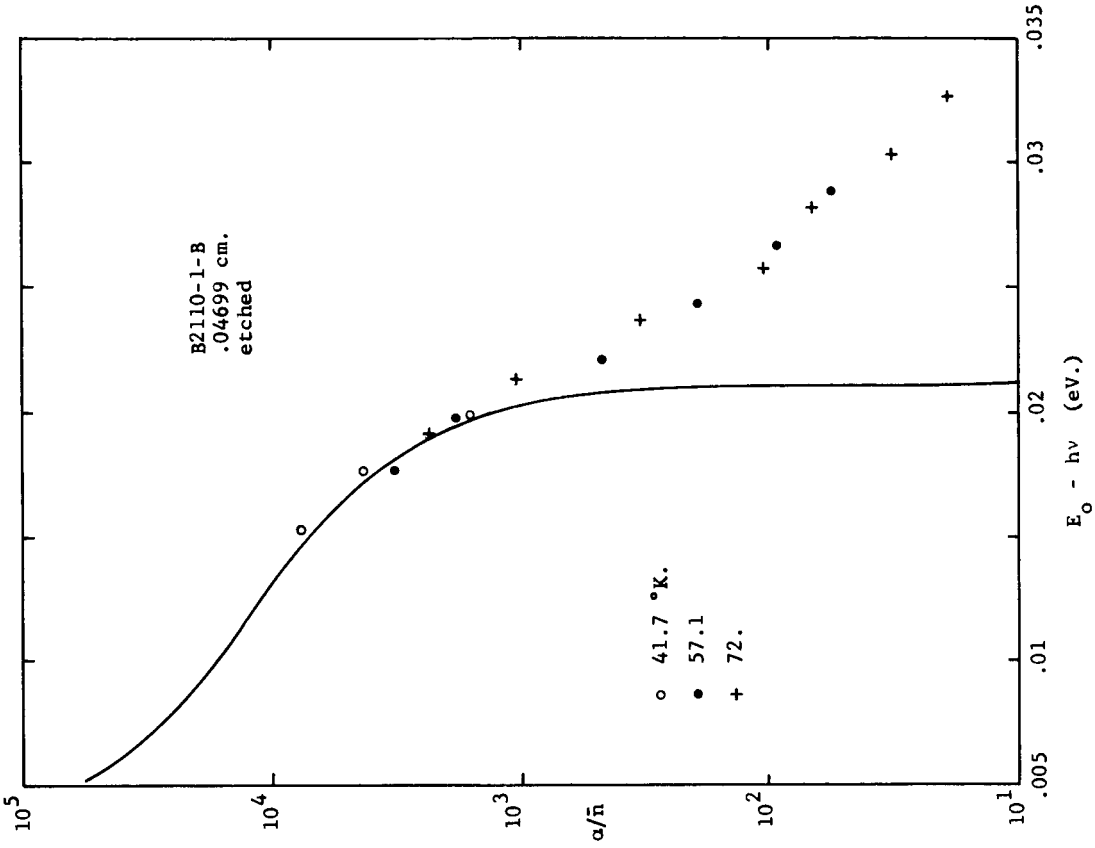

Fig. 2.5 NORMALIZED RESULTS FOR SAMPLE B2110-1-B

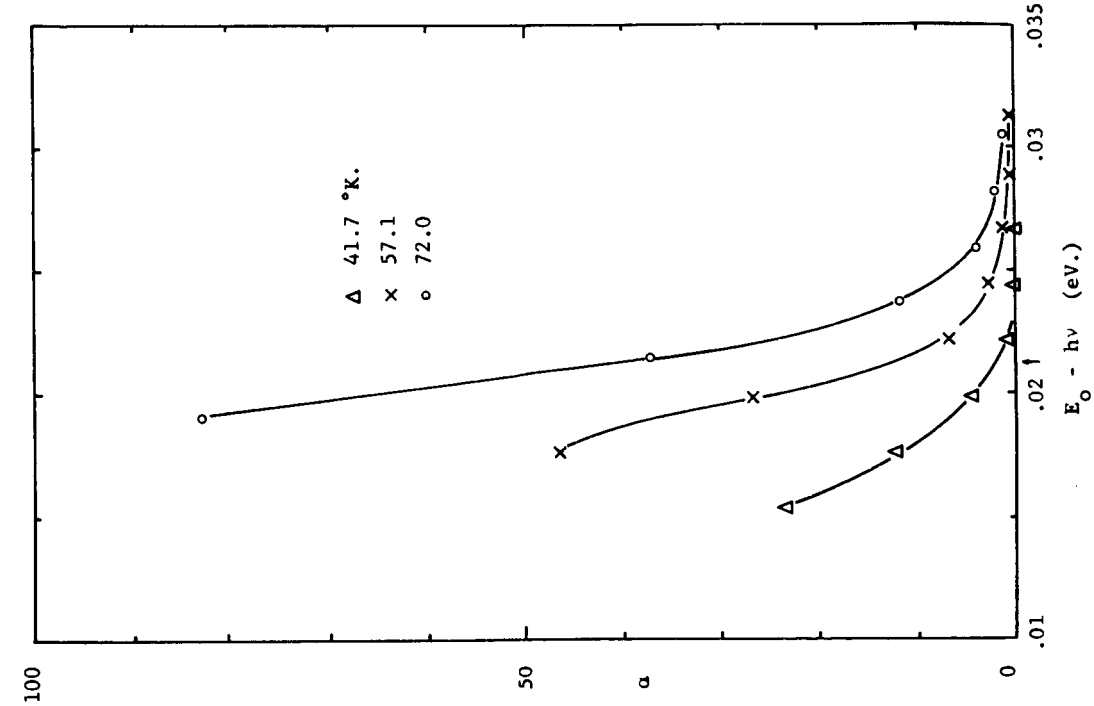

Fig. 2.4 TEMPERATURE DEPENDENT COMPONENT CORRECTED FOR BACKGROUND ABSORPTION

agree with this theory. However, a component appears below the predicted "one phonon threshold" which also is observed to exhibit a magnitude which is proportional to the occupation probability of one LO phonon.

this pattern of behavior was observed on several additional samples for which a composite presentation is shown in Figure 2.6. The quantitative agreement of theory and experiment is satisfactory over a substantial range of values. However, it is also apparent that another process involving one LO phonon is effective in contributing in the range of energy below the predicted threshold.

For purposes of comparison, the experimental results of D.T.F. Marple are shown in Figure 2.7. The only significant disagreement between the two sets of results lies in the magnitude of the component of absorption below the threshold. The qualitative dependence, however, appears to be similar. The difference of behavior between material of different sources suggests that a defect of impurity of variable concentration is involved.

2.1.6 Surface preparation

Transmission samples were lapped and then polished to a final finish with 0.5μ chromium oxide on a silk wheel. However, the residual damage causes an observable amount of optical absorption. For this reason, a subsequent chemical preparation was employed. The etch consisted of 3 parts concentrated H_2SO_4 and 7 parts saturated $K_2Cr_2O_7$ [by volume].[14] A total time of 8 minutes removed approximately 60μ from each side. The last minute of etching was carried out in fresh solution.

A comparison of two samples with surfaces which were mechanically and chemically prepared in the manner prescribed is shown in Figure 2.8. There is a difference between the two samples which is much larger than could be caused by the approximate means used to obtain the absolute bulk absorption values.

A difficulty arises in interpreting the transmission data for samples with surfaces which are irregular as a result of etching. For small absorption values, a multiple reflection correction must be applied. The reflections are accompanied by a large angular scattering. This is characteristic of the statistical distribution of angles present on the surface. Snell's law predicts a magnification of these angles by at least a factor $\bar{n}$, the optical

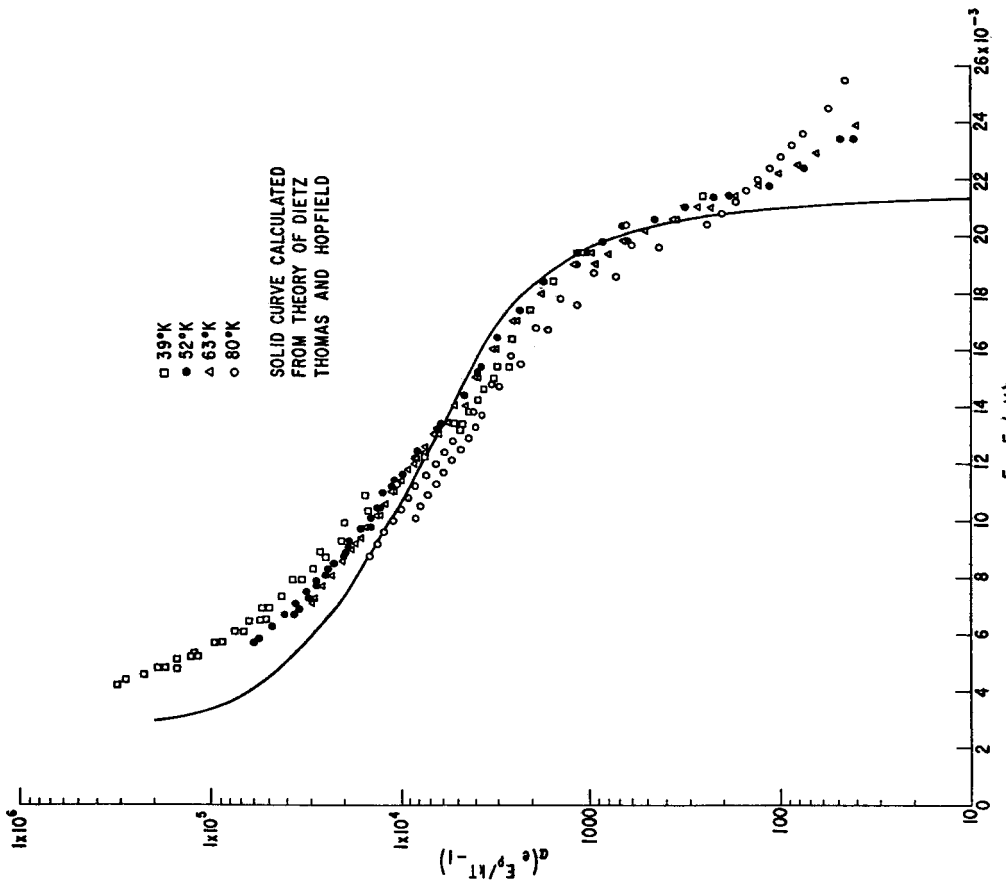

Fig. 2.7 NORMALIZED ABSORPTION DATA OF MARPLE[6]

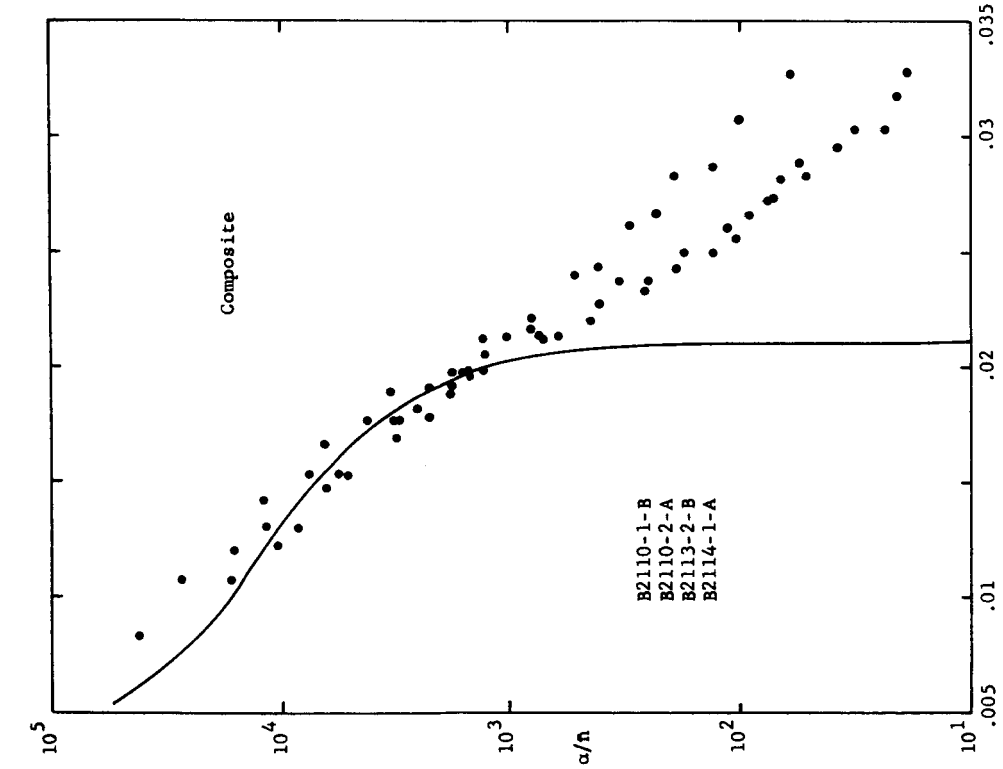

Fig. 2.6 COMPOSITE PRESENTATION OF NORMALIZED RESULTS

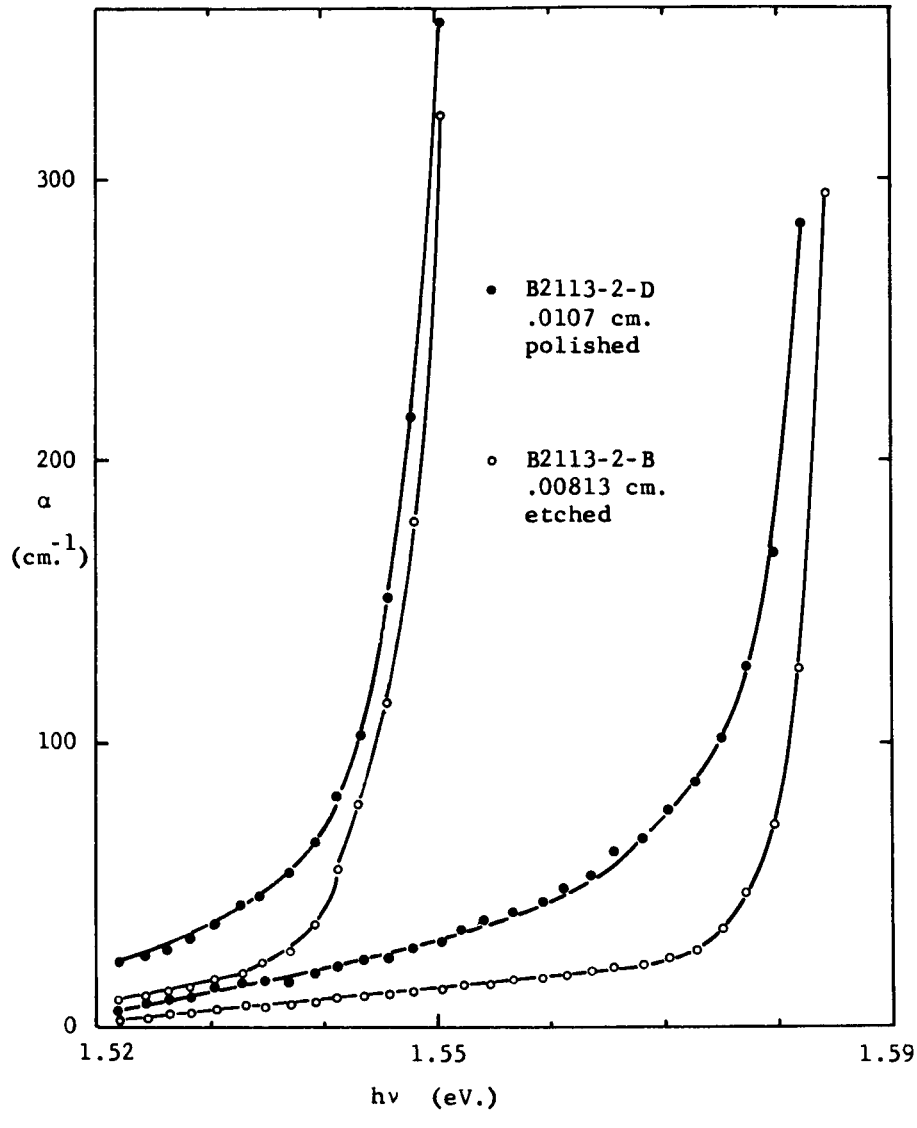

Fig. 2.8 COMPARISON OF RESULTS FROM AN ETCHED SAMPLE WITH THOSE FROM A POLISHED ONE

index, on transmission for the medium.

The solid angle subtended at the sample position by the access windows must, in order to minimize heating by ambient radiation, be small. As a consequence, some of the transmitted radiation is intercepted. This results in an imperfect measurement of the absolute transmission. The maximum angle that an axially symmetric distribution of transmitted radiation can have, and not be intercepted, is 3.5 degrees.

2.2 Theoretical Considerations

2.2.1 The relation of observed transmission to bulk absorption

For a transmission sample with plane and parallel surface the relation between absolute transmission, t, and specific bulk absorption αD is[15]

$$t = \frac{(1-R)^2}{e^{\alpha D} - R^2 e^{-\alpha D}} \tag{2.1}$$

or alternately stated,

$$\alpha D = \log \frac{(1-R)^2}{t} \frac{1}{2} \left\{1 + \left[1 + \frac{4R^2 t^2}{(1-R)^2}\right]^{1/2}\right\} \tag{2.2}$$

where R is the reflectivity a dielectric discontinuity of n, the index of refraction, i.e.,

$$R = \left(\frac{n-1}{n+1}\right)^2 \tag{2.3}$$

In recovering the temperature dependent component of absorption, a subtraction was made in order to correct for the effects of reflection. Denoting by primes the parameters associated with the lower temperature this procedure written in the formalism of equation 2.2 is

$$\alpha D - \alpha' D = \log \frac{t'}{t} + \log \frac{1 + \left[1 + \frac{4R^2 t^2}{(1-R)^4}\right]^{1/2}}{1 + \left[1 + \frac{4R'^2 t'^2}{(1-R')^4}\right]^{1/2}} \tag{2.4}$$

The quantity log t'/t is effectively that which is directly observed, and αD-α'D is the physically significant value of importance. The remaining

term in equation 2.4 provides an estimate of the error inherent to the method. In the worst possible case, i.e.,

$$t' = 0$$
$$t = t_{max} = \frac{(1-R)}{(1+R)}$$

the specific error is

$$\varepsilon = \log \frac{1}{2} \left\{1 + \left[1 + \frac{4\,R^2}{(1-R^2)^2}\right]^{1/2}\right\}$$

With R = .25 corresponding in equation 2.3 to an index of refraction, n = 3, the error is

$$\varepsilon = 0.0552$$

That this is a small error can be seen by a simple example. Consider

$$D = .01 \text{ cm}$$
$$\alpha - \alpha' = 100 \text{ cm}^{-1}$$

which are values typical of those used, then the error,

$$\alpha_\varepsilon = \varepsilon/D = 5.52$$

in a worse case estimate, is of reasonable proportion.

However, in cases studied, the effect of mechanical damage has required that chemically prepared surfaces be employed. If a measure of absolute bulk absorption were required, imperfections peculiar to the etched surface would cause a serious problem. For small specific absorption, a multiple reflection correction must be made. When the surfaces are irregular, reflection is accompanied by scattering. Even if an exact statistical description of the surfaces was available, this correction would be formitable.

It is important, however, to understand the general features of transmission through an optical medium which lacks the ideal geometry of plane and parallel surfaces. Accordingly, a description of the situation has been formulated in statistical terms and a numerical solution of the model obtained. From this the conclusion can be drawn that the contribution to the transmission by multiple internal reflections is relatively less important in the case of

imperfect surfaces.

The problem is formulated physically in terms of the off-normal incident of electromagnetic radiation on a dielectric. Here, within the range of validity of geometric optics, boundary conditions provide vector relations for the transmission and reflection. The medium is taken to be optically inactive so that an averaging over polarizations is a meaningful simplification. A large angular dispersion upon leaving a medium of high refractive index arises as a consequence of Snell's law.

The statistical features of the surface are generated by scanning a geometric model. In particular, a surface is described as being uniformly dovered by "mounds" of the analytic form

$$z = S(x^2 + y^2)$$

where S is a very small constant $\simeq .05$. Viewed from within the medium a cross sectional appearance is shown in Figure 2.9. When viewed from an angle of incidence, θ_i, part of the surface is "shadowed". The "illuminated" portion, when scanned by superposing a mesh and evaluating the surface normal vectors at the mesh points, provides a statistical distribution.

The logic of the calculation is shown in Figure 2.10. The distribution of transmitivity which is axially symmetric is shown in Figure 2.11. Results are shown for one value of the parameter S and for the initial and first order of internal reflection. In the geometry of Figure 2.9, this distribution is intercepted by a slot.

The absolute transmission for the surface parameter indicated and a slit angle $\theta_s = 3.5$ for the initial and second orders of transmission are

$$S = .02$$
$$\theta_s = 3.5°$$

Order	Transmission
0	.3555
1	.0088

This is to be compared with the case of perfect surfaces where

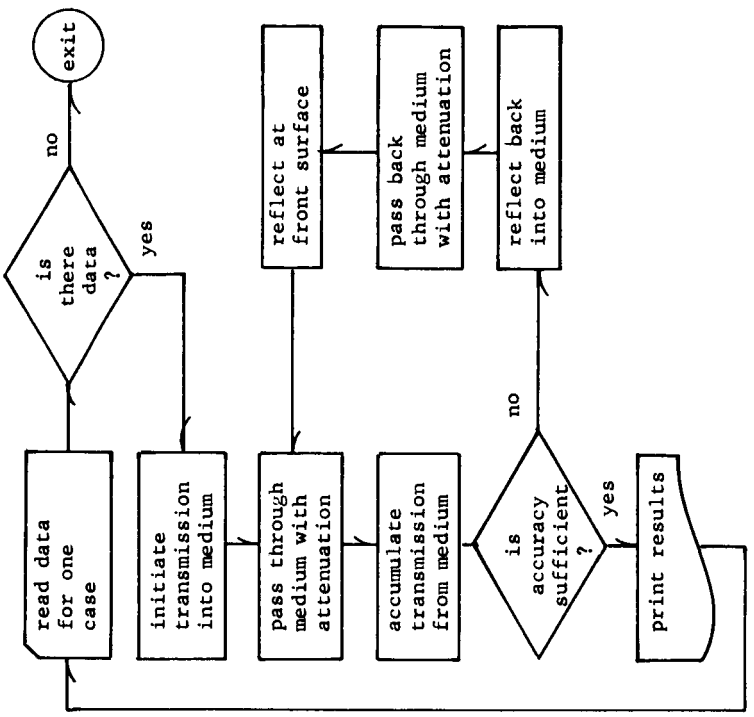

Fig. 2.10 LOGIC FOR THE MULTIPLE REFLECTION CALCULATION

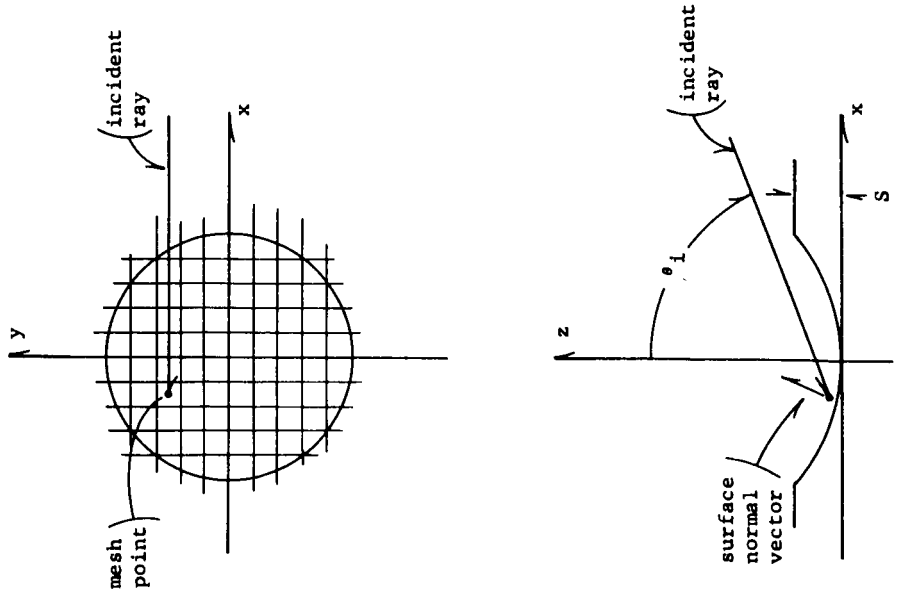

Fig. 2.9 GEOMETRY OF THE SURFACE MODEL

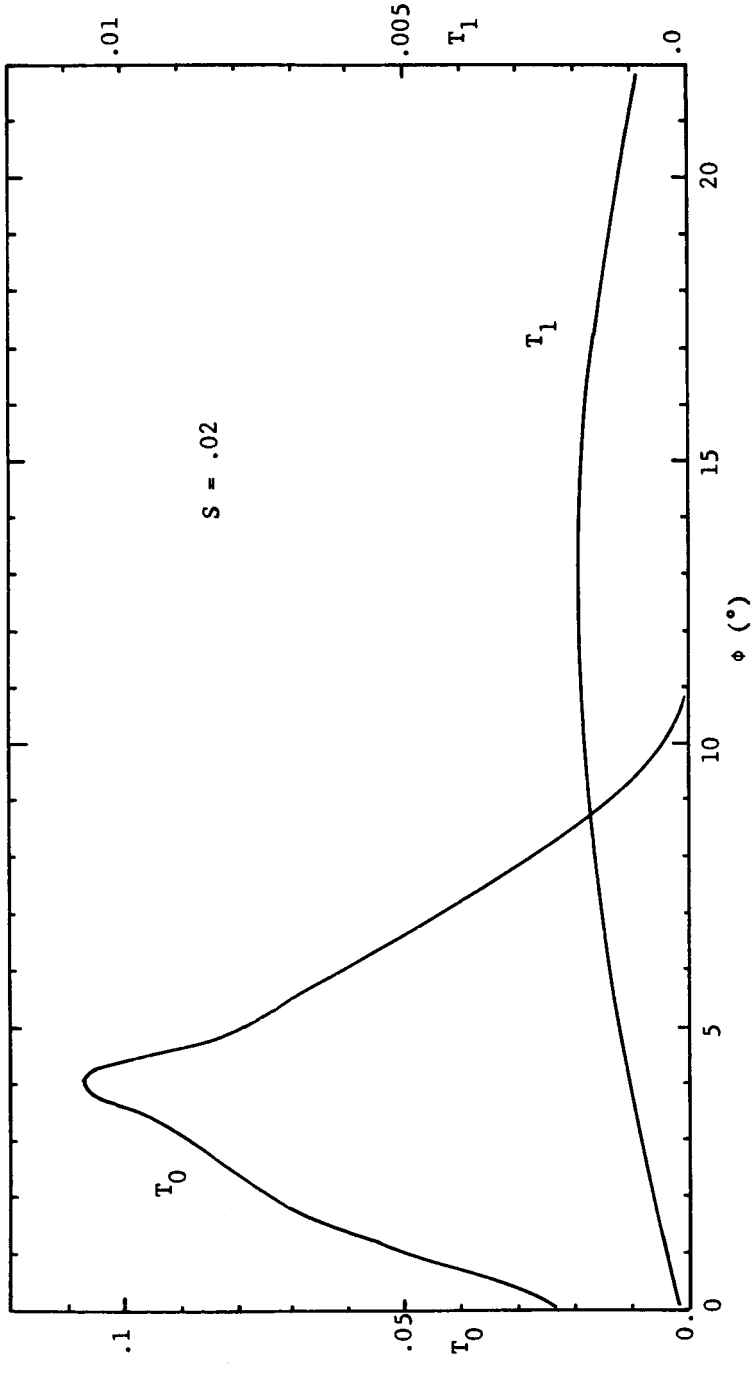

Fig. 2.11 DISTRIBUTION OF SCATTERED TRANSMISSION PROBABILITY
INITIALLY AND FOR THE FIRST ORDER OF INTERNAL REFLECTION

Order	Transmission
0	.5625
1	.0351

It is apparent that both the magnitude of the zero order and the relative magnitude of the first order are less in the case of imperfect surfaces.

2.2.2 Contribution to the optical absorption below the "one phonon threshold"

The threshold predicted by theory at one quantum of LO phonon energy below the exciton has been observed to be "soft". The mechanism responsible for this cannot be uniquely assigned. However, the behavior exhibited does provide a basis for analysis. The properties of the anomolous optical absorption are:

1. The temperature dependence is characteristic of a one LO phonon absorption.
2. The magnitude of the effect varies according to the source of the material.

From this two deductions are made:

1. An optically active level exists, the excitation energy of which lies below the lowest exciton energy.
2. The origin of this level is associated with a defect or impurity, the concentration of which can vary.

The energy of the level, E_i, can be roughly fixed as lying one quantum of LO phonon energy, $h\omega_{LO}$, above the region of observation, i.e.

$$E_o - 2h\omega_{LO} < E_i < E_o - h\omega_{LO}$$

where E_o is the excitation energy of the lowest exciton. Alternately stated, the "binding energy" of this level is

$$E_d = E_g - E_i$$

Numerically, this binding energy is expected to be about

$$E_d \simeq 0.025 \text{ ev.}$$

where, for purposes of comparison, the binding energy of the lowest exciton is about

$$E \approx .01 \text{ ev.}$$

Since the binding energy is small, the level may be described in terms of effective mass particles.[16] Since there are no known acceptor levels having a binding energy with respect to the valence band edge less than that of the C_d vacancy, 0.15, ev., the center involved is not an acceptor. However, De Nobel[17] quotes a possible donor level at $0.022 \pm .002$ ev. Since the hydrogenic model of a single charged donor predicts a binding energy of about .01 ev., his level probably arises from a doubly charged center in analogy with atomic He.[18] The shallow levels of such a center would have a binding energy of about 0.025 ev.

In the absence of more detailed information, and approximate model for the purpose of estimating an optical matrix element is taken to be that of 1s hydrogen. In a quantitative calculation of the absorption arising from such a center, two disposable parameters are required, E_d the binding energy of the level and, n_d, its concentration.

Transitions from all valence band states are allowed in the first order, i.e., in the absence of phonon assistance. Dumke has considered this case, in detail.[19] In the second order case, the valence band provides initial states, and the conduction band the intermediate states. The final states are electrons bound to the donor center. This process is schematically illustrated in Figure 2.12.

Bound levels contain components from all Bloch states. In the effective mass approximation[19] the hydrogenic wavefunction for the model assumed is

$$\psi(r) = (\pi a_d^3)^{-1/2} \, u_c(r) \, e^{-r/a_v}$$

This can be expanded as

$$\psi(r) = \sum_{k_c} A_{k_c} \, u_c(r) \, e^{ik_c \cdot r}$$

where A_{k_c} may be found by Fourier transformation as

$$A_{k_c} = 8 \, (\pi a_d^3/V)^{1/2} \, (1 + a_d^2 \, k_c^2)^{-2}$$

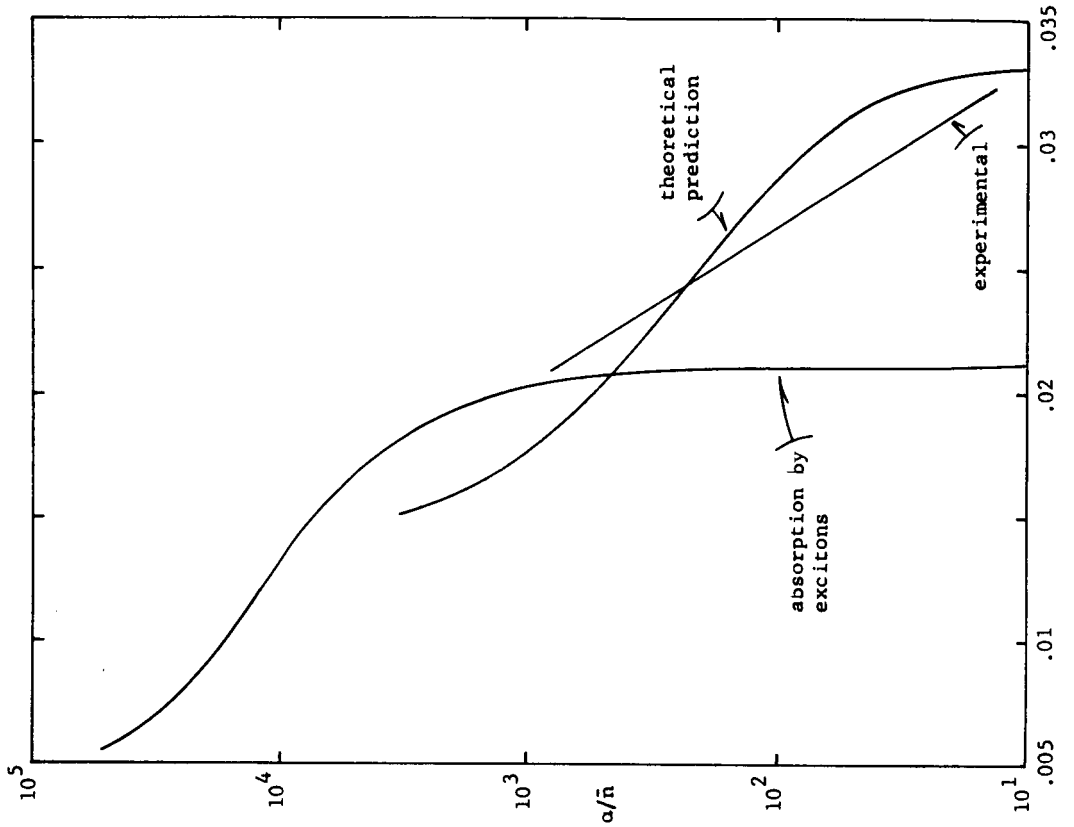

Fig. 2.13 NORMALIZED THEORETICAL PREDICTION OF ABSORPTION BY DONORS

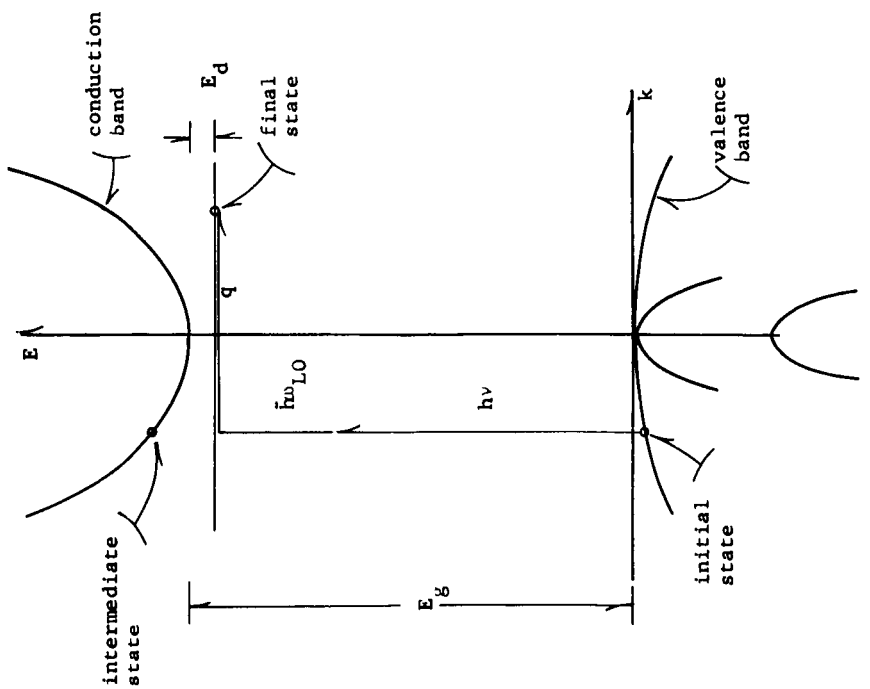

Fig. 2.12 SCHEMATIC ILLUSTRATION OF OPTICAL ABSORPTION BY A DONOR WITH ASSISTANCE FROM A PHONON

Derivation of optical absorption by second order perturbation theory requires calculation of matrix elements connecting initial and intermediate then intermediate and final states and a subsequent summations over the density of initial states and over final states. The initial and intermediate state wavefunctions are

$$\psi_o = V^{-1/2} u_v(r) e^{ik_v \cdot r}$$

and

$$\psi_i = V^{-1/2} u_c(r) e^{ik_c \cdot r}$$

The photon interaction Hamiltonian is

$$H(h\nu) = \frac{e}{m} \frac{z}{(2\pi\nu)} p_z$$

and the corresponding matrix element is

$$H_{io} = \frac{e}{m} \frac{z}{(2\pi\nu)} p_{cv} \delta_{k_c, k_v}$$

The final state wave function is

$$\psi_f = (\pi a_d^3)^{-1/2} u_c(r) e^{-r/a_d}$$

and the LO phonon interaction Hamiltonian is

$$H(h\omega_{LO},T) = H'(h\omega_{LO},T) \frac{1}{q} e^{iq \cdot r}$$

where

$$H'(h\omega_{LO},T) = e \left\{ \frac{h\omega_{LO}}{2V} \left(\frac{1}{\epsilon_\infty} - \frac{1}{\epsilon_s}\right) \frac{1}{e^{h\omega_{LO}/kT} - 1} \right\}^{1/2}$$

The matrix element is

$$H_{fi} = H' \, 8(\pi a_d^3/V)^{1/2} \, (1 + a_d^2 \, k_i^2)^{-2}$$

The transition rate arising from all LO phonons of the spectrum is

$$W_{if} = \frac{2}{h} \sum_q \left| \sum_i \frac{H_{fi} \, H_{io}}{E_{io} - h\nu} \right|^2 (E_{fo} - h\nu - h\omega_{LO})$$

The summation may be converted to integration by

$$\sum_\tau = \frac{V}{(2\pi)^3} \int d\underline{\tau}$$

The density of initial states, valence band electrons, is

$$g(E_v) = (1/2\pi)^2 \, (2m_h/\bar{h}^2)^{3/2} \, E_v^{1/2}$$

where

$$E_v = \frac{\bar{h}^2 \, k_v^2}{2m_h}$$

The number of final states is in the limit of zero (Fermi) occupation

$$N_d = n_d \, V$$

The resulting expression for the optical absorption written in a normalized form is

$$\alpha_d(h\nu, T) = \alpha_{do} \, \frac{1}{(e^{h\omega_{LO}/kT} - 1)} \, \left(\frac{E_g - E_d + h\omega_{LO} - h}{E_g - E_d} \right)^{1/2} \int_0^\infty dx \, \frac{1}{[(x-x')^2 + A]^2 [(x-x')^2 + 1]^4}$$

$$\alpha_{do} = \frac{2\,h\nu}{n\,c\varepsilon_o \mathcal{E}_z^2} \cdot \frac{2\pi}{\bar{h}} \cdot \frac{e^2}{m^2} \frac{\mathcal{E}_z^2}{(2\pi\nu)^2} |P_{cv}|^2 \frac{8\pi a_d^3}{V}$$

$$\cdot e^2 \frac{h\omega_{LO}}{2V} \left(\frac{1}{\varepsilon_\infty} - \frac{1}{\varepsilon_s}\right) a_d^2 \cdot$$

$$\cdot \frac{1}{(2\pi)^2} \left(\frac{2m_h}{\bar{h}^2}\right)^{3/2} (E_g - E_d)^{1/2}$$

$$\left(\frac{2m_h a_d^2}{\bar{h}^2}\right)^2 \cdot \frac{V}{2\pi^2} \frac{1}{a_d^3} \cdot n_d V$$

$$A = \frac{2m_h a_d^2}{\bar{h}^2} (E_g - E_d - h\nu)$$

and

$$x' = a_d k_v = \frac{2m_h a_d^2}{\bar{h}^2} (E_g - E_d + h\omega_{LO})^{1/2}$$

Numerical means were employed to evaluate the expression. To effect a comparison with the process involving excitons a common energy coordinate is required. Consider

$$\Delta' = E_g - E_d - h\nu = E_i - h\nu$$

as a measure of photon energy with respect to the direct excitation. A similar quantity

$$\Delta = E_g - E_x - h\nu = E_o - h\nu$$

appears in the process involving excitons. In terms of Δ as the common coordinate of energy

$$\Delta' = E_d - E_x + \Delta$$

The temperature dependences are the two process are the same and a fully normalized form

$$\alpha_{dn}(\Delta) = \alpha_d(\Delta,T) \cdot (e^{h\omega_{LO}/kT} - 1)$$

can be similarly be employed. The results of evaluation for the parameters

$$E_d = .022 \text{ ev.}$$
$$n_d = 2.5 \times 10^{15} \text{ cm}^{-3}$$

presented in the normalized form along with the corresponding quantity for the process involving excitons is shown in Figure 2.13. Also shown is a line which represents the dependence of the effect observed experimentally and previously reported in detail.

A unique identification of the mechanism actually involved cannot be made. Thus, this calculation series primarily to show how sensitive the presence of a sharp threshold is to a relatively small concentration of donors having the properties described. However, a level actually exists with the binding energy required.

In a sample of relatively poor optical quality, a line structure was observed. Further, the observed structure did show a magnetic field dependence. The optical absorption for the sample in question is shown in Figure 2.14. The positions of the (weak) absorption peaks which appear as "humps" on a monotonically increasing background are

$$E_p(0) = 1.584 \pm .001$$
$$E_p(5w/m^2) = 1.586 \pm .0005$$

With an exciton energy, $E_o = 1.5955 \pm .0005$ ev., and a binding energy of $E_x = .01 \pm .001$ ev., the binding energy of the observed level, E_d, is

$$E_d = E_o + E_x - E_p(0)$$
$$= 0.0215 \pm .0025$$

Thus the presence of an optically active level having an energy consistant with that of the model previously assumed is demonstrated.

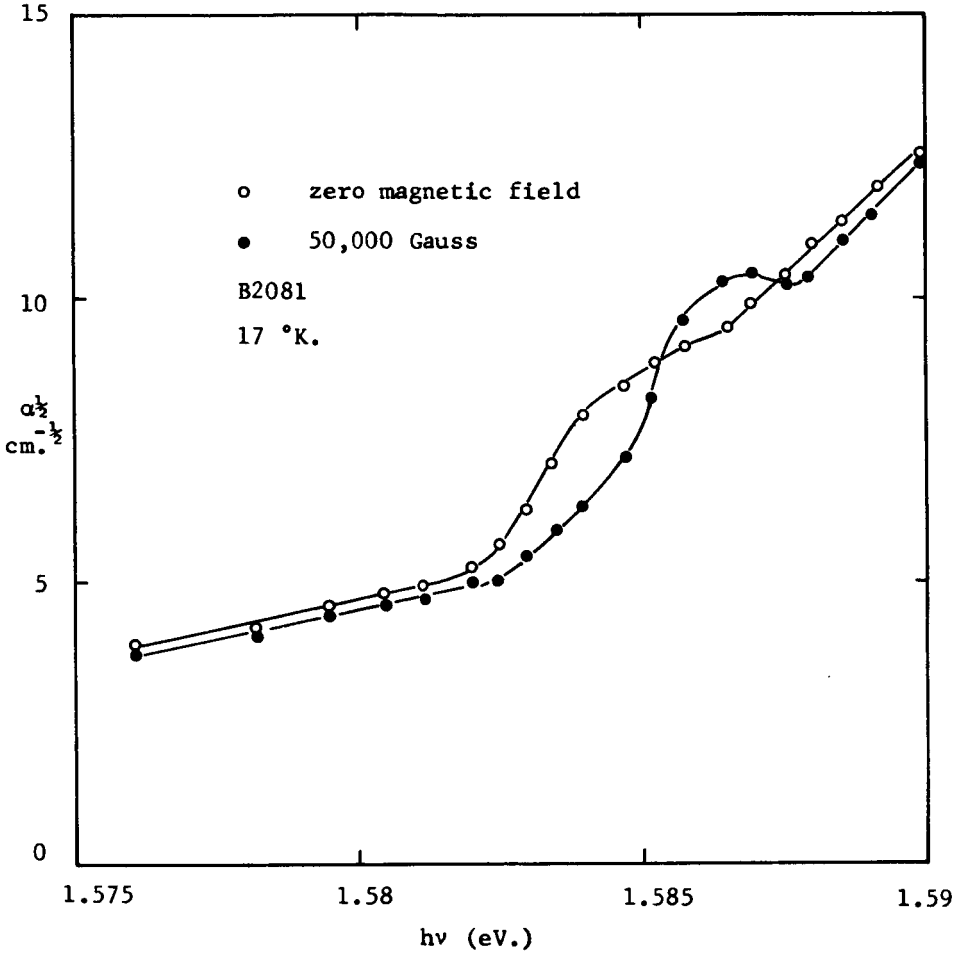

Fig. 2.14 OBSERVATION OF AN ANOMALOUS MAGNETO-OPTICAL EFFECT

2.3 References

1. "Semiannual Technical Summary Report No. 2", NASA NsG 496, M.I.T., June, 1964.

2. Marple, D.T.F. and B. Segall, Bull. Amer. Phys. Soc., 9, 223 (1964).

3. Segall, B. and D.T.F. Marple, loc. cit.

4. Andonian Associates, Inc., Waltham, Mass., Model 1237, Liquid Helium Dewar.

5. Ohmite Mfg. Co., Chicago, Ill., Little Devil (R) 1/2 w. 5% 180 ohms.

6. Carborundum Co., Electronics Div., Latrobe, Pa., Kovar to Pyrex Graded Seal 96.1028.

7. Thermo Electric Co., Inc., Saddle Brook, N.J., premium grade copper-constantan thermocouple wire N/N-36-DDT.

8. Powell, R.L., Caywood, L.P., and Bunch, M.D., "Temperature", Reinhold, New York.

9. "M.I.T. Wavelength Tables", Wiley, New York, (1939).

10. "Handbook of Chemistry and Physics", 49th ed., Chemical Rubber, Cleveland, Ohio (1962).

11. Bausch and Lomb Inc., Rochester, New York, grating 35-50-09-550.

12. Baumeister, T. and Marguardt, D.W., IBM SHARE Distribution no. 1428 (1963).

13. Halsted, R.E., (unpublished data).

14. Ischimiya, T. et al. "Solid State Physics in Electronics and Telecommunication", Academic Press, New York (1960).

15. Fan, H.Y., "Reports on Progress in Physics", Phys. Soc. London, XIX, 107, (1956).

16. Kohn, W., "Solid State Physics", 5, 274 (1960).

17. De Nobel, D., Phillips Research Reports 14, 430 (1961).

18. Lampert, M.A., Phys. Rev. Letters 1, 450 (1958).

19. Dumke, W.P., Phys. Rev., 132, 1998 (1963).

CHAPTER 3

A MULTI-TRANSITION PN JUNCTION PHOTOVOLTAIC CELL

3.0 Introduction

High efficiency solar cells can be achieved with a proper material which provides a good match to the solar spectrum. Direct transition processes make use only of photons with energy equal to or higher than the energy gap. Indirect transition processes, made possible by the presence of impurity levels in the forbidden gap, can absorb low energy photons and bring them to the conduction band.

The basic problem is the study of the relevant properties of the material, such as impurity concentration and location in the forbidden gap, capture cross section, and the engineering of the most favorable material in order to achieve the maximum efficiency. Little is known about the physical properties of traps deliberately added to the material, especially high concentration traps.

3.1 The Material

CdS has been chosen as the most suitable material. Workers in the field have reported an efficiency as high as 7 or 8 percent with solar cells made out of CdS. CdS single crystals are orange in color and very photosensitive. They can be handled easily and are not brittle. Some properties of CdS are listed below:

Energy gap : 2.42 ev. at 300°K
Hall mobility : 300 cm^2/volt sec at 300°K
Resistivity : 1 to 100 ohm-cm (bought from Clevite Corp.)
Melting point : 1480°C
Effective mass of free carriers: $.2m_e$ for electrons
$2.1m_e$ for holes

Available data on impurities in CdS shows that the material has much promise.

3.2 Contact Making and Sample Preparation

The crystals are cut by sandblasting to 1 mm x 2mm x 10mm, then cleaned with acetone and distilled water. Ohmic contacts can be obtained with indium. An ultrasonic soldering iron gives better results than electroplating. Indium does not addhere well at first, and very high contact resistance arises. If the heat is applied long enough, the contact resistance can be observed to decrease drastically from about 100K to 50 ohms. The soldering iron, the solder and the sample should be very clean in order to insure ohmic contacts which can be tested on a curve tracer. A straight and symmetric characteristic means that the contacts are ohmic.

3.3 Hall Measurements

Hall measurements have been performed in order to determine carriers concentration, hall mobility and conductivity, at room temperature and as a function of temperature, from liquid nitrogen to room temperature.

The results agree with published data. The resistivity has been found to be 3.0 ohm-cm at room temperature. Such a low resistivity is favorable. The plot of mobility as a function of temperature shows that imperfection scattering is dominant ($\mu \alpha T^{3/2}$). The material is strongly n-type. At 77°K the carrier concentration is $10^{15}/cm^3$.

3.4 Photoconductivity

Trapping action and recombination processes can be studied using the relaxation kinetics of the photocurrent and its steady state under the excitation of short light pulses. A typical oscillogram of the photocurrent is as shown.

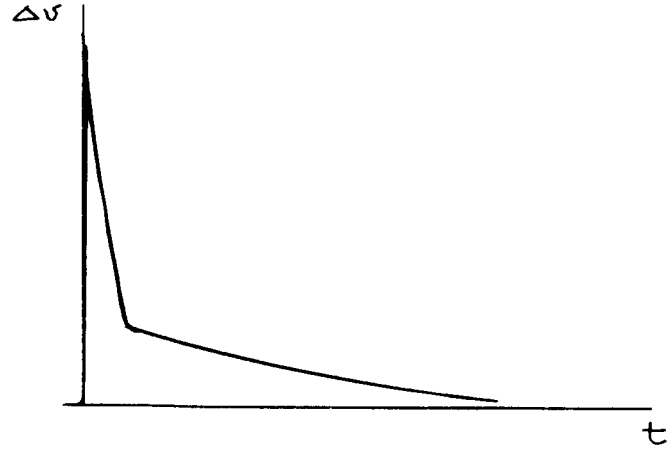

It can be observed that there are two distinct decay time constants: One very short, of the order 10 microseconds, comparable to the decay time of the light pulse which makes it hard to draw any conclusion, the second decay time is of the order 20 milliseconds. It is also observed that only high illumination shows a strong difference between the two regions. These observations agree with the results found by other workers (Soviet Physics-Solid State, Vol. 5, no. 2, Aug. 1963 p. 289 and no. 1 July, 1963 p. 174).

3.5 Some Conclusions

There is some fast action due to shallow traps. At low level excitation, trap concentration is high enough to recapture all freed electrons, only one decay time is observed. At high level excitation, deeper traps come into play. When all shallow traps have been filled, electrons are captured by deeper ones, giving rise to a much longer decay time.

We are interested in those deep traps and would like to investigate further on their nature. An experiment shall be designed to learn about their location, their capture cross-section and their concentration. If they prove to be effective photon-interaction centers and stepping stones for electrons from the valence band, possible ways of incorporating them into the material shall also be investigated.

CHAPTER 4

THERMAL AND ELECTRONIC TRANSPORT PROPERTIES OF ZINC ANTIMONIDE

4.0 Introduction

Zinc antimonide is an anisotropic semiconductor with good thermoelectric characteristics in the moderate temperature range.

The objects of this work are to gain information about the basic electronic conduction processes in ZnSb through thermoelectric and galvanomagnetic studies of single crystal samples and to empirically evaluate the thermoelectric properties of ZnSb near room temperature.

Large single crystals of ZnSb have been produced. Copper is used as an acceptor dopant. A number of attempts to produce n-type ZnSb by doping with Al, Se, or In have failed. All electrical and thermal measurement programs are progressing satisfactorily. Thus far, measurements on this orthorhombic semiconductor indicate no anisotropy in the thermoelectric power, about a 20 percent variation in the thermal conductivity, and a 200 percent variation in electrical conductivity between the three principal axes. Due to the relatively large anisotropy in the electrical conductivity, electric and thermal currents should be along the "c" axis of the crystal to give the largest thermoelectric figure of merit.

4.1 Macroscopic Symmetry Considerations in the D_{2h} Point Group

It is obviously important to have a knowledge of the number of independent tensor elements required to characterize the physical properties of a crystalline material before measurements are begun. Using symmetry considerations, Nye[1] has tabulated the possible non-zero tensor elements for the common physical properties of crystals in each of the 32 point groups. This tabulation does not include properties which relate to dependence upon magnetic field strength. Reed and Marcus[2] have published the non-zero tensor coefficients of an expansion of the electrical resistivity up to second order in magnetic field strength for the D_{2h} point group. In the principal coordinate system of the crystal, there are 3 independent zero magnetic field resistivities, 3 independent Hall coefficients (when Onsager symmetry is included), and 12 independent magnetoresistance coefficients.

TABLE 4.1

POSSIBLE NON-ZERO TENSOR ELEMENTS FROM MACROSCOPIC CRYSTAL SYMMETRY CONSIDERATIONS IN THE D_{2h} POINT GROUP

Second rank tensor elements are given up through fourth order terms in a phenomenological expansion in magnetic field strength. Onsager symmetry has not been included.

The crystal is referenced to its principal coordinate system. The numbers in parentheses indicate the multiplicity of equivalent coefficients.

Element of Tensor	$T_{11}(H)$	$T_{22}(H)$	$T_{33}(H)$	$T_{12}(H)$	$T_{13}(H)$	$T_{23}(H)$	$T_{21}(H)$	$T_{31}(H)$	$T_{32}(H)$
0^{th} order in H	T°_{11}	T°_{22}	T°_{33}						
1^{st} order in H				T_{123}	T_{132}	T_{231}	T_{213}	T_{312}	T_{321}
2^{nd} order in H	T_{1111}	T_{2211}	T_{3311}	$(2)T_{1212}$	$(2)T_{1313}$	$(2)T_{2323}$	$(2)T_{2121}$	$(2)T_{3131}$	$(2)T_{3232}$
	T_{1122}	T_{2222}	T_{3322}						
	T_{1133}	T_{2233}	T_{3333}						
3^{rd} order in H	$(6)T_{11123}$	$(6)T_{22213}$	$(6)T_{33312}$	T_{12333}	T_{13222}	T_{23111}	T_{21333}	T_{31222}	T_{32111}
				$(3)T_{12113}$	$(3)T_{13112}$	$(3)T_{23122}$	$(3)T_{21113}$	$(3)T_{31112}$	$(3)T_{32122}$
				$(3)T_{12223}$	$(3)T_{13233}$	$(3)T_{23133}$	$(3)T_{21223}$	$(3)T_{31233}$	$(3)T_{32133}$
4^{th} order in H	T_{111111}	T_{221111}	T_{331111}						
	T_{112222}	T_{222222}	T_{332222}						
	T_{113333}	T_{223333}	T_{333333}						
	$(6)T_{111122}$	$(6)T_{221122}$	$(6)T_{332233}$	$(4)T_{121112}$	$(4)T_{131333}$	$(4)T_{232333}$	$(4)T_{211222}$	$(4)T_{311333}$	$(4)T_{322333}$
	$(6)T_{111133}$	$(6)T_{221133}$	$(6)T_{331122}$	$(4)T_{122221}$	$(4)T_{131113}$	$(4)T_{232223}$	$(4)T_{212111}$	$(4)T_{311113}$	$(4)T_{322223}$
	$(6)T_{112233}$	$(6)T_{222233}$	$(6)T_{331133}$	$(12)T_{121233}$	$(12)T_{131223}$	$(12)T_{232311}$	$(12)T_{211233}$	$(12)T_{311223}$	$(12)T_{322311}$

Example: Through 4^{th} order in H

$$T_{11}(H) = T^{\circ}_{11} + T_{1111} H_1^2 + T_{1122} H_2^2 + T_{1133} H_3^2 + 6T_{11123} H_1H_2H_3 + T_{111111} H_1^4 + T_{112222} H_2^4 + T_{113333} H_3^4 + 6T_{111122} H_1^2H_2^2 + 6T_{111133} H_1^2H_3^2 + 6 T_{112233} H_2^2H_3^2 + \cdots$$

Since higher order terms may appear in the experimental data, a calculation of all of the possible non-zero tensor coefficients in a phenomenological expansion in the magnetic field of a second rank tensor was made for the D_{2h} point group. The calculation includes terms up through those of 4th order in magnetic field.

The results of this calculation are given in Table 4.1 along with an example of the use of the table. Onsager symmetry has not been applied in this table. Hence, it can be used for any physical property which can be represented as a second rank tensor. Benzol, TiO_2, CdSb, gallium and materials with the Olivine structure are a few crystalline materials that have the same point group as ZnSb.

When applied to electrical resistivity Onsager symmetry requires that:

$$\rho_{ij}(\hat{H}) = \rho_{ji}(-\hat{H})$$

where $\hat{H}$ is the magnetic field intensity vector. Hence, using Table 4.1 along with this additional symmetry consideration, the electrical resistivity may be written down immediately. Assigning subscripts according to the following table of permutations:

i	j	k
1	2	3
2	3	1
3	1	2

where 1, 2, and 3 are the principal directions in the orthorhombic crystal unit cell, the electric field which is produced by an arbitrarily oriented electric current density may be written as:

$$E_i = J_i \left(\rho^{\circ}_{ii} + \rho_{iiii} H_i^2 + \rho_{iijj} H_j^2 + \rho_{iikk} H_k^2\right)$$

$$+ J_j \left(\rho_{ijk} H_k + 2 \rho_{ijij} H_i H_j\right)$$

$$+ J_k \left(\rho_{ikj} H_j + 2 \rho_{ikik} H_i H_k\right)$$

with the following higher order terms:

$$+ J_i \left(\rho_{iiiiii} H_i^4 + \rho_{iijjjj} H_j^4 + \rho_{iikkkk} H_k^4\right.$$

$$+ 6 \rho_{iiiijj} H_i^2 H_j^2 + 6 \rho_{iiiikk} H_i^2 H_k^2$$

$$\left. + 6 \rho_{iijjkk} H_j^2 H_k^2\right)$$

$$+ J_j \left(\rho_{ijkkk} H_k^3 + 3 \rho_{ijiik} H_i^2 H_k + 3 \rho_{ijjjk} H_j^2 H_k\right.$$

$$+ 4 \rho_{ijiiij} H_i^3 H_j + 4 \rho_{ijijjj} H_i H_j^3$$

$$\left. + 12 \rho_{ijijkk} H_i H_j H_k^2\right)$$

$$+ J_k \left(\rho_{ikjjj} H_j^3 + 3 \rho_{ikiij} H_i^2 H_j + 3 \rho_{ikjkk} H_j H_k^2\right.$$

$$+ 4 \rho_{ikikkk} H_i H_k^3 + 4 \rho_{ikiiik} H_i^3 H_k$$

$$\left. + 12 \rho_{ikijjk} H_i H_j^2 H_k\right)$$

4.2 Magnetic Field Dependence of the Hall Effect and Magnetoresistance in P-Type Zinc Antimonide

4.2.1 Hall effect

The Hall effect has been measured in undoped ($p \simeq 3 \times 10^{16}$ cm^{-3}) and copper doped ($p \simeq 4 \times 10^{17}$ cm^{-3} and $p \simeq 1 \times 10^{19}$ cm^{-3}) ZnSb at room temperature and at liquid nitrogen temperature for magnetic fields between 250 gauss and 12.5 kilogauss. The measured Hall voltages were linear in B, showing only an apparently non-systematic $\pm$ 2 percent maximum deviation from a linear field dependence. These fluctuations are within the experimental accuracy of the measurement.

4.2.2 Magnetoresistance

Magnetoresistance has been measured in the undoped and the lightly copper doped samples referred to above at liquid nitrogen temperature for magnetic field densities between 8 and 12.5 kg. The magnetoresistance follows a simple B^2 magnetic field dependence within $\pm$ 5 percent. This is within the experimental accuracy of the measurement. No systematic deviations from a B^2 dependence are observed in the magnetic field range of 8 to 12.5 kg.

4.3 Carrier Precipitation in Undoped P-Type ZnSb Crystals

Most of the researchers who have worked with single crystals of ZnSb have reported that the carrier concentrations increase with time when the crystal is held at elevated temperatures. This observation was first made by Kot and Kretsu[3] in 1958 and is very apparent in their published data. This behavior was also noticed by R. Mazelsky in 1960.[4] More recently in 1964, Komiya, Masumoto and Fan,[5] have mentioned the same observation. Justi, Rasch and Schneider[6] do not report this behavior, but neither do they report any high temperature data.

The only explanation of this observation was advanced by Kot and Kretsu who said that the crystals were possibly subject to "thermal dissociation". However, they and Mazelsky report that the apparent carrier concentrations would slowly decrease with time under room temperature storage.

This behavior of ZnSb has been observed and some preliminary results will be reported. At this time it seems reasonable to hypothesize that this process is similar to the precipitation of Te in PbTe crystals which

has been reported by Scanlon.[7]

Our experiments are conducted by annealing Hall samples of single crystal ZnSb in an open tube furnace. The ambient atmosphere is either nitrogen or argon with a flow rate of about one s.c.f.h. The results are not dependent on which gas is used. Annealing temperatures have been varied between 65 and 240°C and it has been found that an equilibrium condition is apparently reached in several hours of annealing time.

Most of the data has been taken on samples that are annealed with the electrical contacts in place. The electrical contacts are copper wires soldered with 50-50 lead-tin solder using Rosin flux. A typical experimental run consists of measuring the room temperature Hall effect and resistivity of the sample, demounting from the sample holder, washing the sample in trichlorethylene, acetone and methyl alchol, annealing, air quenching to room temperature, remounting in the sample holder, and monitoring the Hall effect and resistivity as a function of time. The first electrical measurements are taken within 1/3 to 1 hour of the moment when the temperature drops to end the annealing cycle.

At the present time, two samples have been annealed without the electrical contacts in place. These samples were provided with sidearms to which the voltage contacts were attached. The usual galvanomagnetic samples are simple rectangular parallelepipeds. The sidearm samples were subjected to the same experimental procedure already outlined except that all traces of lead-tin solder contact material were removed by sandblasting before an annealing cycle took place.

The apparent hole concentration was obtained by simply inverting the measured Hall coefficient. The observed carrier concentrations are plotted as a function of reciprocal annealing temperature in Fig. 4.1. Good straight lines are obtained. The slopes correspond to an apparent activation energy of 1.0 ev. The points obtained for the contactless samples lie below the points which are obtained for the samples annealed with the contacts in place. This could result from contact diffusion, gross structural defects in the contactless samples, anistropy in the Hall coefficient, or the differences in gross geometry between the sidearm samples and the samples which had small area contacts soldered directly to their surfaces. Present experimental evidence indicates that this

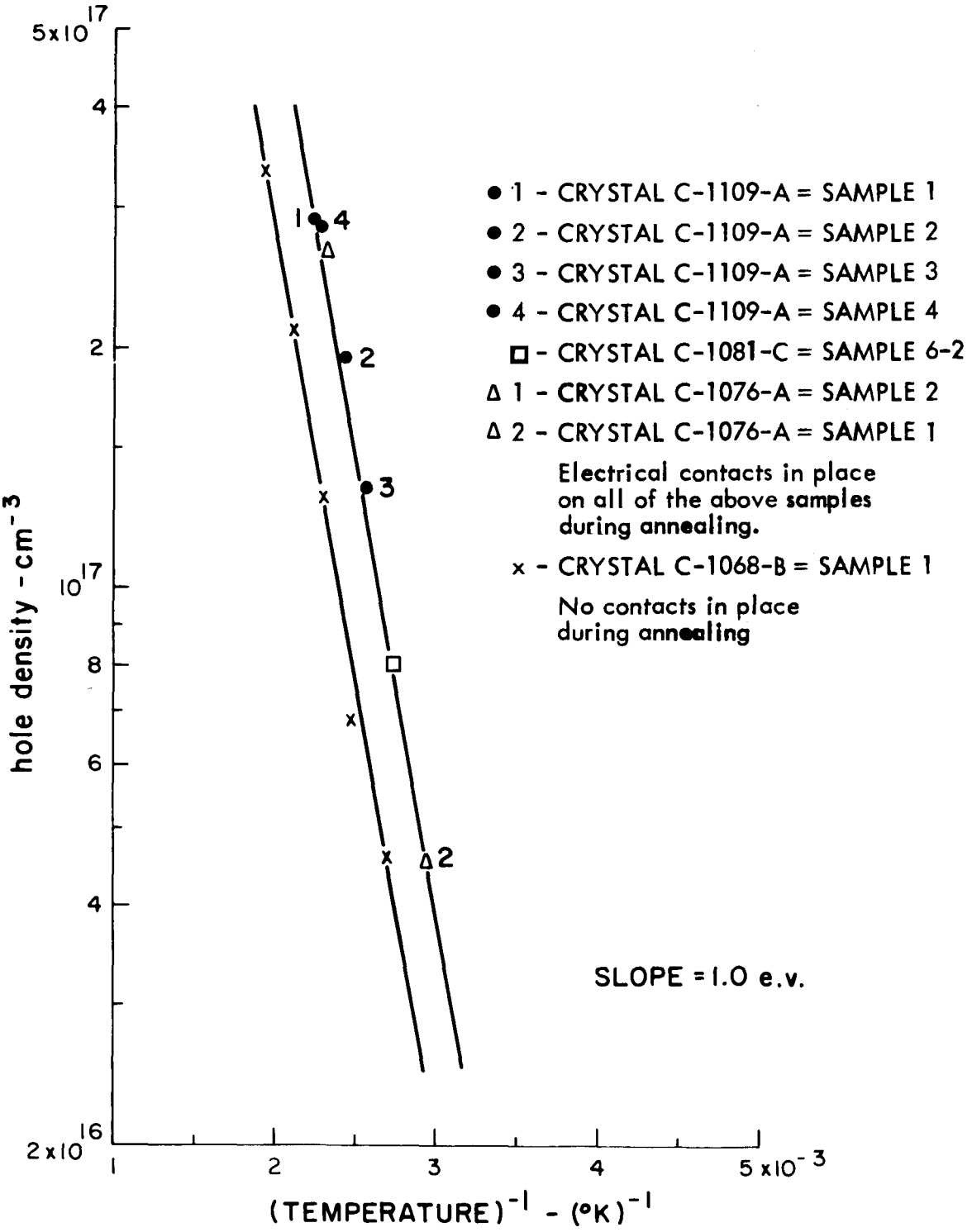

Fig. 4.1 Carrier Concentration vs. Reciprocal Annealing Temperature - p type ZnSb

discrepancy mainly results from the difference in geometry between the side-arm and the small area contact samples.

After annealing the apparent hole concentration decreases with time. This recovery has been monitored as several samples. A typical result is plotted as Fig. 4.2. The initial slope of the recovery curves indicate an initial $t^{2/3}$ time dependence. At large times, the curves seem to approach a $(1-e^{-t})$ behavior.

A tentative explanation of what may be happening can be briefly stated. This model is essentially the same as that advanced for the similar behavior of p-type lead telluride.[7]

This model states that Fig. 4.1 is essentially a representation of the ZnSb retrograde solidus line on the Zn-Sb phase diagram. The ZnSb lattice can be thought of as containing more antimony at the higher temperature. Of course, it is uncertain whether excess antimony or zinc is incorporated into the lattice at higher temperatures. The nature of the electrically active point defect in the lattice is also open to speculation. At any rate, at higher temperatures, it is possible that additional antimony is supplied by crystal dislocations which act as a source or a sink for antimony depending upon the annealing temperature involved and the exact shape of the retrograde solubility line.

Hence when a crystal is annealed at an elevated temperature, a new concentration of electrically active antimony (or zinc) is incorporated into the lattice and the hole concentration increases. This new equilibrium is reached in a fairly short time - several hours. Afterwards, when the crystal is allowed to remain at room temperature, the antimony (or zinc) precipitates out on dislocation lines in the crystal as electrically neutral atoms. This room temperature precipitation process is slow. taking hundreds or thousands of hours. Ham[8] has presented a theory for diffusion assisted precipitation. The theory predicts a slope of $t^{2/3}$ for the initial portion of the precipitation curve and a long time limiting behavior of $(1-e^{-t})$. Apparently, these time functions are being observed here.

Once again, it is emphasized that the interpretation of these physical measurements is still under consideration. The given model seems to be the most reasonable one at the present time. It seems apparent that this

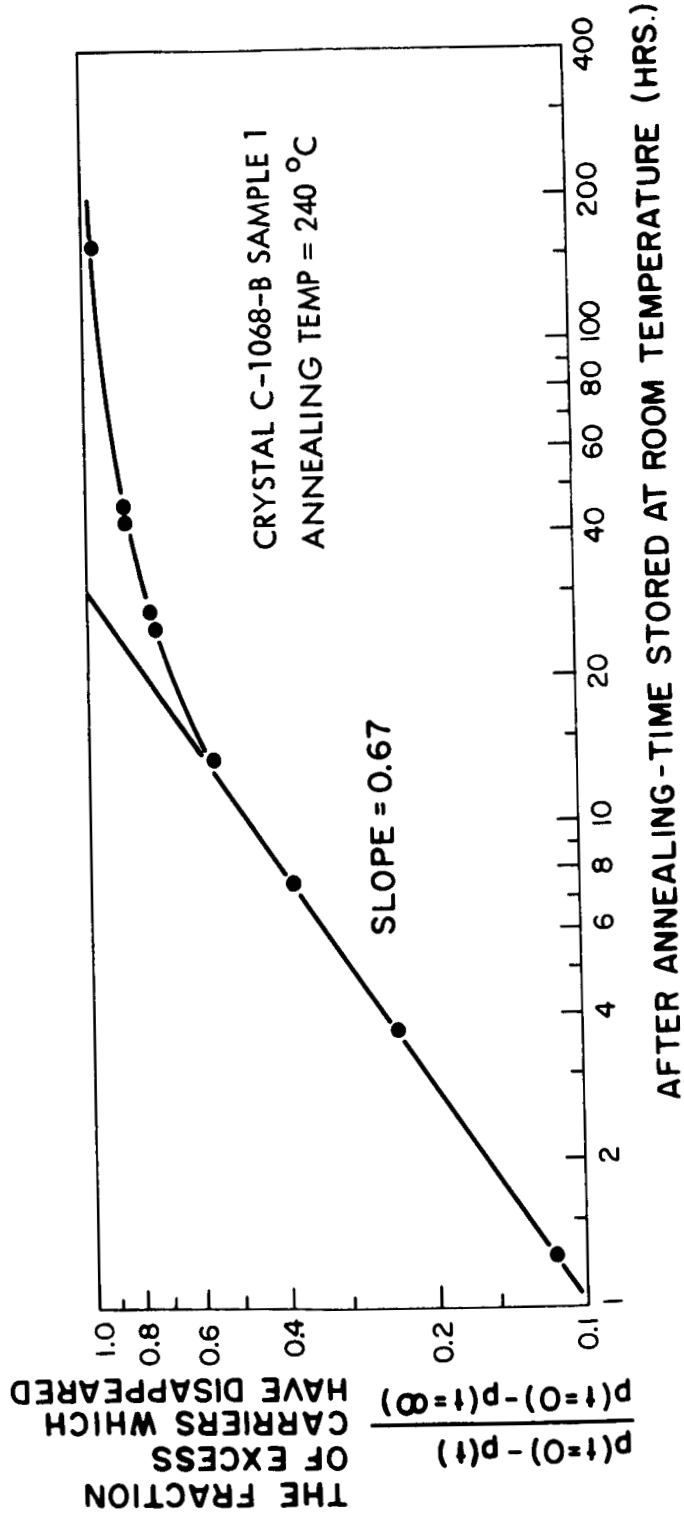

Fig. 4.2 Recovery of p-type ZnSb after Annealing

phenomena can have a profound influence on the results of electrical measurements or ZnSb - especially on undoped crystals. For example, crystals are usually cycled down to room temperature in a matter of hours after growth. But, the hole concentrations in a newly grown crystal may take weeks or months to equilibrate at room temperature. This complicates the determination of the anisotropy of the galvanomagnetic properties of ZnSb.

4.4 Hall Mobility as a Function of Temperature in p-type ZnSb

4.4.1 Undoped samples $p \sim 3 \times 10^{16}$ cm^{-3}

Measurements of the electrical conductivity and Hall effect have been made between liquid nitrogen temperature and room temperature. The resulting Hall mobilities are plotted in Fig. 4.3. This data is similar to that presented by Komiya, Masumoto and Fan,[5] except that the slopes of the straight lines are about 10 percent lower and the Hall mobilities are about 20 percent higher than in their material. Their crystals were grown by the Czochralski technique.

4.4.2 Copper doped samples $p \sim 4 \times 10^{17}$ cm^{-3}

Copper is being used as an acceptor impurity in ZnSb. Copper is added to the molten zone in the horizontal zone recrystallization process and is incorporated into the crystal during its growth. There is some evidence that copper has higher solubility limits than silver or gold in ZnSb.[9] Measurements have been completed on a copper doped crystal with a carrier concentration of about 4×10^{17} cm^{-3}. The Hall mobilities are shown in Fig. 4.4. Evidently, a considerable amount of impurity scattering is present near liquid nitrogen temperatures. These measurements are being extended to more heavily copper doped samples.

4.4.3 Anisotropy of the electrical conductivity

The above results may be used to give a good indication of the degree of anisotropy of the electrical conductivity of ZnSb. Results are also taken from Fig. 2 of the recent paper by Komiya, Masumoto, and Fan.[5] Table 4.2 provides a summary of the anisotropy. The results are fairly consistent and indicate that $\sigma_c = 1.5\ \sigma_a = 3\ \sigma_b$ at 0°C.

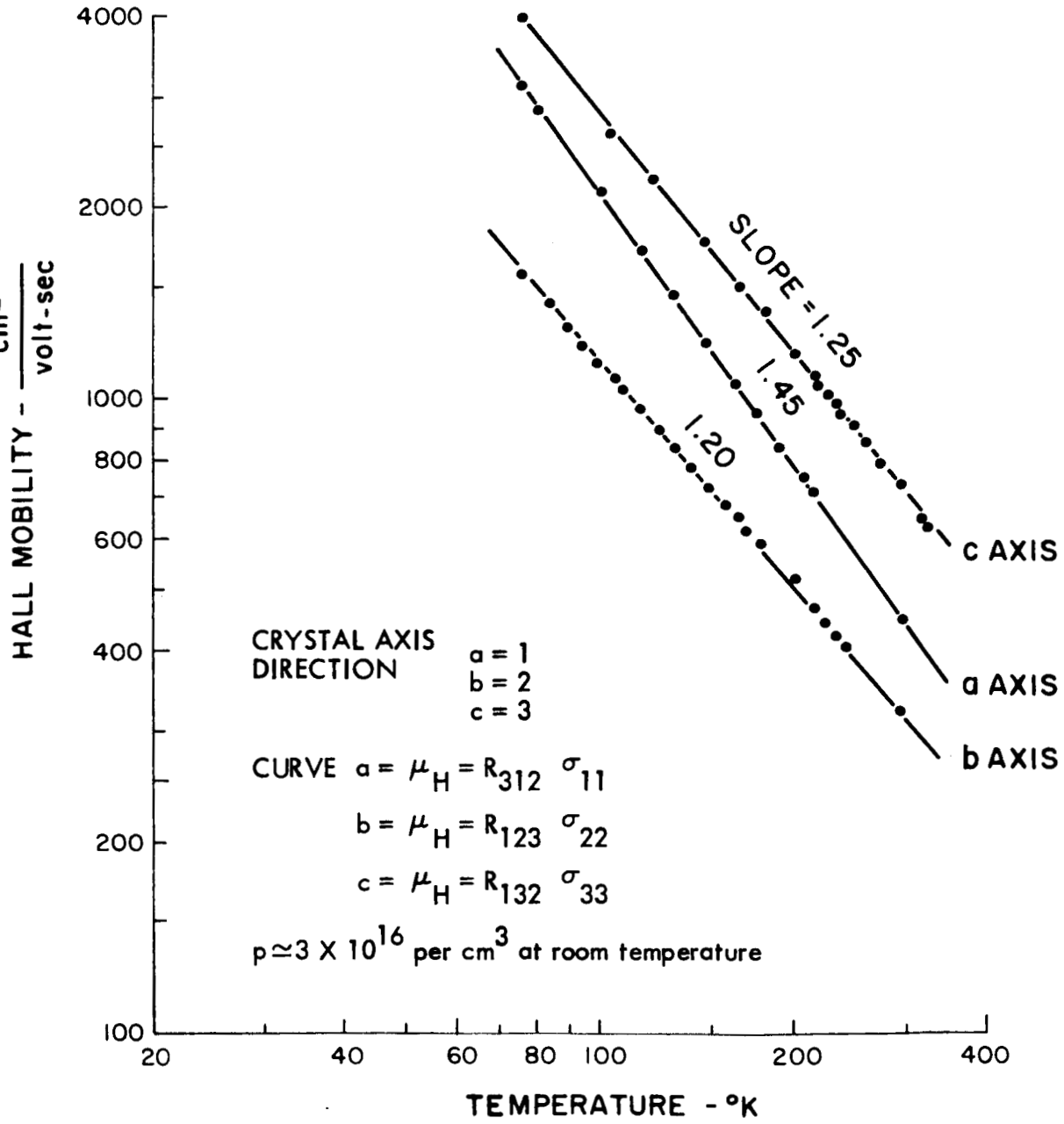

Fig. 4.3 Hall Mobilities of Undoped p-type ZnSb

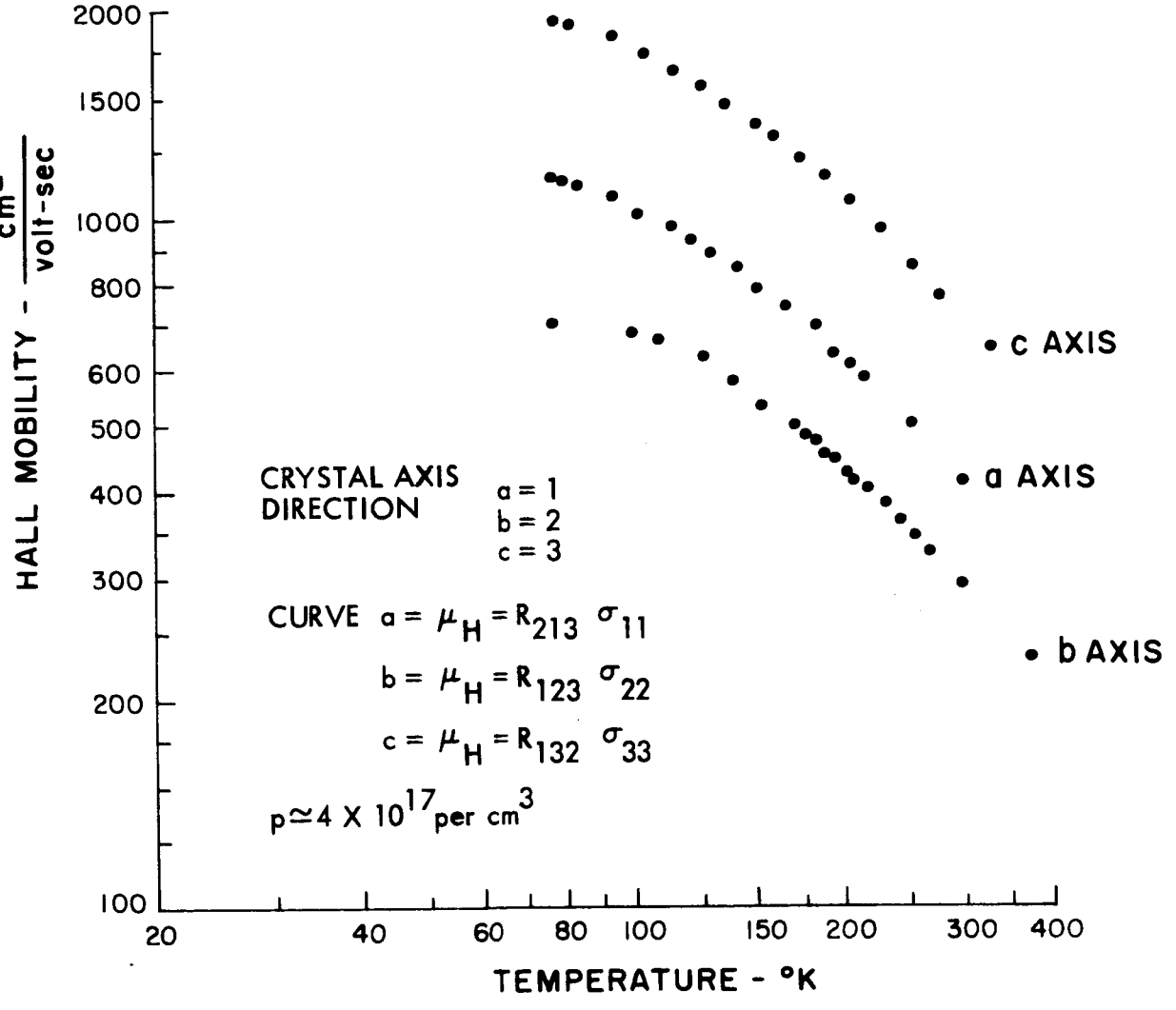

Fig. 4.4 Hall Mobilities as a function of Temperature p-type ZnSb-Copper Doped

TABLE 4.2

ANISOTROPY IN THE ELECTRICAL CONDUCTIVITY
OF P-TYPE ZnSb AT 0°C

Crystal C-1081-C Undoped $p \simeq 3 \times 10^{16}$ cm^{-3}

Ratio of Hall Mobilities in $\frac{cm^2}{volt\text{-}sec.}$

$$\frac{\mu_b}{\mu_a} = \frac{330}{530} = 0.62 \qquad \frac{\mu_c}{\mu_a} = \frac{820}{530} = 1.55$$

Komiya, Masumoto and Fan[5] Undoped Crystal

Ratio of Hall Mobilities in $\frac{cm^2}{volt\text{-}sec.}$

$$\frac{\mu_b}{\mu_a} = \frac{180}{400} = 0.45 \qquad \frac{\mu_c}{\mu_a} = \frac{620}{400} = 1.55$$

Crystal C-1078-C Copper Doped $p \simeq 4 \times 10^{17}$ cm^{-3}

Ratio of Electrical Conductivities in $(ohm\text{-}cm)^{-1}$

$$\frac{\sigma_b}{\sigma_a} = \frac{21.5}{35.6} = 0.60 \qquad \frac{\sigma_c}{\sigma_a} = \frac{55}{35.6} = 1.55$$

Crystal C-1075-B Copper Doped $p \simeq 1.1 \times 10^{19}$ cm^{-3}

Ratio of Electrical Conductivities in $(ohm\text{-}cm)^{-1}$

$$\frac{\sigma_b}{\sigma_a} = \frac{370}{614} = 0.60 \qquad \frac{\sigma_c}{\sigma_a} = \frac{950}{614} = 1.55$$

4.5 Magnetoresistance in P-Type ZnSb

Magnetoresistance data are presented in Figs. 4.5 and 4.6 for two p-type zinc antimonide crystals. Instead of plotting a very large number of individual data points, brackets have been drawn that represent the total excursion for all of the data points that correspond to a given angle between the magnetic field and current axis of the sample.

The scatter of the individual data points within a given bracket seems to bear no correlation to magnetic field strength. Hence, it must be concluded that the observed magnetoresistance is quadratic in magnetic field strength. The scatter of the individual data points mainly arises from the fact that the magnetoresistance effect is so small in ZnSb. For instance, at 77.3°K in a 12.5 kg magnetic field, the largest observed changes in resistance are 1.5 percent and 0.3 percent for the undoped and copper doped samples, respectively. At 12.5 kg, the electric field component which gives rise to the Hall voltage is roughly two orders of magnitude larger than the change in the longitudinal component of the electric field which is caused by the magnetoresistance. As a result, the slightest departures from ideal galvanomagnetic sample geometry will introduce a spurious Hall voltage component into the voltage measured at the magnetoresistance probes. In practice, the measured magnetoresistance voltage contains roughly an equal amount of spurious Hall voltage at 12.5 kg. By suitably averaging voltages measured for both directions of the magnetic field, the actual magnetoresistance voltage can be obtained. However, especially below 10 kg, this procedure can amount to taking the difference of two large numbers and can possibly introduce considerable error into the magnetoresistance results. The absolute accuracy of the magnetoresistance measurement, $\Delta\rho/\rho B^2$, is estimated to be between 5 percent and 10 percent, depending upon the numerical magnitudes involved. The data scatter indicated by the size of the brackets in Figs. 4.5 and 4.6 are generally in agreement with this estimate.

Data taken with the electric current along the a and b axes (the <100> and <010> directions) is reproducible to within at least 10 percent between different samples cut from crystal C-1078-C (copper doped). This is reasonable reproducibility when sample cutting and mounting misorientation errors are added to the above error estimate. Data for current

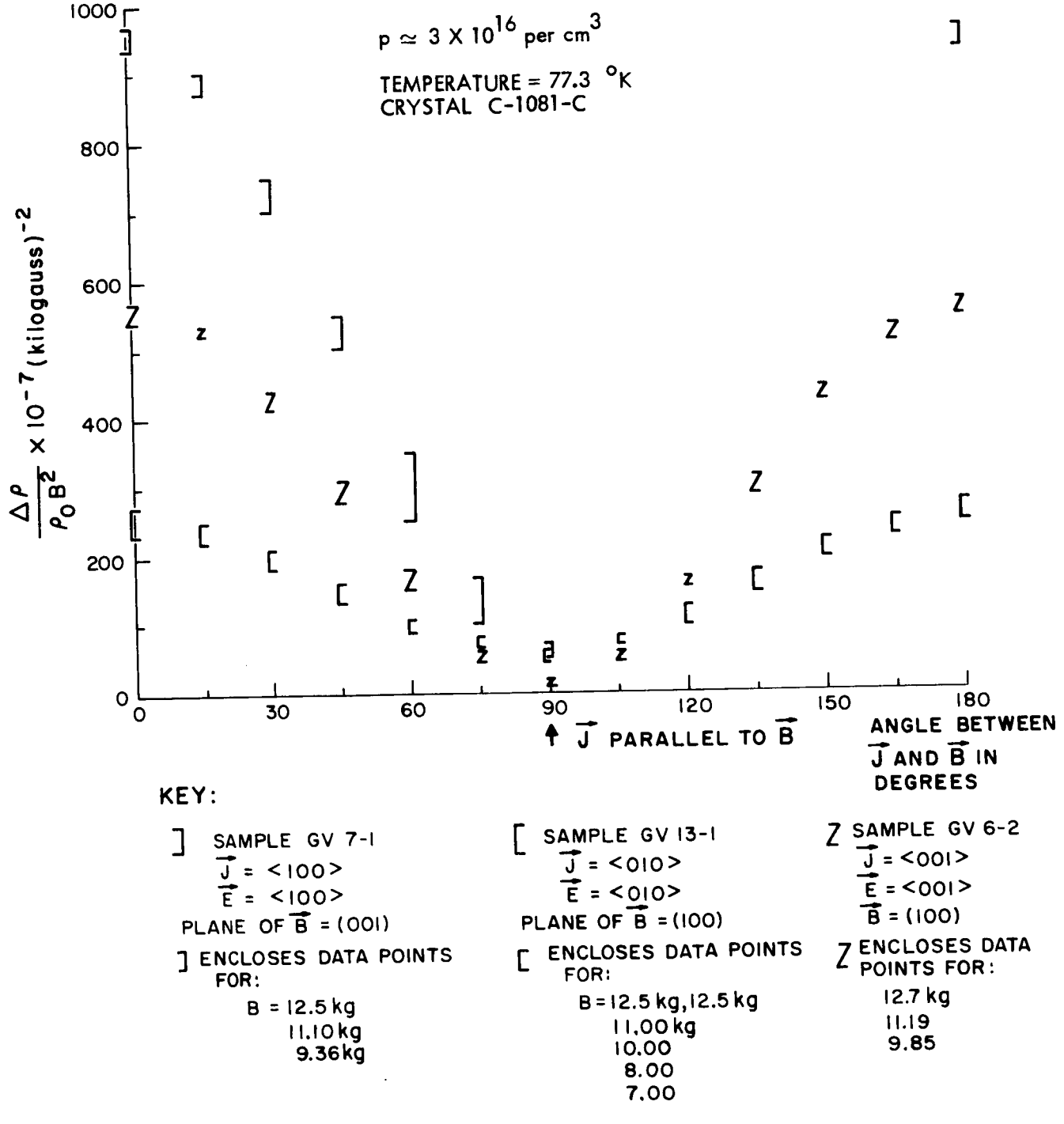

Fig. 4.5 Magnetoresistance in Undoped p-type ZnSb

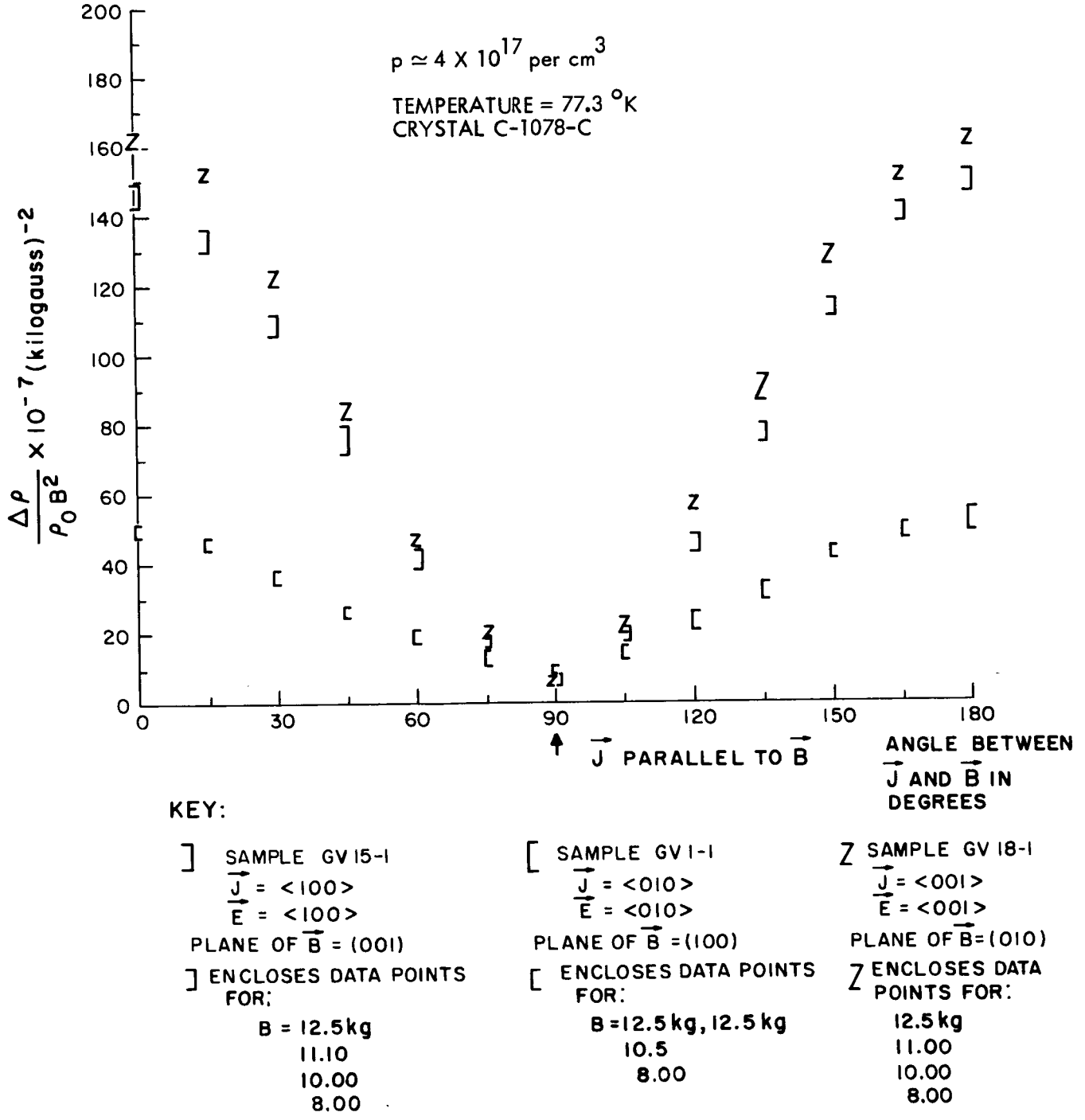

Fig.4.6 Magnetoresistance in Copper Doped ZnSb

along the c axis of the copper doped crystal have not been reproduced as yet. Hence, the c axis (the <001> current direction) results should be regarded as tentative.

The data which is presented indicates a longitudinal magnetoresistance effect which is so small that it is reasonable to regard it as being residual. The observed longitudinal effect probably arises from local departures from sample uniformity. These nonuniformities are principally local crystalline imperfections and the finite size of the voltage contacts on the samples. Similar amounts of residual longitudinal magnetoresistance appear in published data for n-type GaAs[10] and n-type Si.[11]

The approximately zero longitudinal magnetoresistance for electric currents directed along each of the principal crystal axes indicates that the energy surfaces of p-type ZnSb might be characterized by one or more general ellipsoids which are oriented with their principal axes parallel to the edges of the orthorhombic Brillouin zone.

Numerical evaluation of the magnetoresistance data will begin as soon as experimental checks of the reproducibility of the data are complete.

4.6 Thermal Measurements on P-Type ZnSb

Measurements of thermoelectric power and thermal conductivity as a function of electrical conductivity are now in progress. Measurements are being made on samples which are cut from single crystals that have six different carrier concentrations.

The thermal conductivity, thermoelectric power, and electrical conductivity are being measured simultaneously in the apparatus which is shown in Figs. 4.7 and 4.8. The samples are approximately cube-shaped and measure 3 to 5 mm on a side. The cubes are cut so that they are bounded by the 3 principal crystal planes.

In order to minimize mechanical strains due to differential thermal expansion between any two principal axes and the copper heat source or sink, a low temperature soldering technique is needed. Two opposite faces of the sample are carefully electroplated with indium in a room temperature bath of indium sulfamate solution. The copper heat source and sink are pretinned with gallium. The sample is raised to slightly above room temperature (to about 30°C) and the indium plated faces are tinned with

THERMAL AND ELECTRICAL CONTACT
IS MADE TO THE INDIUM PLATED CONTACT
AREAS OF THE CRYSTAL WITH GALLIUM. ALL
SOLDERING IS DONE AT ROOM TEMPERATURE

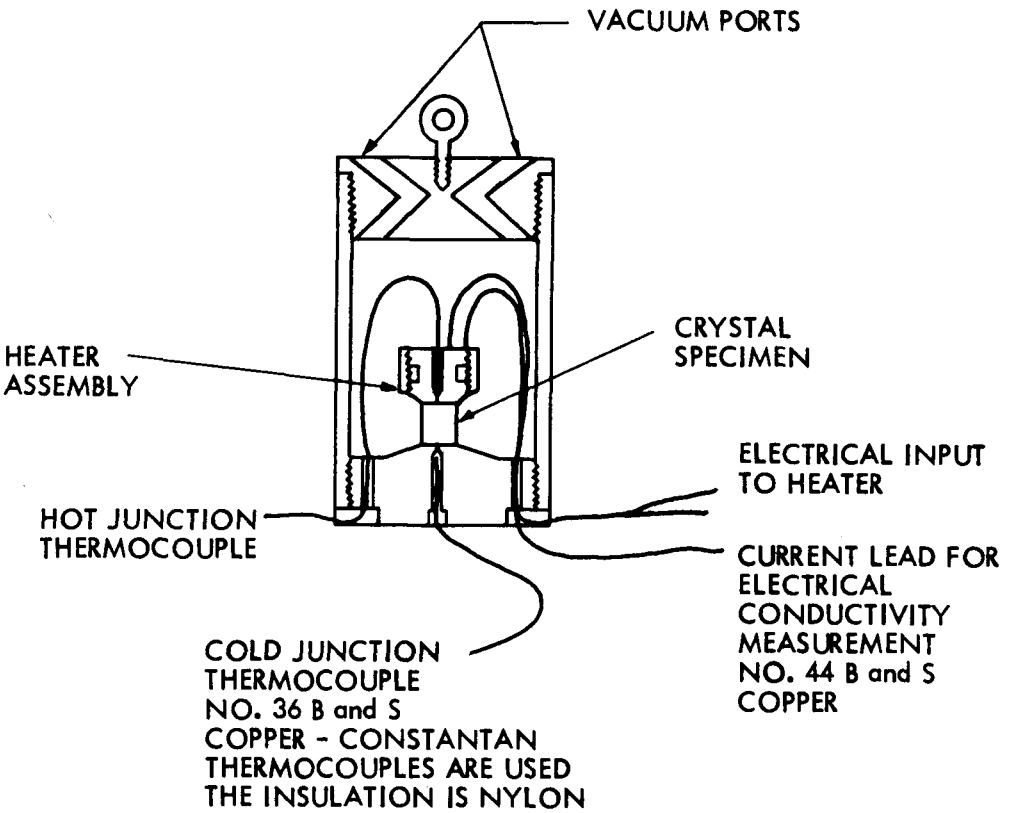

Scale: FULL SIZE

Material: GOLD PLATED COPPER

Fig. 4.7 Thermal Conductivity Chamber

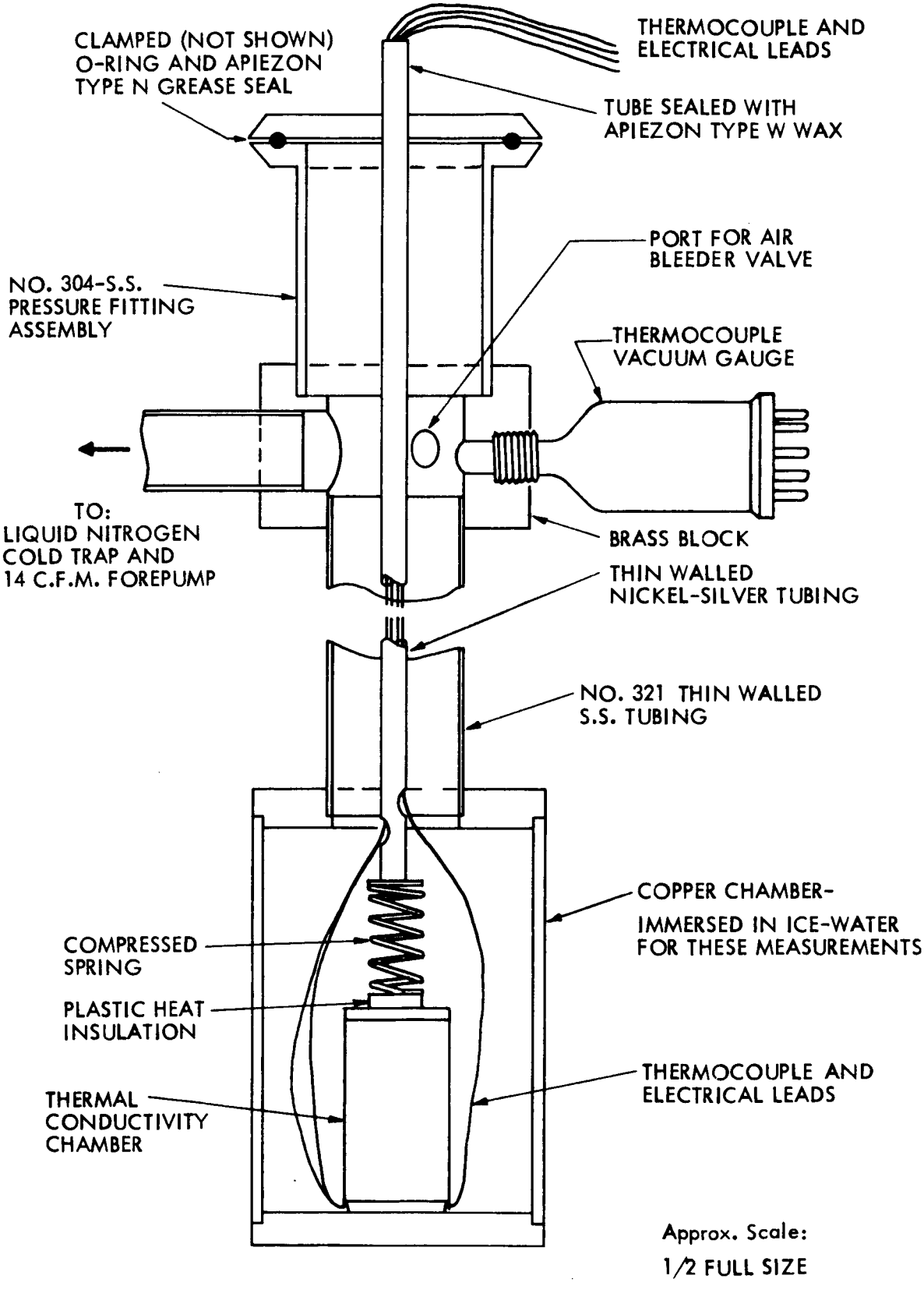

Fig. 4.8 Vacuum Cryostat for Thermal Conductivity Measurement

gallium. The sample is then attached to the heat source and sink and the copper chamber cooled to below room temperature (to about 10 or 15°C) where the gallium solder freezes. The copper thermal conductivity chamber is then placed in the vacuum crystal and evacuated. All measurements are made at 0°C with the cryostat immersed in an ice bath.

Using this technique, it has been possible to make successive thermal measurements along the three principal axes of the same single crystal cube. The empirical probability of taking 3 sets of measurements on the same cube without fracturing it is about 90 percent.

Some preliminary results of the thermal measurements are shown in Table 4.3. This data indicates that there is about a 20 percent anisotropy in the thermal conductivity and no anisotropy in the thermoelectric power of p-type ZnSb.

TABLE 4.3

PRELIMINARY RESULTS OF THERMAL MEASUREMENTS
ON P-TYPE ZnSb AT 0°C

Crystal Axis	Sample Number	Approx. Hole Concentration	Thermal Conductivity milliwatts/cm-°K			Thermoelectric Power μV/°K			Electrical Conductivity (ohm-cm)$^{-1}$		
			a	b	c	a	b	c	a	b	c
C-1081-C	2	3×10^{16} cm^{-3}	32.0	34.0	37.0	677	-	664	-	-	-
	2*	undoped	-	33.3	-	-	707	-	-	-	-
C-1078-C	1	4×10^{17}	31.3	34.0	35.0	408	424	409	-	-	-
	2	copper doped	31.3	33.0	34.8	418	412	432	-	-	-
	2**		31.3	32.7	35.0	426	437	434	35.6	21.5	55.0
	2†		-	-	34.7	-	-	429	-	-	53.6
C-1075-B	2	1×10^{19}	30.0	-	37.0	176	-	177	-	-	-
	3	copper doped	33.5	34.5	40.0	170	180	173	614	370	950

*This reading taken after 2 months storage at room temperature. Refer to section 4.0 of this report.

**The measured electrical conductivities agree well with those measured on galvanomagnetic samples.

†The c-axis dimension was cut in half for this measurement. Designation of crystal axes;
a = 6.20 Å, b = 7.74 Å, c = 8.10 Å.

4.7 References

1. Nye, J.F., Physical Properties of Crystals, Oxford University Press, London, 1960.

2. Reed and Marcus, Phys. Rev., 130, (1957), 1963.

3. Kot and Kretsu, Gov. Phys. Solid State, 2, (1134) 1960.

4. R. Mazelsky, Private Communication.

5. Komiya, Masumoto, Frank, Phys. Rev., 133, (A1679), 1964.

6. Justi, Rasch and Schneider, Adv. Energy Conversion, 4, 27 (1964).

7. W.W. Scanlon, Phys. Rev., 126, (509) 1962).

8. F.S. Ham, J. Appl. Phys., 30, 915 (1959).

9. R. Mazelsky, R. Eisner, Scientific Paper 23-929-8902-P5, Westinghouse Research Laboratories, Pittsburgh, Pa., April 4, 1961.

10. Woods and Chen, Phys. Rev., 135, (A1462) 1964.

11. Putley, E.H., The Hall Effect and Related Phenomena, Butterworths, London, 1960, p. 19.